UNIVERSIDADE ESTADUAL PAULISTA "JÚLIO DE MESQUITA FILHO"
FACULDADE DE MEDICINA

Gabriel Bacil Prata

Estabelecimento de modelo murino de esteatohepatite não alcoólica: tratamento com compostos bioativos de alimentos

Dissertação apresentada à Faculdade de Medicina, Universidade Estadual Paulista "Júlio de Mesquita Filho", Câmpus de Botucatu, para obtenção do título de Mestre em Ciências, com ênfase em Patologia, pelo Programa de Pós-Graduação em Patologia.

Orientador: Prof. Dr. Luis Fernando Barbisan

Coorientador: Prof. Dr. Guilherme Ribeiro Romualdo

Botucatu

2022

Gabriel Bacil Prata

Estabelecimento de modelo murino de esteatohepatite não alcoólica: tratamento com compostos bioativos de alimentos

Dissertação apresentada à Faculdade de Medicina, Universidade Estadual Paulista "Júlio de Mesquita Filho", Campus de Botucatu, para obtenção do título de Mestre em Ciências, com ênfase em Patologia, pelo Programa de Pós-Graduação em Patologia.

Orientador: Prof. Dr. Luis Fernando Barbisan

Coorientador: Prof. Dr. Guilherme Ribeiro Romualdo

Botucatu

2022

FICHA CATALOGRÁFICA ELABORADA PELA SEÇÃO TÉC. AQUIS. TRATAMENTO DA INFORM.
DIVISÃO TÉCNICA DE BIBLIOTECA E DOCUMENTAÇÃO - CÂMPUS DE BOTUCATU - UNESP
BIBLIOTECÁRIA RESPONSÁVEL: ROSEMEIRE APARECIDA VICENTE-CRB 8/5651

Prata, Gabriel Bacil.
Estabelecimento de modelo murino de esteatohepatite não alcoólica : tratamento com compostos bioativos de alimentos / Gabriel Bacil Prata. - Botucatu, 2022

Dissertação (mestrado) - Universidade Estadual Paulista "Júlio de Mesquita Filho", Instituto de Biociências de Botucatu
Orientador: Luís Fernando Barbisan
Coorientador: Guilherme Ribeiro Romualdo
Capes: 40105008

1. Esteatose hepática. 2. Hepatopatia gordurosa não alcoólica. 3. Polifenóis. 4. Brassica.

Palavras-chave: Esteatohepatite não alcoólica; Esteatose hepática; Isotiocianatos; Polifenóis; Vegetais Brassica.

Agradecimentos

Inicialmente, gostaria de agradecer ao Instituto de Biociências de Botucatu (IBB), pela construção e formação oferecida no período 2016-2020, e à Faculdade de Medicina de Botucatu (FMB), na qual finalizo a primeira etapa da minha Pós-Graduação. Dessa forma, gostaria também de agradecer à Universidade Estadual Paulista (UNESP), que por todos esses anos foi minha casa, nos melhores e piores momentos. Aos docentes e servidores que me acompanharam, aconselharam e foram companheiros durante esses anos, minha eterna gratidão. Gostaria também de agradecer à Fundação de Amparo à Pesquisa do Estado de São Paulo (FAPESP, #2020/01944-6) e à Coordenação de Aperfeiçoamento de Pessoal de Nível Superior (CAPES, #88887.481152/2020-00) pelo financiamento dos projetos vinculados à dissertação em questão.

Ressalto também a disponibilidade, apoio e dedicação brilhante dos membros e amigos do Laboratório de Carcinogênese Química e Experimental (LCQE), que desde 2017 é a minha casa, em especial aos meus quase irmãos Isadora Penedo de Souza, que me acompanhou até 2020, e Guilherme Ribeiro Romualdo, que continua sendo meu mentor, exemplo e companheiro diário, sem os quais não seria capaz de trilhar essa jornada. Por todos os momentos críticos e divertidos, discussões calorosas e construtivas e levezas da nossa rotina, saiba que sem elas eu não chegaria até esse ponto e, ironicamente, sou eternamente grato por todas elas. Sem dúvidas foram nos momentos difíceis em que puder aprender mais. Aos orientadores e Professores Luís Fernando Barbisan e Guilherme Ribeiro Romualdo, por me abrirem as portas do LCQE em 2017, para a realização da iniciação científica, em 2020, para a realização do meu Mestrado, e novamente em 2022, para a realização do Doutorado, a minha gratidão e admiração. Espero ser digno de levar adiante nossas discussões e contribuir para a formação de outros, tal qual fizeram comigo. Obrigado por acreditarem em mim quando eu mesmo não enxergava potencial. Sem vocês, eu jamais encontraria a rota certa nessa jornada.

Aos meus irmãos da República Põe na Mão de Deus, sem vocês, nada faria sentido. O primeiro passo para fora de casa é sempre o mais crítico, sem a leveza, amizade e carinho de todos (sim, mais velhos e novos) essa trajetória seria impossível. Agradeço em especial ao Renan Augusto Pereira, Marcel Rodrigues Ferreira, Matheus Naville, Luis Eduardo Taguchi, Gustavo Camargo, Thiago Cobra e Monteiro, Marcos Bottaro e Silva e Gabriel Gasparini por me abrirem as portas e me receberem em sua casa. Em especial, aos irmãos Ivan Rossi Moraes, Marcel Rodrigues Ferreira, Thiago Cobra e Monteiro, Renan Augusto Pereira dos Santos e Guilherme Gazolla Santana, que desde 2016/2017 são meus conselheiros, a que sempre estiveram ao meu lado nos momentos de conquista e batalha. Obrigado por todo o carinho, apoio e dedicação, sem vocês nada seria possível. Aos que sempre tentaram me levar para o "mal caminho" universitário, tenham certeza que sem essas festas, confraternizações, e momentos marcantes, a vida em Botucatu não seria a mesma. Espero que as nossas vidas estejam entrelaçadas até o fim.

Aos meus irmãos de longa data João Rafael Peres Prado, Alan Pontes Polverini e Vitor Tramontin Tornello, agradeço a sua amizade e carinho de sempre. Essa conquista não seria viável sem vocês. Espero que logo estejamos novamente juntos e próximos uns dos outros.

Finalmente, gostaria de agradecer aos meus pais Sérvulo do Sacramento Prata e Sandra Maria Bacil, por todos os esforços realizados durante todos estes anos. A sua dedicação incessante e irrestrita para que sejamos capazes de alcançar os nossos sonhos são o combustível que nos mantém nessa jornada. Esse título e todas as demais conquistas também são de vocês. Aos meus avós Roberto Bacil e Eunice de Oliveira Bacil, o ponto de partida da nossa família. Sem vocês, não haveria perspectiva, coragem e portas abertas. A minha eterna gratidão e carinho. O meu sonho seria ter ambos comemorando comigo essa conquista. Em especial, ao meu avô, conselheiro, pai, amigo, espero um dia chegar perto do que você representou para nós todos. Por fim, gostaria de agradecer às duas pessoas mais importantes da minha vida. Agradeço à Gabrielle Rodrigues Domingues, minha companheira e melhor amiga a 10 anos, a fortaleza dos meus

sentimentos e que sempre será o meu porto-seguro. Eu jamais teria conseguido ir além sem o seu carinho e apoio. Obrigado por se preocupar comigo mais do que eu mesmo. Amo você. Enfim, ao meu exemplo desde jovem. Ao meu irmão Raphael Bacil Prata, meu espelho, símbolo de dedicação e competência, companheiro nos melhores e piores momentos, e conselheiro nas demais horas. Por sua causa tive as portas de um laboratório abertas para mim. Sem o seu apoio, dedicação irrestrita, paciência e irmandade eu jamais teria escolhido seguir esse caminho e encontrado a minha paixão na área acadêmica. Amo todos vocês.

Resumo

Atualmente, estima-se que a doença hepática gordurosa não alcoólica (NAFLD, do inglês Nonalcoholic Fatty Liver Disease) afeta cerca de 25% da população mundial, enquanto o seu grau mais severo, a estatohepatite não alcoólica (NASH), afeta 5%. O aumento da prevalência da NAFLD/NASH, por sua vez, acontece em paralelo com o aumento do número de indivíduos com diabetes do tipo II e obesidade, associadas à adesão populacional à dieta ocidental (WD), rica em carboidratos simples e gorduras saturadas, e de hábitos sedentários. No entanto, não existem métodos terapêuticos aprovados pelas agências de saúde governamentais para os pacientes com NAFLD/NASH, assim como é urgente o estabelecimento de modelos experimentais translacionais que recapitule as características da doença correspondente em humanos. Então, foi estabelecido um modelo experimental híbrido de NASH em camundongos C57BL/6J e BALB/c, no qual observamos o aumento do grau *Nonalcoholic fatty liver activity score* (NAS), além de acúmulo de lipídios do parênquima hepático ($p<0.0001$, em ambos) e fibras colágenas na região centro-lobular ($p<0.0001$, em ambos), aumento da ativação de células estreladas hepáticas, infiltração de células $CD68^+$ ($p<0.0001$, em ambos) e do número de hepatócitos caspase-3 clivada$^+$ ($p<0.0001$, em ambos). Ademais, ambas as linhagens apresentaram a redução dos níveis proteicos de Nrf2 ($p<0.0001$, em ambos), enquanto somente os animais C57BL/6J apresentaram o aumento dos níveis de NF-κB (p65) ($p<0.0001$), além de um perfil metabolômico linhagem-dependente. Nesse contexto, os compostos bioativos dos vegetais da família *Brassicaceae* indol-3-carbinol (I3C) e ácido clorogênico (CGA) foram capazes de reduzir o grau NAS, a ativação de CEH e a infiltração de células $CD68^+$ ($p<0.0001$), além de uma tendência de redução no conteúdo lipídico e acúmulo hepático de fibras de colágeno ($p<0.0001$).

Abstract

Recently, nonalcoholic fatty liver diseases (NAFLD) have been indicated as a potential most common chronic liver disease worldwide, as well as affecting ~25% of the population. Likewise, its most severe form, nonalcoholic steatohepatitis (NASH) affects 5% of the global population. The NAFLD prevalence, however, has been linked to the adhesion of a western diet (WD), which is enriched with simple carbohydrates and high levels of saturated fatty acid, as well as adherence to a sedentary lifestyle. Moreover, there are no approved therapies for patients, by the governmental agencies, as well as an urgent need of establishing a reliable experimental model that resembles the morphologic and molecular traits of the corresponding human disease. Thus, we sought to establish a hybrid model of NASH in C57BL/6J and BALB/c mice. Indeed, the hybrid model increased the Nonalcoholic fatty liver activity score (NAS), whereas enhanced the lipid ($p<0.0001$, on both strains) and collagen content ($p<0.0001$, on both strains), increased the number of active hepatic stellate cells (HSC) ($p<0.0001$, on both strains), $CD68^+$ cells ($p<0.0001$, on both strains) and cleaved caspase-3^+ hepatocytes ($p<0.0001$, on both strains). Additionally, both strains featured reduced protein levels of Nrf2 ($p<0.0001$, on both strains), while only C57BL/6J featured increased levels of NF-κB ($p<0.0001$). We also assessed the hepatic metabolomic profile, and a strain-dependent response was observed. On the other hand, the bioactive compounds of *Brassicaceae* family vegetables indole-3-carbinol (I3C) and chlorogenic acid (CGA) reduced the NASH severity, besides reducing the HSC activation ($p<0.0001$) and the number of hepatic $CD68^+$ ($p<0.0001$), besides presenting a decreasing trend of hepatic collagen and lipid content, although no statistical difference were observed.

Summary

ARTICLE

Are isothiocyanates and polyphenols from *Brassicaceae* vegetables emerging preventive/therapeutic strategies for NAFLD? The landscape of recent preclinical findings

Received 00th January 20xx,
Accepted 00th January 20xx

DOI: 10.1039/x0xx00000x

Gabriel P. Bacil[a], Bruno Cogliati[b], Daniel R. Cardoso[c], Luís Fernando Barbisan[d] and Guilherme R. Romualdo[ad]*

Nonalcoholic fatty liver disease (NAFLD) is a lipid impairment-related chronic metabolic disease that affects almost 25% of the worldwide population and has become the leading cause of liver transplantation in the United States of America (USA). NAFLD may progress from simple hepatic steatosis to nonalcoholic steatohepatitis (NASH), which occurs simultaneously to an inflammatory and fibrotic microenvironment, and affects aorund 5% of the global population. Recently NASH has been suggested as a relevant driver of progressive liver cirrhosis and a populational attributable fraction in hepatocellular carcinoma patients. Moreover, predictions show that NAFLD-related annual health costs in the USA reach ~$100 bi., but effective therapies still scarce. Thus, it is urgent to develop new preventive strategies for this hepatic disease. The *Brassicaceae* vegetable family comprises almost 350 genus and 3500 species, being one of the main kinds of harvest and produced vegetables worldwide. These vegetables are well-known sources of glucobrassicin-derivative molecules, as isothiocyanates, and phenolic compounds, showing anti-oxidant and anti-lipogenic effects in preclinical findings of NAFLD. In this review, we sought to gather prominent evidence of *in vivo* and *in vitro* effects of these vegetable-derived nutraceutical compounds on the gut-liver-adipose axis, which is a well-known regulator of NAFLD and may represent a new strategy for disease control.

Introduction

Nonalcoholic fatty liver disease (NAFLD) comprises a wide spectrum of chronic liver disease which affects ~25% of the global population, displaying the highest prevalence in South America and the Middle East, ~31 and ~32%, respectively. Moreover, nonalcoholic steatohepatitis (NASH), the most severe stage observed in the NAFLD spectrum, occurs in ~5% of the global population1. Currently, NAFLD emerges as the most common chronic liver disease and is expected to become the main cause for liver transplantation in the United States of America (USA)[1–3]. Indeed, the global trends suggest that NAFLD-related incidence of liver cancer increased by ~26% from 2012-2017, while in highly industrialized countries, NAFLD-associated mortality is expected to double in the 2016-2030 period[4,5]. It has been observed that type 2 diabetes mellitus (T2D) and obesity are closely linked to ~23% and ~52% of NAFLD patients, respectively, suggesting the metabolic syndrome (MS) as a major risk factor for this disease[1,6]. In parallel, the global populational lifestyle has suffered drastic changes regarding nutritional habits and sedentarism, which might be responsible for growing NAFLD incidence[7,8]. The development of NAFLD is related to a high intake of western diet (WD), which is mostly composed of food enriched with high amounts of saturated fatty acids (SFA) and simple carbohydrates (e.g.: high-fructose corn syrup, fructose, glucose, and sucrose) - both extensively used by the food industry since the last century -and the sedentary lifestyle[9]. Conversely, only ~9% of USA adults meet the daily recommendations for vegetable intake (~450g /day), according to the Centers for Disease Control and the USDA[10,11]. Besides, NAFLD also displays a high economic burden since, in the USA and Europe (Germany, Italy, France, and the United Kingdom), the annual medical costs are estimated to reach US$ 103 billion and € 35 billion, respectively[12]. These data elicit the rising importance of this chronic liver disease as a contemporary public health problem.

Otherwise, several studies show that adherence to the Mediterranean diet (MD), constituted of high intake of vegetables, fruits, grains, monounsaturated (MUFA) and polyunsaturated fatty acids (PUFA), and low intake of sugar, reduce the related risk for T2D (19%) and hepatocellular carcinoma (44-49%) occurrence, while it also improves HS and insulin resistance (IR) in patients with NAFLD[13–16]. These beneficial effects are attributed to the bioactive compounds of food, which compose a pharmacopeia of antioxidant, anti-inflammatory, and lipid metabolism-modulating molecules, like glucosinolates (GLS), isothiocyanates (ITC), phenolic

[a.] *São Paulo State University (UNESP), Botucatu Medical School, Department of Pathology, Botucatu, SP, Brazil.*
[b.] *University of São Paulo (USP), School of Veterinary and Animal Science, Department of Pathology, São Paulo, SP, Brazil.*
[c.] *University of São Paulo (USP), São Carlos Institute of Chemistry (IQSC), São Carlos, SP, Brazil.*
[d.] *São Paulo State University (UNESP), Department of Structural and Functional Biology, SP, Brazil.*
* Corresponding author

compounds, and others[17]. Indeed, the Brassicaceae, or Cruciferae, family has been appointed as a reliable dietary source of bioactive compounds – especially ITC and polyphenols – and comprises around 350 genera and 3500 species of vegetables, like cabbages, broccoli, cauliflower, and brussel sprouts, all variations of Brassica oleracea specie[18,19].

Since there is plenty of evidence indicating that the Brassicaceae family vegetables are composed of a myriad of bioactive compounds with potential beneficial influence on liver chronic disease, we sought to gather prominent preclinical in vivo and in vitro data of the effects of ITC and phenolic compounds available in Brassicaceae vegetables over the gut-liver-adipose axis and hallmarks of NAFLD.

NAFLD: a contemporary disease

NAFLD has a basal stage of hepatic steatosis (HS) with macrovesicular or microvesicular profile features, while NASH remarks the simultaneous occurrence of HS and inflammatory foci, and hepatocellular lesions, all relevant for grading and staging of patients[20]. The lipid homeostasis impairment induces the steatotic profile of hepatocytes, comprising the first hit for NAFLD establishment. Further HS progression to NASH depends on the occurrence of the inflammatory process, caused by lipotoxicity-induced oxidative stress and mitochondrial metabolic impairment, leading to the activation of death-related signaling that promotes the endoplasmic reticulum stress (ERS) in the hepatocytes. The ERS triggers the systemic inflammatory response, contributing to the pro-inflammatory hepatic milieu and featuring the second hit for NASH development[21]. Of note, lipid homeostasis and oxidative stress are closely linked, suggesting that both mechanisms act in a positive feedback manner during NAFLD progression. In addition, the high intake of fat and sugars leads to adipose tissue (AT) stress, further associated with the synthesis of cytokines and lipolysis of fatty acids (FA), contributing to the establishment of systemic sublethal grade inflammation in which NASH is more susceptible to develop. Additionally, it is well reported that the gut microbiome dysbiosis exerts a pivotal activity during NASH progression, by modulating both liver and AT inflammation and inducing metabolic disorders[22,23]. Taken together, the interplay of liver-gut-adipose dynamics suggests multiple hit-driven mechanisms that modulate NASH progression[23]. In its more advanced stages, NAFLD can progress to extensive fibrosis, cirrhosis, and, further, hepatocellular carcinoma (HCC)[24]. Remarkably, NASH is attributed to 32% of HCC cases in the USA, overcoming chronic viral hepatitis (~25%) and alcohol consumption (~13%) as the main risk factor for this malignancy[25].

Recently, the emergence of NAFLD has been related to dietary and lifestyle factors, especially the high intake of SFA, fructose, and glucose, and lack of physical activities, due to their impacts on the gut-liver-adipose axis[26]. According to Dietary Guidelines for Americans (2015-2020) from the Department of Agriculture (USDA), the recommended intake of SFA is less than 22 g/day (~10% of daily caloric intake), although there was a current average of 11% of daily caloric intake in the USA population. Additionally, sugar consumption is associated with high caloric beverages, like sugar-sweetened beverages (SSB), the most common source of sugars in the USA and epidemiologically related to MS, T2D, obesity, and NAFLD in a dose-dependent manner[27–29]. Furthermore, the mean daily intake of sugar by individuals in the USA is 89.8 g/day (~16% of daily caloric intake recommendations), while American Heart Association recommends the utmost daily intake of 37.5 g/day (~6.7% of daily caloric intake recommendations), suggesting that an unbalanced dietary habits could be responsible for metabolic disorders, and further NAFLD development[30,31]. On the other hand, sedentary behavior increases the risk of developing MS by 73%, while regular physical activity reduces lipid storage in the liver, and hence, NAFLD grading[32,33]. Thus, it remains unknown whether NAFLD development may be attributed to simple carbohydrates/excessive fat consumption, sedentary lifestyle or both.

The ectopic lipid storage in the liver that culminates in HS is mainly caused by the following mechanisms: (1) increased FA influx, derived from the diet; (2) enhanced de novo lipogenesis; (3) inefficient lipid oxidation; and (4) inadequate lipid exportation activity (Figure 1)[21]. Overall, the uptake of FA by hepatocytes depends on the FA transporters activity, especially the CD36 and caveolins, located at the plasma membrane, and FA transport proteins (FATP), responsible for the lipid trafficking and organization into intracellular lipid droplets, which are essential to the adequate metabolism of FA[34,35]. In patients with NAFLD, the lipid accumulation in hepatocytes occurs as TG droplets, derived mostly from the non-esterified fatty acids (NEFA) pool influx (~60%) and the hepatic de novo lipogenesis (~26%)[36]. The hepatic de novo lipogenesis pathways are triggered by the high intake of carbohydrates, like fructose and glucose, and fat, which are catabolized into acetyl-CoA, further related to the tricarboxylic acid cycle (TCA) and palmitate synthesis. The FA synthesis dynamics, however, are modulated by the activation of the sterol regulatory element-binding protein-1c (SREBP-1c) and the carbohydrate regulatory element-binding protein (ChREBP), under influence of insulin and fed state, which interact with sterol and carbohydrate response elements located at the promoter region of FA synthesis-related genes (*Acc1*, *Fas*, and *Scd*)[37–40]. In addition to the above-cited mechanisms, the FA oxidation (FAO) disturbance in mitochondria displays great importance in steatosis emergence and its modulation has been defined as a potential therapeutic approach[41]. The mitochondrial energetics activity encompasses several mechanisms that act coordinately to maintain the adequate FAO rate (β-oxidation, TCA cycle, ketogenesis, respiratory chain activity, and ATP synthesis), Also, it has been appointed that the peroxisome proliferator-activated receptor α (PPARα) activity, which is strikingly reduced in NAFLD patients, might be related to the FAO impairment, leading to the accumulation of FA byproducts (eg.: ceramides, diacylglycerol, and long-chain acylcarnitine), which cause the lipotoxicity of hepatocytes[42–44].

Additionally, subjects with IR feature impaired insulin homeostasis, which plays a pivotal metabolic role in glucose uptake and endogenous synthesis in several tissues [e.g: liver,

skeletal muscle, and adipose tissue (AT)], and NEFA synthesis. Indeed, it has been suggested that large amounts of NEFA pool are available due to increased levels of lipolysis in adipocytes, as a result of obesity-induced inflammation driven by adipose tissue macrophages (ATM, resident macrophages, and/or infiltrating monocytes), demonstrating that the liver-adipose axis is intrinsic for NAFLD development (Figure 1)[45,46]. During obesity, the excessive intake of FA induces adipocyte hypertrophy and alters its functional activity, promoting systemic low-grade inflammation, as previously discussed[47]. Also, adipocytes overexpress monocyte chemoattractant protein-1 (MCP-1), leading to monocyte recruitment to AT and local ATM activation. Thus, active ATM becomes responsible for significant amounts of TNF-α and interleukin (IL)-6 expression released, essential for IR and lipolysis-promoting activity (Figure 1)[48,49]. Likewise, several studies reported that intestinal microbiota dysbiosis modulates NAFLD progression, as previously reviewed[50]. Le Roy et al.[51] demonstrated that germ-free animals that received gut microbiome transplants from mice fed with WD develop metabolic features of NAFLD, like glucose and lipid homeostasis impairment. Indeed, it was observed in patients that the gut microbiome dysbiosis implies higher NAFLD severity and liver fibrosis grade, by modulating the Bacterioides and Ruminococcus genus dynamics (higher abundance) compared to patients without NAFLD, providing evidence about the pivotal role of the gut-liver axis, and its potential activity as a metabolic regulator and noninvasive biomarker (Figure 1)[22]. Moreover, it has been reported that gut dysbiosis induces the disruption of gut epithelium tight junctions [(zonula occludens-1 (ZO-1) e occludin], enabling bacterial metabolite byproducts, that interfere with lipid metabolism and systemic inflammation, like ethanol, choline, bile acids, and lipopolysaccharides (LPS), to reach the liver and impair the hepatocytes metabolism, as well as promote metabolic disorders and systemic low-grade inflammation (Figure 1)[52–54]. In addition, the WD-induced dysbiosis dysregulates tryptophan metabolism, via the kynurenine pathway, and modulates key metabolic processes and inflammation in AT, establishing a direct cross-talk between AT and gut microbiota[55]. By these terms, the gut-liver-adipose axis is pivotal to the establishment of NAFLD, as well as to the emergence of metabolic disorders, especially obesity and IR, that contribute to the disease progression (Figure 1).

Isothiocyanates and phenolic compounds are preventive/therapeutic options for NAFLD?

Estimated intake of Brassicaceae vegetables

From 1994 to 2019, the Brassica genus vegetables worldwide production increased ~65%, and China features as the greatest producer (33.5 million tons)[56]. However, data on the daily human intake are still imprecise. According to the International Agency for Research on Cancer (IARC), there are geographical differences among countries, since the Asian and Middle East daily intake (~100 g/day) is higher than in Europe (32 g/day) and North and South American (~30 g/day and ~13 g/day, respectively) populations, and, overall, the worldwide population daily intake is ~21 g/day57. However, most studies focus on food frequency questionnaires (FFQ) or 24-hours recalls, lacking Brassica vegetable information and biasing the results, since when a FFQ focused on Brassica vegetables were applied, the estimated adult daily intake was ~84 g/day[58]. The health promotion properties of Brassica vegetables are related to the high content of GLS, phenolic compounds, vitamins, and minerals, which may act directly or indirectly in the reduction of the systemic inflammation and pro-oxidant state[49]. GLS are stable and water-soluble groups of molecules that share β-D-thioglucose moiety with a sulfonate oxime group and a variable side chain. They are classified according to their molecular structure (e.g.: aliphatic, aromatic, or indolic) and the side chain which is derived (e.g.: alanine, methionine, phenylalanine, tyrosine, or tryptophan), and are widely found in vegetable cells of Brassica genus[19]. When the vegetable is damaged by harvesting or masticating, the GLS are hydrolyzed by myrosinase activity, a constitutively expressed enzyme, and turned into reactive molecules like ITC, thiocyanates, and nitriles, that may exert several bioactive properties18. Besides, there is evidence that gut microbiota may also induce GLS conversion into bioactive compounds, due to the activity of bacterial myrosinase-like enzymes[18]. Under neutral pH conditions, glucobrassicin is converted into the ITC indole-3-carbinol (I3C, PubChem CID 3712), and further converted into 3,3'-diindolylmethane (DIM, PubChem 3071), which is the major I3C-derivative molecule that exerts bioactive effects, whereas the acidic conditions induce the GLS conversion into nitriles[50]. On the other hand, phenolic compounds are the largest and a well-known group of phytochemical molecules (~8,000 molecules) with antioxidant and anti-inflammatory properties. Briefly, phenolic compounds can be classified into phenolic acids (benzoic and cinnamic acids), flavonoids (anthocyanins and flavonols), and non-flavonoids, according to their structure, which also determines their bioactive properties[60]. Moreover, they can be found in a plethora of vegetables, fruits, and grains, including Brassica vegetables, in which their biosynthesis occurs by the Shikimate pathway. The Shikimate pathway is employed by microorganisms and plants as an alternative route to convert carbohydrates to aromatic compounds and aromatic amino acids61. Thus, it is suggested that the phenolic content in food might be responsible for beneficial effects on chronic liver diseases. In fact, there is evidence that some well-known phenolic compounds, like chlorogenic acid (CGA, PubChem CID 1794427), the most bioavailable hydroxycinnamic acid among Brassica vegetables, and trans-resveratrol, display antioxidant, anti-inflammatory, and lipid metabolism-modulating properties, linking phenolic molecules to a potential beneficial effect on NAFLD[18,62].

Vegetable content and pharmacokinetics of ITC and polyphenols

The bioactive compounds of Brassicaceae vegetables, especially the GLS and phenolic compounds, are well-characterized as unstable molecules, due to influences of pH, temperature, and myrosinase-activated conditions (in this case, only GLS), triggering the degradation and metabolization pathways of these compounds[19]. Moreover, it has been previously reported that both storage and cooking processes modulate the abundance of GLS on vegetables, due to the freeze-thaw cycles and high temperature and cutting processes used in cooking practices[63,64]. Regarding the storage conditions, fresh vegetables (broccoli, brussel sprouts, cauliflower, and green cabbage) stored under 4-8º and -85ºC featured decreased levels of GLS (11-27% and 33%, respectively), whereas no significant difference was observed when stored under ambient conditions (12-22ºC). Similarly, cooking techniques like boiling, microwaving, and pressuring have been related to reducing the total phenolic content level on food (38%, 46%, and 53%, respectively)[65]. Indeed, heating processes (above 100ºC) have been previously described as independent modulators of GLS and indoles levels, by a heat-induced instability mechanism[66]. Likewise, phenolic compounds are also sensitive to thermal processes. Chamorro et al.[67] reported that long-term autoclave heating led to hydrolysis of antioxidant molecules, like catechin (70%), epicatechin (61%), procyanidin dimer B1 (75%), and procyanidin dimer B2 (73%). Of note, although the phenolic content profile was disturbed by the heating process, the antioxidant activity of grape seed extract and pomace was maintained. Additionally, post-shredding assessments show striking decreases of the total GLS levels (up to 75%) in Brassica vegetables, suggesting the activation of a myrosinase-dependent metabolization of these molecules results in unstable isothiocyanates[63]. Taken together, these findings suggest that cooking processes - especially heating, and cutting - and storage are pivotal to the profile determination of bioactive compounds in food, including Brassicaceae vegetables.

The liquid chromatography targeted identification of GLS content in Brassica vegetables showed that the profile and concentration of these molecules depend on both growth stages and crops, and glucobrassicins feature as the most commonly found molecules among these vegetables, although in lower quantities than the other compounds (Figure 2)[68]. Overall, broccoli and cabbage sprouts feature as the Brassica vegetable with the higher concentrations and diversity of GLS, compared to others (cauliflower, cabbage, kale, leaf mustard, pakchoi, and radish). In addition, broccoli and cabbage sprouts display a higher concentration of glucoerucin (123.7 and 34.9 µmol/g of dry weight, respectively) and progoitrin (28.5 and 33.8 µmol/g of dry weight, respectively). Regarding glucobrassicins, they are widely found in cauliflower and broccoli (1.98 and 1.05 µmol/g of dry weight, respectively) (Figure 2)[68]. However, the GLS might be turned into isothiocyanates, responsible for some of the bioactive properties of Brassica vegetables. Indeed, the isothiocyanates identification in Brassica vegetables (kale, cabbage, and broccoli) showed that allyl isothiocyanate (~0.33 mmol/g of dry weight) in cabbage, and 3-butenyl isothiocyanate, in both kale and broccoli, were the most abundant in these vegetables (~0.68 and ~1.22 mmol/g of dry weight, respectively) (Figure 2)[69]. Similarly, the identification of phenolic compounds showed that Brassica vegetables contain high levels of these molecules, as well as a wide diversity (almost 165 phenolic compounds), featuring flavonoids, anthocyanins, and hydroxycinnamic acids, mainly[70]. Martinez-Sanchez et al.[71] findings suggested that Brassicaceae species (watercress, mizuna, salad rocket, and wild rocket) are a source of phenolic compounds (~263, ~99, ~132, and ~100 mg/fresh weight of vegetable), especially flavonoid compounds, like glycosylated quercetin, isorhamnetin, and kaempferol-derivative molecules. Moreover, a wide spectrum of anthocyanins (23 compounds) was identified in red cabbage, in which cyanidin-3-diglucoside-derivative molecules were predominant [cyanidin 3-diglucoside-5-glucoside, cyanidin 3-(sinapoyl)diglucoside-5-glucoside, and cyanidin 3-(p-coumaroyl)diglucoside-5-glucoside] (Figure 2)[72]. Furthermore, hydroxycinnamic acids have been identified by liquid chromatography-mass spectrometry in Brassica vegetables (kale and cabbage), indicating 3-caffeoylquinic acid, 3-p-coumaroylquinic acid, sinapoyl glucoside, 4-caffeoylquinic, and 4-feruloylquinic as the most abundant molecules (Figure 2)[73]. Thus, these findings indicate that the high diversity and abundance of phenolic compounds and GLS presented above might be responsible for the antioxidant and anti-inflammatory properties of Brassica vegetables.

The elevated intake of GLS leads to the I3C synthesis, as a consequence of the myrosinase activity. Furthermore, under gastric acidic conditions, I3C is oligomerized into derivatives like DIM that exert bioactive effects[74]. In CD-1 mice, the determination of the peak concentration of plasmatic and hepatic levels of I3C, following an intragastric administration of oil-diluted I3C (250 mg/Kg of b.wt.), was observed 15 minutes after the administration (~4.1µg/mL and ~25 µg/g of tissue, respectively), while DIM peak concentration featured after 2 hours (~0.8 µg/ml and ~4.0 µg/g of tissue, respectively)[75]. In a radiolabeled monitoring of dietary I3C supplementation, DIM featured as the most abundant hepatic metabolite derivative from I3C, reaching a relative proportion of 22% of the total eluted radioactivity. Regarding the I3C absorption, it is suggested that the stomach and the lower gastrointestinal tract might be pivotal since there is also the detection of radioactivity traits in those tissues. However, the specific mechanism related to it remains imprecise[19,76]. DIM has become a molecule of great interest, due to its chemopreventive properties and high abundance after I3C metabolism[74]. The DIM oral administrations (250 mg/Kg of b.wt.) by gavage showed that in both formulations (crystalline or suspension solution), the liver

is the main site of deposition and metabolism of DIM formulations, similarly to dietary I3C-derivative DIM. Besides, the peak concentration in both liver and plasma occurs after 0.5-1.0 hours of the oral administration of DIM, reaching a peak concentration of 207 and 25.4 μg/mL, respectively, when administered the suspension of DIM, whereas reached 129 and 19.0 μg/mL, respectively, when administered a crystalline DIM-diluted solution[77].

Likewise, the CGA is a group of acyl-quinic acids extensively studied that exerts bioactive effects. This group of molecules comprises molecules like caffeoylquinic (CQA), feruloylquinic (FQA), and other kinds of acyl-quinic acids, which can be absorbed by the stomach and small intestine in a hydrolyzed or untransformed form, or under the activity of the microbiota-mediated metabolism[78]. Besides, it is suggested that CGA metabolites are hydrolyzed or microbiota-mediated converted in the small intestine and colon, respectively[79,80]. Indeed, male Wistar rats submitted to the dietary CGA supplementation (0.25% weight/weight) show increased plasmatic and levels of CGA after 1.5 and 3.0 hours, that received a gastric infusion (~12.4 mg of CGA) showed an increased absorption level of CGA (~16%) after 0.5 hours, concluding that the stomach is a CGA absorption site. In addition, it was observed high levels of CGA in the stomach and small intestine, while only traces of caffeic acid (~1.0% of total CGA) were found. On the other hand, a significant amount of caffeic acid was observed in the cecum (~15-32% of total CGA)[81]. Similarly, the flavonoids represent one of the largest groups of phenolic compounds, as well as the widely consumed in the worldwide population (eg.: quercetin, catechins, anthocyanins). Overall, flavonoids absorption occurs in the small and large intestines by different mechanisms. For instance, quercetin absorption was described by Graefe et al.[82]. They observed that the quercetin absorption occurs by a glucoside conjugation-dependent mechanism, confirming that free quercetin (or aglycone quercetin) is not effectively absorbed in the stomach, small intestine, and colon (under the microbiota activity), since only conjugated quercetin is observed in the plasma after oral intake, in agreement with previous findings[82,83]. The quercetin-4'-O-glucoside featured a quick absorption level, compared with peak plasmatic levels of 2.1±1.6 μg/mL, after ~0.7 hours, whereas its excretion occurs after 9-12 hours. Of note, only 3'-O-methyl quercetin metabolite was detectable after the phase I conjugation process preceding excretion, corresponding to 10% of quercetin-4'-O-glucoside concentration[82].

Recent in vivo and in vitro findings

The indoles have been targeted as potential therapeutic approaches, due to their antioxidant and anti-inflammatory properties. Indeed, I3C was previously evaluated in male C57BL/6J mice subjected to a HFD for 10 weeks[84]. Briefly, I3C-treated mice featured a reduction in HS profile, serum markers of dyslipidemia and hepatic damage (total cholesterol, alanine aminotransferase, and aspartate aminotransferase) (Table 1). Overall, diet-induced murine models elicit a translational burden resembling metabolic traits, like obesity and IR, by feeding mice a high-fat diet (HFD) or a high-fat-cholesterol diet (HFCD), along with great similarity to the transcriptomic profile of patients and NAFLD/NASH hallmarks (enhanced lipogenic and inflammatory activity)[85,86]. In fact, the diet-induced animal model of nonalcoholic fatty liver disease (DIAMOND), in which animals were fed with WD, a HFCD chow (42% of kcal derivative from fat and 0.1% wt/wt addition of cholesterol) and sugar-added water (23.1 and 18.9 g/L of fructose and glucose, respectively) resulted in liver changes that, resembled the transcriptomic profile of patients with the corresponding disease[86]. In vitro findings suggests that I3C (50 μmol/L, for 24 hours) modulates FA dynamics of lipid metabolism axis in HepG2 cells, inhibiting the FA synthesis and trafficking by down-regulation of SREBP-1c and FASN genes and apoB levels (Table 2)[87]. Likewise, in vivo findings suggests that I3C reduces both liver-related ER stress and lipogenesis-associated proteins levels, which are responsible for triggering the hepatic lipotoxic milieu and the inflammatory response, as well as inducing the FA de novo synthesis (Figure 3)[88]. In another study[89], the I3C oral treatment prevented obesity development in male C57BL/6N mice submitted to a HFD protocol, by alleviating the visceral fat pad weight gain, suggesting an antiobesity activity (Table 1). In agreement, I3C-treated mice submitted to a DIO protocol featured normal levels of serum glucose and glucose tolerance, as well as reduced the number of F4/80+ cells in the epididymal AT, known as responsible for inducing the systemic low-grade inflammation, contributing to NAFLD emergence[90] (Table 1) (Figure 3). Of note, I3C has also been suggested as a modulator of the redox balance dynamics, which are disrupted during NAFLD progression, by attenuating the levels of hepatic 4-hydroxynonenal (4-HNE) and malondialdehyde, both indicators of lipid peroxidation processes, and restoring the glutathione (GSH) levels, as well as may act directly by scavenging radicals and oxidant molecules[84,91]. Similarly, I3C-treated HepG2 cells displayed increased nuclear levels of phosphorylated Nrf2, a master regulator of enzymes associated with the antioxidant defense in hepatocytes (Table 2) (Figure 3). As expected, I3C increased the protein levels of catalase (CAT), superoxide dismutase (SOD), glutathione reductase (GR), and glutathione peroxidase (GPx), confirming that the above-cited bioactive compound exerts an antioxidant effect with the potential to attenuate NAFLD progression (Table 2) (Figure 3)[92].

Recently, macrophages were described as pivotal drivers of the pro-inflammatory milieu and oxidative stress conditions, in which NAFLD progression to NASH occurs, suggesting that modulating macrophages ROS/RNS and cytokines synthesis might be an effective approach against NASH[93]. The I3C treatment reduced in a dose-dependent-manner the synthesis of pro-inflammatory cytokines IL-1β and IL-6 by LPS-activated

RAW264.7 cells, in an IRF3-IFN-β-STAT1/3 underlying mechanism[94] (Table 2). Thus, I3C displays bioactive properties that suppress the pro-inflammatory activity of macrophages modifying the microenvironment in which NASH is susceptible to emerge. Besides, it has been described that I3C is a ligand of aryl hydrocarbon receptor (AhR), modulating the inflammatory milieu in the gastrointestinal tract in a Treg-dependent manner and microbiota profile[95,96] (Table 1) (Figure 3). Indeed, in a colitis-induced model, I3C was responsible for preventing colitis-associated microbial dysbiosis and increasing the levels of Roseburia gram-positive bacteria, known as producers of butyrate, a SCFA linked to intestinal integrity reestablishment (Table 1) (Figure 3)[97,98]. Thus, it is suggested that I3C might be a potential strategy by targeting multiples underlying mechanisms associated with NAFLD/NASH emergence, as oxidative stress and inflammatory hepatic milieu, lipid and glucose metabolism, obesity-associated stress, intestinal integrity, and microbiota composition (Figure 3).

DIM, the major I3C-derivative molecule as previously discussed, has become a compound of high interest due to its bioactive properties that might alleviate NAFLD progression19,75. Indeed, female C57BL/6 mice treated with DIM (20.0 or 40.0 mg/kg of b.wt.), in especial the higher dose, attenuated the methionine-choline-deficient (MCD) diet-induced steatosis, hepatic damage (reduced the levels of serum transaminases), and CD4+ cells infiltration by modulating the Treg/Th17 cells ratio (increasing the number of Treg+ cells and reducing the number of Th17+ cells) (Table 1) (Figure 3)[99]. Of note, Th17+ cells have been previously described as potential drivers of NASH in several experimental models, by modulating the hepatic pro-inflammatory microenvironment and further activation of HSC, leading to fibrosis/cirrhosis[100]. Likewise, DIM is suggested as a modulator of macrophages activation, by attenuating LPS-induced RAW264.7 cells and inhibiting tumor necrosis factor-α (TNF-α), IL-6, and IL1β, by inhibiting the activation of JNK/AP-1-NF-κB pathway[101]. Thus, DIM modulates the Treg/Th17 ratio and further synthesis of both IL-17 and IL-21, a pivotal axis for NASH progression (Table 1)[99]. Moreover, there is evidence that DIM modulates IR, by reducing the plasma glucose and insulin levels, in male mice fed a HFD, along with attenuating the hepatic levels of IR-related oxidative stress markers, like thiobarbituric acid reactive substances (TBARS) and lipid hydroperoxides, whereas enhancing the activity of antioxidant-related enzymes, in especial SOD, GPx, and CAT (Figure 3). Hence, it is suggested that DIM may modulate the oxidative stress state by enhancing attenuating the oxidative stress and enhancing the activity of the antioxidant cell line defense[102]. Indeed, it has been reported that DIM mitigates the noxious effects of CCl4-induced acute liver injury, by enhancing the hepatic protein levels of Nrf2, associated with the attenuation of the oxidative stress (Table 1) (Figure 3)[103]. Regarding intestinal barrier integrity, it has been shown that DIM ameliorates intestinal selective permeability, by increasing the protein levels of ZO-1 and occludin in Caco-2 cells, when exposed to IL-1β, mimicking the pro-inflammatory milieu in which HFD-induced microbiota shift occurs (Figure 3)[104].

In addition, some studies reported beneficial effects of glucobrassicins-derivative molecules, like phenethyl isothiocyanate (PEITC, PubChem CID 16741) and benzyl isothiocyanate (BITC, PubChem 2346), on well-known NAFLD hallmarks[105,106]. Regarding PEITC, it has been described as a potential activity on NAFLD-related hallmarks, especially lipogenic-, glucose-, and AT-related axis. The PEITC-treated mice, mainly the higher dose (75 mg/Kg of b.wt.) reduced the epididymal fat pad weight and restored the normal concentration of serum total cholesterol, TG, low-density lipoprotein cholesterol (LDL), glucose, and insulin, whereas the homeostasis assessment-estimated IR (HOMA-IR) index was also decreased by the PEITC treatment (Figure 3). Along with it, PEITC restored the lipid metabolism dynamics, by reducing the protein levels of CD36 and increasing ATP binding cassette subfamily A member 1 (ABCA1) and the synthesis and efflux of the high-density lipoprotein cholesterol (HDL) instead of LDL, LXR-α, and peroxisome proliferator-activated receptor γ (PPARγ) levels. Finally, PEITC modulated the hepatic inflammatory milieu by reducing the mRNA and protein levels of NF-κB (Table 1) (Figure 3)[105]. Similar to PEITC, BITC (chow added 0.05 or 0.1% wt./wt.) features a dose-dependent antiobesity effect, suppressing the body weight (b.wt.) and fat weight pad gain in male mice fed with HFD (Table 1) (Figure 3). Moreover, BITC was able to mitigate the HFD-induced IR, as well as restore plasma markers associated with NAFLD (total cholesterol, TG, and NEFA), suggesting a potential underlying mechanism linking BITC to glucose and lipid metabolism. Indeed, BITC reduced the protein levels of SREBP-1c, FAS, LXRα, and ACC in both the liver and AT (Table 1) (Figure 3)[106]. Therefore, both PEITC and BITC features as reliable strategies to contain the hepatic and AT inflammatory milieu, as well as lipid-glucose axis, usually impaired during NAFLD progression to NASH. However, no information regarding their effects on gut integrity and microbiota was found (Figure 3).

Beneficial effects against NAFLD/NASH are also attributable to the other bioactive molecules, like phenolic compounds, widely found in vegetables and fruits60. In an obese-induced model of mice, CGA displayed a beneficial effect on lipid-related metabolism markers, restoring the plasma levels of TG, total cholesterol, and adiponectin levels, whereas suppressed the lipid-synthesis pathways and enhanced the β-oxidation activity (Figure 4)[107]. Additionally, male ICR CGA-treated mice CGA displayed reduced epididymal and perirenal fat weights, as well as reduced adipocyte size, which is usually hypertrophic in obesity-induced models and patients, due to the redox dynamics disturbance and oxidative stress (Table 1)[107–110]. In agreement, Ma et al.[111] reported that CGA alleviates oil-red-O staining area and markers of inflammatory processes of obese

mice, suggesting that hepatic steatosis is attenuated by the interplay between lipid metabolism and inflammation. Indeed, CGA reduced the hepatic TG levels, as well as Cd36, Fabp4, and Mgat1 mRNA levels, which encode protein receptors that promote the FA influx. Regarding inflammation, CGA reduced the mRNA levels of Cd68, encoding CD68, a marker of activated hepatic macrophages exerting phagocytic activity (Table 1) (Figure 4)[111]. In vitro assays also confirmed that GCA exerts an anti-fibrotic activity, modulating the HSC. Taken together, it is suggested that CGA exerts an anti-obesity effect, by modulating the oxidative stress-lipid metabolism axis and microbiota (Figure 4). Likewise, the oral administration of CGA modulates the HFD-induced microbiota shift. Although the HFD protocol increases the Escherichia coli and Enterococcus and reduced Bifidobacterium bacteria abundance, CGA displayed the opposite effect, reestablishing the normal abundance of these bacteria, besides restoring the expression of enterocyte ZO-1 and occludin (Figure 4). The CGA also reduced the protein levels of TNF-α, p-NF-κB, and toll-like receptor 4 (TLR4) (Table 1) (Figure 4)[112,113]. Thus, it is suggested that CGA might act in the gut reestablishing the intestinal integrity and, further, attenuating systemic endotoxemia and NF-κB-TLR4 pathway, usually impaired in patients with NASH (Figure 4).

Anthocyanins are a large spectrum of flavonoids, responsible for the color of foods, that can be found in plenty of vegetables and fruits of daily basis consumption by the population. Regarding their structure, anthocyanins are heterosides consisting of an aglycone or anthocyanidin derived from 2-phenyl-benzopyrylium skeleton diversely hydroxylated or methoxylated, that is linked to sugar moieties that can be further acylated. Although there are several classes of anthocyanins, the most commonly found are cyanidin, delphinidin, pelargonidin, malvidin, and petunidin[114]. Recently, they have been the focus of studies due to their bioactive properties that can be a potential strategy to alleviate NAFLD, as well as cyanidin-derived glucosides, which have been widely found in Brassica vegetables[62,115,116]. Regarding in vitro assays, it has been reported that both delphinidin and cyanidin-derivative molecules modulate the oxidative stress axis by upregulating the Nrf2 pathway (Figure 4)[117,118]. Delphinidin-treated (10.0, 20.0, and 40.0 µmol/L, for 24 hours) HepG2 cells showed a reduction in the H2O2-induced oxidative stress by modulating a Nrf2-dependent mechanism, similarly to CGA findings, suggesting that isolated delphinidin might be a reliable strategy against NAFLD (Table 2)[117,119]. Likewise, cyanidin-3-glucoside features as the major cyanidin-derivative compound, and it is suggested to play a similar role to delphinidin, modulating the oxidative stress axis on both in vitro and in vivo models[118]. Cyanidin-3-glucoside-pre-treated HepG2 cells displayed reduced H2O2-induced apoptosis, associated with a lower protein level of both cleaved caspase-3 and Bax, as well as increasing Bcl-2 protein levels, suggesting that the anthocyanins modulate the oxidative-stress-induced death of hepatocytes (Table 2) (Figure 4). Similarly, male C57 mice submitted to a CCl4-induced acute liver injury model featured reduced apoptosis of hepatocytes when treated with cyanidin-3-glucoside, by upregulating the Nrf2-related antioxidant enzymes SOD and GPx, whereas reduced the MDA levels f, a marker of oxidative stress[118]. Likewise, cyanidin-3-glucoside was able to modulate the AT metabolism, inhibiting the IR of db/db knockout male mice fed with HFD. Additionally, cyanidin-3-glucoside reduced the pro-inflammatory state of the AT, reducing the adipocytes death ratio and AT macrophages infiltration (F4/80+ cells), as well as inhibiting Tnfa, Il6, and Mcp-1 expression, in a JNK-dependent mechanism (Figure 4)[120]. Thus, anthocyanins provide a potential reliable strategy on NAFLD, by modulating both redox and AT inflammation dynamics, targeting the Nrf2 and JNK pathway, increasing the antioxidant defense, and reducing the AT-associated inflammation, further alleviating the disease progression (Figure 4).

Conclusions

Several preclinical evidence suggests that ITC and/or phenolic compounds are widely consumed among the worldwide population and commonly found in Brassicaceae family vegetables, prospecting as a reliable strategy that counters the well-established hallmarks of NAFLD (hepatic steatosis and inflammation, IR, dyslipidemia, systemic low-grade inflammation, impaired intestinal barrier integrity, and microbiota dysbiosis), especially the lipid-inflammation-redox-microbiota axis, and the accepted natural history of the disease ("Two hits" and "Multiple hits" theories). Although still necessary to unravel molecular mechanisms related to the protective effects of these bioactive compounds on NAFLD/NASH in vivo and in vitro models (Figures 3 and 4), we suggest that the ITC and/or polyphenol might be a potential preclinical/clinical strategy against this chronic liver disease, by modulating the gut-liver-adipose axis. Our narrative review elicited that ITC and phenolic compounds, when individually administered in preclinical studies, modulate common molecular targets directly implicated in lipid-inflammation-redox-microbiota axis (Tables 1 and 2). Therefore, it is still unknown whether the beneficial effects of Brassica vegetable-based diets in humans (as MD) may be attributed to a specific class or to the combination of different classes of bioactive compounds found in these plants. The present work may inspire future preclinical and clinical investigations.

Author Contributions

Conceptualization: G.P.B and G.R.R.; writing - original draft preparation: G.P.B.; writing - review & editing: G.P.B., B.C., D.R.C., L.F.B. and G.R.R. All authors have read and agreed to the published version of the manuscript.

Conflicts of interest

The authors declare no conflict of interest.

Acknowledgements

This review paper was supported by the fellowship from São Paulo Research Foundation (FAPESP, Brazil; Grant #2020/01944-6) and Coordination of Superior Level Staff Improvement (CAPES, Brazil; Grant #88887.481152/2020-00) for G.P.B.

References

1 Z. M. Younossi, A. B. Koenig, D. Abdelatif, Y. Fazel, L. Henry and M. Wymer, Hepatology, 2016, 64, 73–84.
2 R. J. Wong, M. Aguilar, R. Cheung, R. B. Perumpail, S. A. Harrison, Z. M. Younossi and A. Ahmed, Gastroenterology, 2015, 148, 547–555.
3 Z. M. Younossi, M. Stepanova, M. Afendy, Y. Fang, Y. Younossi, H. Mir and M. Srishord, Clin. Gastroenterol. Hepatol., 2011, 9, 524-530.e1.
4 J. M. Paik, P. Golabi, Y. Younossi, A. Mishra and Z. M. Younossi, Hepatology, 2020, 72, 1605–1616.
5 C. Estes, Q. M. Anstee, M. T. Arias-Loste, H. Bantel, S. Bellentani, J. Caballeria, M. Colombo, A. Craxi, J. Crespo, C. P. Day, Y. Eguchi, A. Geier, L. A. Kondili, D. C. Kroy, J. V. Lazarus, R. Loomba, M. P. Manns, G. Marchesini, A. Nakajima, F. Negro, S. Petta, V. Ratziu, M. Romero-Gomez, A. Sanyal, J. M. Schattenberg, F. Tacke, J. Tanaka, C. Trautwein, L. Wei, S. Zeuzem and H. Razavi, J. Hepatol., 2018, 69, 896–904.
6 M. Hamaguchi, T. Kojima, N. Takeda, T. Nakagawa, H. Taniguchi, K. Fujii, T. Omatsu, T. Nakajima, H. Sarui, M. Shimazaki, T. Kato, J. Okuda and K. Ida, Ann. Intern. Med., 2005, 143, 722.
7 E. Sathiaraj, M. Chutke, M. Y. Reddy, N. Pratap, P. N. Rao, D. N. Reddy and M. Raghunath, Eur. J. Clin. Nutr., 2011, 65, 533–537.
8 S. Ryu, Y. Chang, H. Jung, K. E. Yun, M. Kwon, Y. Choi, C. Kim, J. Cho, B. Suh, Y. K. Cho, E. C. Chung, H. Shin and Y. S. Kim, J. Hepatol., 2015, 63, 1229–1237.
9 B. M. Popkin and P. Gordon-Larsen, Int. J. Obes., 2004, 28, S2–S9.
10 Centers for Disease Control, 2018 State Indicator Report On Fruits And Vegetables, 2018.
11 U.S. Department of Agriculture, Eat Healthy: Vegetables - My plate, https://www.myplate.gov/eat-healthy/vegetables.
12 1Z. M. Younossi, D. Blissett, R. Blissett, L. Henry, M. Stepanova, Y. Younossi, A. Racila, S. Hunt and R. Beckerman, Hepatology, 2016, 64, 1577–1586.
13 L. Schwingshackl, B. Missbach, J. König and G. Hoffmann, Public Health Nutr., 2015, 18, 1292–1299.
14 M. C. Ryan, C. Itsiopoulos, T. Thodis, G. Ward, N. Trost, S. Hofferberth, K. O. Dea, P. V Desmond, N. A. Johnson and A. M. Wilson, J. Hepatol., 2013, 59, 138–143.
15 L. Schwingshackl, C. Schwedhelm, C. Galbete and G. Hoffmann, Nutrients, 2017, 1–24.
16 F. Turati, D. Trichopoulos, J. Polesel, F. Bravi, M. Rossi, R. Talamini, S. Franceschi, M. Montella, A. Trichopoulou, C. La Vecchia and P. Lagiou, J. Hepatol., 2014, 60, 606–611.
17 M. Suárez, N. Boqué, J. del Bas, J. Mayneris-Perxachs, L. Arola and A. Caimari, Nutrients, 2017, 9, 1052.
18 J. W. Fahey, A. T. Zalcmann and P. Talalay, Phytochemistry.
19 M. Esteve, Front. Nutr., 2020, 7, 1–22.
20 D. E. Kleiner, E. M. Brunt, M. Van Natta, C. Behling, M. J. Contos, O. W. Cummings, L. D. Ferrell, Y. Liu, M. S. Torbenson, A. Unalp-arida, M. Yeh and A. J. Mccullough, Hepatology, 2005, 41, 1313–1321.
21 F. Marra, A. Gastaldelli, G. Svegliati Baroni, G. Tell and C. Tiribelli, Trends Mol. Med., 2008, 14, 72–81.
22 International Agency for Research on Cancer, IARC Monogr. Eval. Carcinog. Risks Chem. Man., 2012, 10F, 1–628.
23 E. Buzzetti, M. Pinzani and E. A. Tsochatzis, Metabolism, 2016, 65, 1038–1048.
24 F. Negro, Liver Int., 2020, 40, 72–76.
25 O. V Makarova-rusher, S. F. Altekruse, T. S. Mcneel, S. Ulahannan, A. G. Duffy, B. I. Graubard, T. F. Greten and K. A. Mcglynn, Cancer, 2016, 1757–1765.
26 Z. M. Younossi, R. Loomba, M. E. Rinella, E. Bugianesi, G. Marchesini, B. A. Neuschwander-Tetri, L. Serfaty, F. Negro, S. H. Caldwell, V. Ratziu, K. E. Coery, S. L. Friedman, M. F. Abdelmalek, S. A. Harrison, A. J. Sanyal, J. E. Lavine, P. Mathurin, M. R. Charlton, N. p. Chalasani, Q. M. Anstee, K. V. Kowdley, J. Geroge, Z. D. Goodman and K. Lindor, Hepatology, 2018, 68, 361–371.
27 V. S. Malik, B. M. Popkin, G. A. Bray, J. P. Després, W. C. Willett and F. B. Hu, Diabetes Care, 2010, 33, 2477–2483.
28 V. S. Malik, A. Pan, W. C. Willett and F. B. Hu, Am. J. Clin. Nutr., 2013, 98, 1084–1102.
29 H. Chen, J. Wang, Z. Li, C. W. K. Lam, Y. Xiao, Q. Wu and W. Zhang, Int. J. Environ. Res. Public Health, 2019, 16, 2192.
30 J. a Welsh, A. Sharma, J. L. Abramson, C. Gillespie and M. B. Vos, J. Am. Med. Assoc., 2010, 303, 1490–1497.
31 R. K. Johnson, L. J. Appel, M. Brands, B. V. Howard, M. Lefevre, R. H. Lustig, F. Sacks, L. M. Steffen and J. Wylie-Rosett, Circulation, 2009, 120, 1011–1020.
32 C. L. Edwardson, T. Gorely, M. J. Davies, L. J. Gray, K. Khunti, E. G. Wilmot, T. Yates and S. J. H. Biddle, PLoS One, 2012, 7, 3–7.
33 L. A. Orci, K. Gariani, G. Oldani, V. Delaune, P. Morel and C. Toso, Clin. Gastroenterol. Hepatol., 2016, 14, 1398–1411.
34 D. P. Y. Koonen, R. L. Jacobs, M. Febbraio, M. E. Young, C. L. M. Soltys, H. Ong, D. E. Vance and J. R. B. Dyck, Diabetes, 2007, 56, 2863–2871.
35 Y. Qiu, S. Liu, H. T. Chen, C. H. Yu, X. D. Teng, H. T. Yao and G. Q. Xu, Hepatobiliary Pancreat. Dis. Int., 2013, 12, 630–636.
36 K. L. Donnelly, C. I. Smith, S. J. Schwarzenberg, J. Jessurun, M. D. Boldt and E. J. Parks, J. Clin. Invest., 2005, 115, 1343–1351.
37 C. Saponaro, M. Gaggini, F. Carli and A. Gastaldelli, Nutrients, 2015, 9453–9474.
38 H. Shimano, N. Yahagi, M. Amemiya-Kudo, A. H. Hasty, J. Osuga, Y. Tamura, F. Shionoiri, Y. Iizuka, K. Ohashi, K. Harada, T. Gotoda, S. Ishibashi and N. Yamada, J. Biol. Chem., 1999, 274, 35832–35839.
39 K. Iizuka, R. K. Bruick, G. Liang, J. D. Horton and K. Uyeda, Proc. Natl. Acad. Sci., 2004, 101, 7281–7286.
40 K. Iizuka, K. Takao and D. Yabe, Front. Endocrinol. (Lausanne)., 2020, 11, 1–10.
41 M. R. Jain, S. R. Giri, B. Bhoi, C. Trivedi, A. Rath, R. Rathod, R. Ranvir, S. Kadam, H. Patel, P. Swain, S. S. Roy, N. Das, E. Karmakar, W. Wahli and P. R. Patel, Liver Int., 2018, 38, 1084–1094.
42 N. E. Sunny, F. Bril and K. Cusi, Trends Endocrinol. Metab., 2017, 28, 250–260.
43 M. Pawlak, P. Lefebvre and B. Staels, J. Hepatol., 2015, 62, 720–733.
44 S. Kersten and R. Stienstra, Biochimie, 2017, 136, 75–84.
45 M. J. Armstrong, J. M. Hazlehurst, D. Hull, K. Guo, S. Borrows, J. Yu, S. C. Gough, P. N. Newsome and J. W. Tomlinson, Diabetes, Obes. Metab., 2014, 16, 651–660.

46 H. Kanda, K. Egashira, M. Kasuga, H. Kanda, S. Tateya, Y. Tamori, K. Kotani, K. Hiasa and R. Kitazawa, J. Clin. Invest., 2006, 116, 1494–1505.
47 A. Asghar and N. Sheikh, Cell. Immunol., 2017, 315, 18–26.
48 S. P. Weisberg, R. L. Leibel, W. Anthony, F. Jr, S. P. Weisberg, D. Mccann, M. Desai, M. Rosenbaum, R. L. Leibel and A. W. Ferrante, J. Clin. Ivestigation, 2003, 112, 1796–1808.
49 N. Kamei, K. Tobe, R. Suzuki, M. Ohsugi, T. Watanabe, N. Kubota, N. Ohtsuka-Kowatari, K. Kumagai, K. Sakamoto, M. Kobayashi, T. Yamauchi, K. Ueki, Y. Oishi, S. Nishimura, I. Manabe, H. Hashimoto, Y. Ohnishi, H. Ogata, K. Tokuyama, M. Tsunoda, T. Ide, K. Murakami, R. Nagai and T. Kadowaki, J. Biol. Chem., 2006, 281, 26602–26614.
50 A. A. Kolodziejczyk, D. Zheng, O. Shibolet and E. Elinav, EMBO Mol. Med., 2019, 11, 1–13.
51 T. Le Roy, M. Llopis, P. Lepage, A. Bruneau, S. Rabot, C. Bevilacqua, P. Martin, C. Philippe, F. Walker, A. Bado, G. Perlemuter, A.-M. Cassard-Doulcier and P. Gérard, Gut, 2013, 62, 1787–1794.
52 A. A. Kolodziejczyk, D. Zheng, O. Shibolet and E. Elinav, EMBO Mol. Med., 2018, 11, 1–13.
53 L. Xue, J. He, N. Gao, X. Lu, M. Li, X. Wu, Z. Liu, Y. Jin, J. Liu, J. Xu and Y. Geng, Sci. Rep., 2017, 7, 1–13.
54 P. D. Cani, R. Bibiloni, C. Knauf, A. M. Neyrinck and N. M. Delzenne, Diabetes, 2008, 57, 1470–81.
55 A. T. Virtue, S. J. McCright, J. M. Wright, M. T. Jimenez, W. K. Mowel, J. J. Kotzin, L. Joannas, M. G. Basavappa, S. P. Spencer, M. L. Clark, S. H. Eisennagel, A. Williams, M. Levy, S. Manne, S. E. Henrickson, E. John Wherry, C. A. Thaiss, E. Elinav and J. Henao-Mejia, Sci. Transl. Med., , DOI:10.1126/scitranslmed.aav1892.
56 Food and Agriculture Organization of the United Nations, FAOStat, https://www.fao.org/faostat/en/#compare.
57 International Agency For Research On Cancer, IARC Handbook of Cancer Prevention: Cruciferous Vegetables, Isothiocyanates and Indoles, International Agency for Research on Cancer, Lyon, France, 2004.
58 C. A. Thomson, T. R. Newton, E. J. Graver, K. A. Jackson, P. M. Reid, V. L. Hartz, E. C. Cussler and I. A. Hakim, J. Am. Diet. Assoc., 2007, 107, 631–643.
59 A. Kaulmann, M.-C. Jonville, Y.-J. Schneider, L. Hoffmann and T. Bohn, Food Chem., 2014, 155, 240–250.
60 H. Zhang and R. Tsao, Curr. Opin. Food Sci., 2016, 8, 33–42.
61 K. Herrmann and L. Weaver, Annu. Rev. Plant Phisiology Plant Mol. Biol., 1999, 50, 473–503.
62 M. E. Cartea, M. Francisco, P. Soengas and P. Velasco, Molecules, 2010, 16, 251–280.
63 L. Song and P. J. Thornalley, Food Chem. Toxicol., 2007, 45, 216–224.
64 N. Pellegrini, E. Chiavaro, C. Gardana, T. Mazzeo, D. Contino, M. Gallo, P. Riso, V. Fogliano and M. Porrini, J. Agric. Food Chem., 2010, 58, 4310–4321.
65 D. Murador, A. R. Braga, D. Da Cunha and V. De Rosso, Crit. Rev. Food Sci. Nutr., 2018, 58, 169–177.
66 K. Oerlemans, D. M. Barrett, C. B. Suades, R. Verkerk and M. Dekker, Food Chem., 2006, 95, 19–29.
67 S. Chamorro, I. Goñi, A. Viveros, D. Hervert-Hernández and A. Brenes, Eur. Food Res. Technol., 2012, 234, 147–155.
68 S. Bhandari, J. Jo and J. Lee, Molecules, 2015, 20, 15827–15841.
69 N. Wang, L. Shen, S. Qiu, X. Wang, K. Wang, J. Hao and M. Xu, Eur. Food Res. Technol., 2010, 231, 951–958.
70 J. Sun, Z. Xiao, L. Lin, G. E. Lester, Q. Wang, J. M. Harnly and P. Chen, J. Agric. Food Chem., 2013, 61, 10960–10970.
71 A. Martínez-Sánchez, A. Gil-Izquierdo, M. I. Gil and F. Ferreres, J. Agric. Food Chem., 2008, 56, 2330–2340.
72 X. Wu and R. L. Prior, J. Agric. Food Chem., 2005, 53, 3101–3113.
73 P. Velasco, M. Francisco, D. A. Moreno, F. Ferreres, C. García-Viguera and M. E. Cartea, Phytochem. Anal., 2011, 22, 144–152.
74 S. Wang, L. Cheng, Y. Liu, J. Wang and W. Jiang, Curr. Drug Metab., 2016, 17, 401–409.
75 M. J. Anderton, M. M. Manson, R. D. Verschoyle, A. Gescher, J. H. Lamb, P. B. Farmer, W. P. Steward and M. L. Williams, Clin. Cancer Res., 2004, 10, 5233–5241.
76 R. H. Dashwood, L. Uyetake, A. T. Fong, J. D. Hendricks and G. S. Bailey, Food Chem. Toxicol., 1989, 27, 385–392.
77 M. J. Anderton, M. M. Manson, R. Verschoyle, A. Gescher, W. P. Steward, M. L. Williams and D. E. Mager, Drug Metab. Dispos., 2004, 32, 632–638.
78 M. N. Clifford, A. Kerimi and G. Williamson, Compr. Rev. Food Sci. Food Saf., 2020, 19, 1299–1352.
79 A. Stalmach, W. Mullen, D. Barron, K. Uchida, T. Yokota, C. Cavin, H. Steiling, G. Williamson and A. Crozier, Drug Metab. Dispos., 2009, 37, 1749–1758.
80 M. Renouf, P. A. Guy, C. Marmet, A. L. Fraering, K. Longet, J. Moulin, M. Enslen, D. Barron, F. Dionisi, C. Cavin, G. Williamson and H. Steiling, Mol. Nutr. Food Res., 2010, 54, 760–766.
81 S. Lafay, A. Gil-Izquierdo, C. Manach, C. Morand, C. Besson and A. Scalbert, J. Nutr., 2006, 136, 1192–1197.
82 E. U. Graefe, J. Wittig, S. Mueller, A.-K. Riethling, B. Uehleke, B. Drewelow, H. Pforte, G. Jacobasch, H. Derendorf and M. Veit, J. Clin. Pharmacol., 2001, 41, 492–499.
83 P. C. H. Hollman, J. M. van Trijp, M. N. C. P. Buysman, M. S. v.d. Gaag, M. J. B. Mengelers, J. H. . de Vries and M. B. Katan, FEBS Lett., 1997, 418, 152–156.
84 Y. Choi, M. A. Abdelmegeed and B.-J. Song, J. Nutr. Biochem., 2018, 55, 12–25.
85 J. Willebrords, I. Veloso, A. Pereira, M. Maes, S. Crespo, I. Colle, B. Van Den Bossche, T. Cristina, D. Silva, C. Pinto, M. Souza, D. Oliveira, W. Andraus, V. Avancini, B. Cogliati and M. Vinken, Prog. Lipid Res., 2015, 59, 106–125.
86 A. Asgharpour, S. C. Cazanave, T. Pacana, M. Seneshaw, R. Vincent, B. A. Banini, D. P. Kumar, K. Daita, H. Min, F. Mirshahi, P. Bedossa, X. Sun, Y. Hoshida, S. V Koduru, D. Contaifer, U. O. Warncke, D. S. Wijesinghe and A. J. Sanyal, J. Hepatol., 2016, 65, 579–588.
87 G. K. Maiyoh, J. E. Kuh, A. Casaschi and A. G. Theriault, J. Nutr. Biochem. Genet. Mech., 2007, 100, 2185–2189.
88 Y. Choi, Y. Yanagawa, S. Kim and T. Park, J. Nutr. Biochem., 2013, 24, 1393–1400.
89 Y. Choi, Y. Kim, S. Park, K. W. Lee and T. Park, J. Nutr. Biochem., 2012, 23, 1732–1739.
90 H.-P. Chang, M.-L. Wang, M.-H. Chan, Y.-S. Chiu and Y.-H. Chen, Nutrition, 2011, 27, 463–470.
91 M. B. Arnao, J. Sanchez-Bravo and M. Acosta, Biochem. Mol. Biol. Int., 1996, 39, 1125–1134.
92 V. Krajka-Kuźniak, J. Paluszczak, H. Szaefer and W. Baer-Dubowska, J. Physiol. Biochem., 2015, 71, 227–238.
93 T. A. Wynn, D. Ph, L. Barron and D. Ph, Semin. Liver Dis., 2011, 30, 245–257.
94 J. Jiang, T. B. Kang, D. W. Shim, N. H. Oh, T. J. Kim and K. H. Lee, Food Chem. Toxicol., 2013, 57, 256–261.
95 E. A. Stevens, J. D. Mezrich and C. A. Bradfield, Immunology, 2009, 127, 299–311.
96 O. Schanz, R. Chijiiwa, S. C. Cengiz, Y. Majlesain, H. Weighardt, H. Takeyama and I. Förster, Int. J. Mol. Sci., 2020, 21, 3189.
97 P. B. Busbee, L. Menzel, H. Alrafas, N. Dopkins, W. Becker, K. Miranda, C. Tang, S. Chatterjee, U. Singh, M. Nagarkatti and P. S. Nagarkatti, JCI Insight, 2020, 5, 1–18.
98 K. Bach Knudsen, H. Lærke, M. Hedemann, T. Nielsen, A. Ingerslev, D. Gundelund Nielsen, P. Theil, S. Purup, S. Hald, A.

Schioldan, M. Marco, S. Gregersen and K. Hermansen, Nutrients, 2018, 10, 1499.
99 Y. Liu, W. She, F. Wang, J. Li, J. Wang and W. Jiang, Int. Immunopharmacol., 2014, 23, 489–498.
100 C. M. Chackelevicius, S. E. Gambaro, C. Tiribelli and N. Rosso, World J. Gastroenterol., 2016, 22, 9096.
101 1H. J. Cho, M. R. Seon, Y. M. Lee, J. Kim, J.-K. Kim, S. G. Kim and J. H. Y. Park, J. Nutr., 2008, 138, 17–23.
102 P. Jayakumar, K. V. Pugalendi and M. Sankaran, J. Physiol. Biochem., 2014, 70, 525–534.
103 S. Munakarmi, L. Chand, H. B. Shin, K. Y. Jang and Y. J. Jeong, Int. J. Mol. Sci., 2020, 21, 2048.
104 J. Y. Kim, T. A. N. Le, S. Y. Lee, D.-G. Song, S.-C. Hong, K. H. Cha, J. W. Lee, C.-H. Pan and K. Kang, J. Agric. Food Chem., 2019, 67, 9277–9285.
105 M.-H. Gwon, Y.-S. Im, A.-R. Seo, K. Y. Kim, H.-R. Moon and J.-M. Yun, Nutrients, 2020, 12, 3657.
106 W.-T. Chuang, Y.-T. Liu, C.-S. Huang, C.-W. Lo, H.-T. Yao, H.-W. Chen and C.-K. Lii, J. Agric. Food Chem., 2019, 67, 7136–7146.
107 A. Cho, S. Jeon, M. Kim, J. Yeo, K. Seo, M. Choi and M. Lee, Food Chem. Toxicol., 2010, 48, 937–943.
108 Z. Wang, K. L. Lam, J. Hu, S. Ge, A. Zhou, B. Zheng, S. Zeng and S. Lin, Food Sci. Nutr., 2019, 7, 579–588.
109 A. Hammarstedt, S. Gogg, S. Hedjazifar, A. Nerstedt and U. Smith, Physiol. Rev., 2018, 98, 1911–1941.
110 S. K. Shin, H. W. Cho, S. E. Song, S. S. Im, J. H. Bae and D. K. Song, Redox Biol., 2020, 37, 101749.
111 Y. Ma, M. Gao and D. Liu, Pharm. Res., 2015, 32, 1200–1209.
112 A. Shi, T. Li, Y. Zheng, Y. Song, H. Wang, N. Wang, L. Dong and H. Shi, Front. Pharmacol., 2021, 12, 1–9.
113 A. A. Shanab, P. Scully, O. Crosbie, M. Buckley, L. O'Mahony, F. Shanahan, S. Gazareen, E. Murphy and E. M. M. Quigley, Dig. Dis. Sci., 2011, 56, 1524–1534.
114 L. Valenti, P. Riso, A. Mazzocchi, M. Porrini, S. Fargion and C. Agostoni, Oxid. Med. Cell. Longev., 2013, 2013, 1–8.
115 D. A. Moreno, S. Pérez-Balibrea, F. Ferreres, Á. Gil-Izquierdo and C. García-Viguera, Food Chem., 2010, 123, 358–363.
116 R. Lo Scalzo, A. Genna, F. Branca, M. Chedin and H. Chassaigne, Food Chem., 2008, 107, 136–144.
117 J. Xu, Y. Zhang, G. Ren, R. Yang, J. Chen, X. Xiang, H. Qin and J. Chen, Oxid. Med. Cell. Longev., 2020, 2020, 1–12.
118 L. Yu, S. Zhang, X. Zhao, H. Ni, X. Song, W. Wang, L. Yao, X. Zhao and Y. Fu, J. Funct. Foods, 2020, 73, 104148.
119 H. Shi, A. Shi, L. Dong, X. Lu, Y. Wang, J. Zhao, F. Dai and X. Guo, Clin. Nutr., 2016, 35, 1366–1373.
120 H. Guo, M. Xia, T. Zou, W. Ling, R. Zhong and W. Zhang, J. Nutr. Biochem., 2012, 23, 349–360.

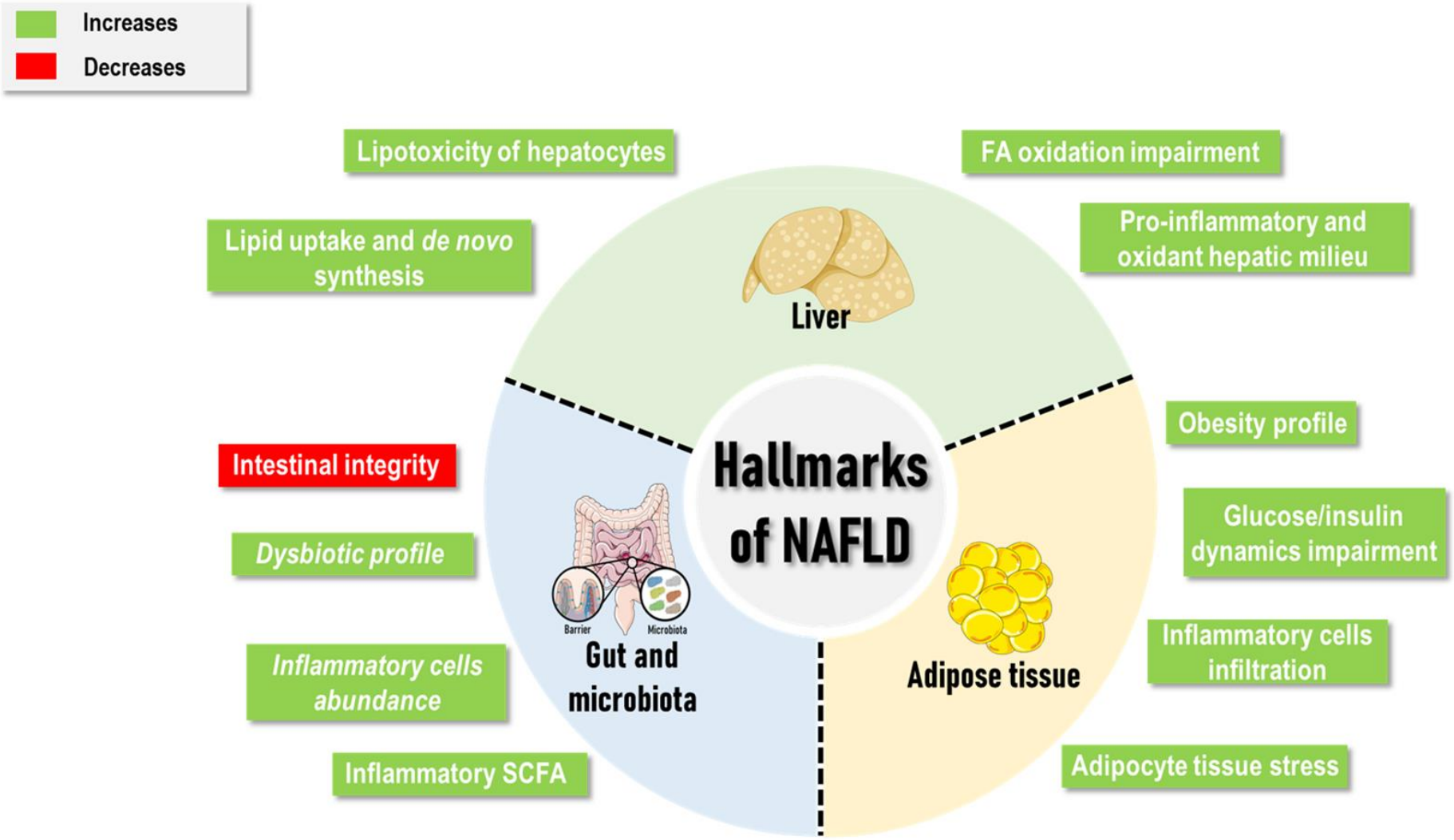

Figure 1. Hallmarks of NAFLD. A comprehensive overview of the molecular mechanism associated with NAFLD development/progression.

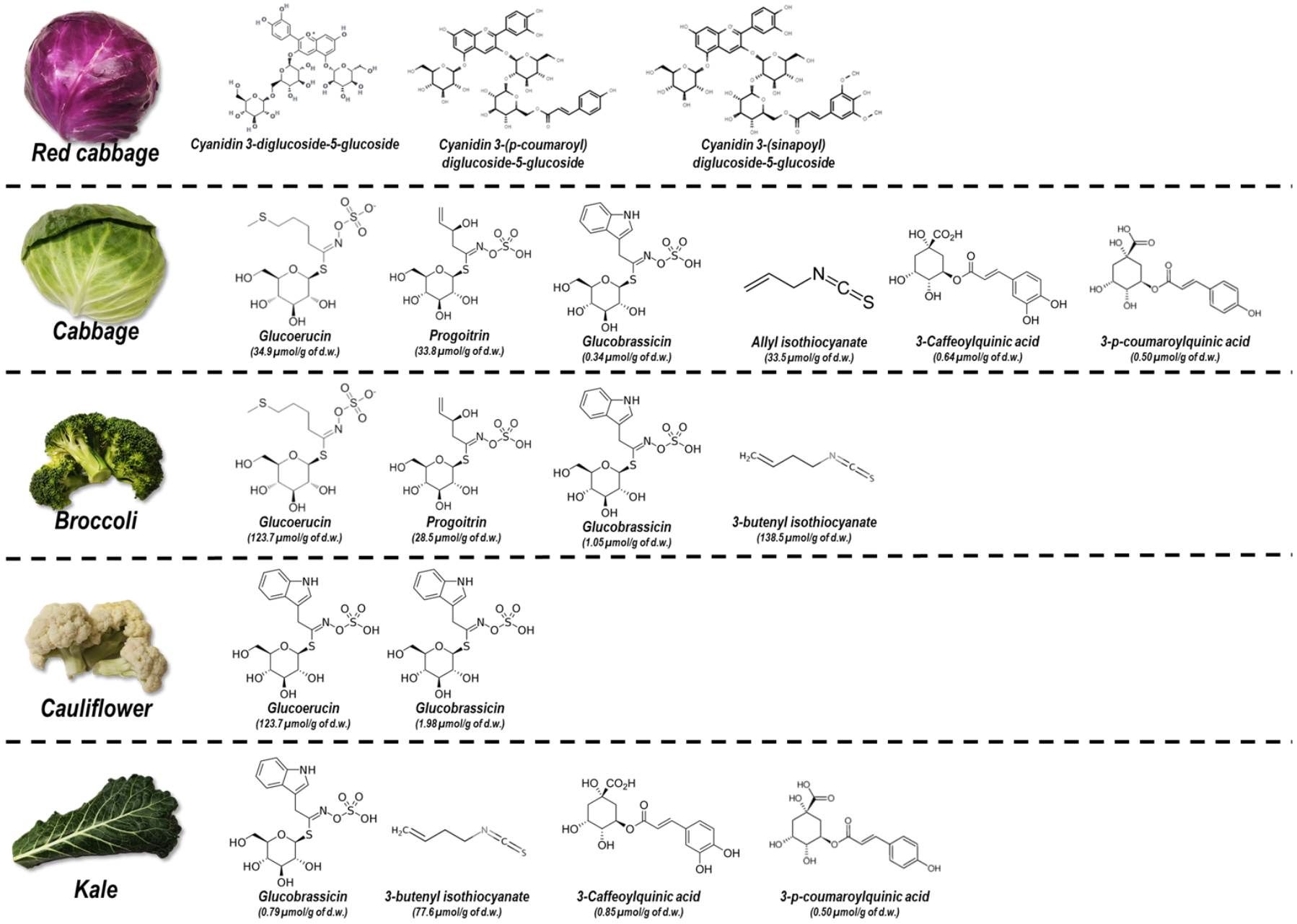

Figure 2. Estimate content of glucosinolates and phenolic compounds in *Brassicaceae* family vegetables.

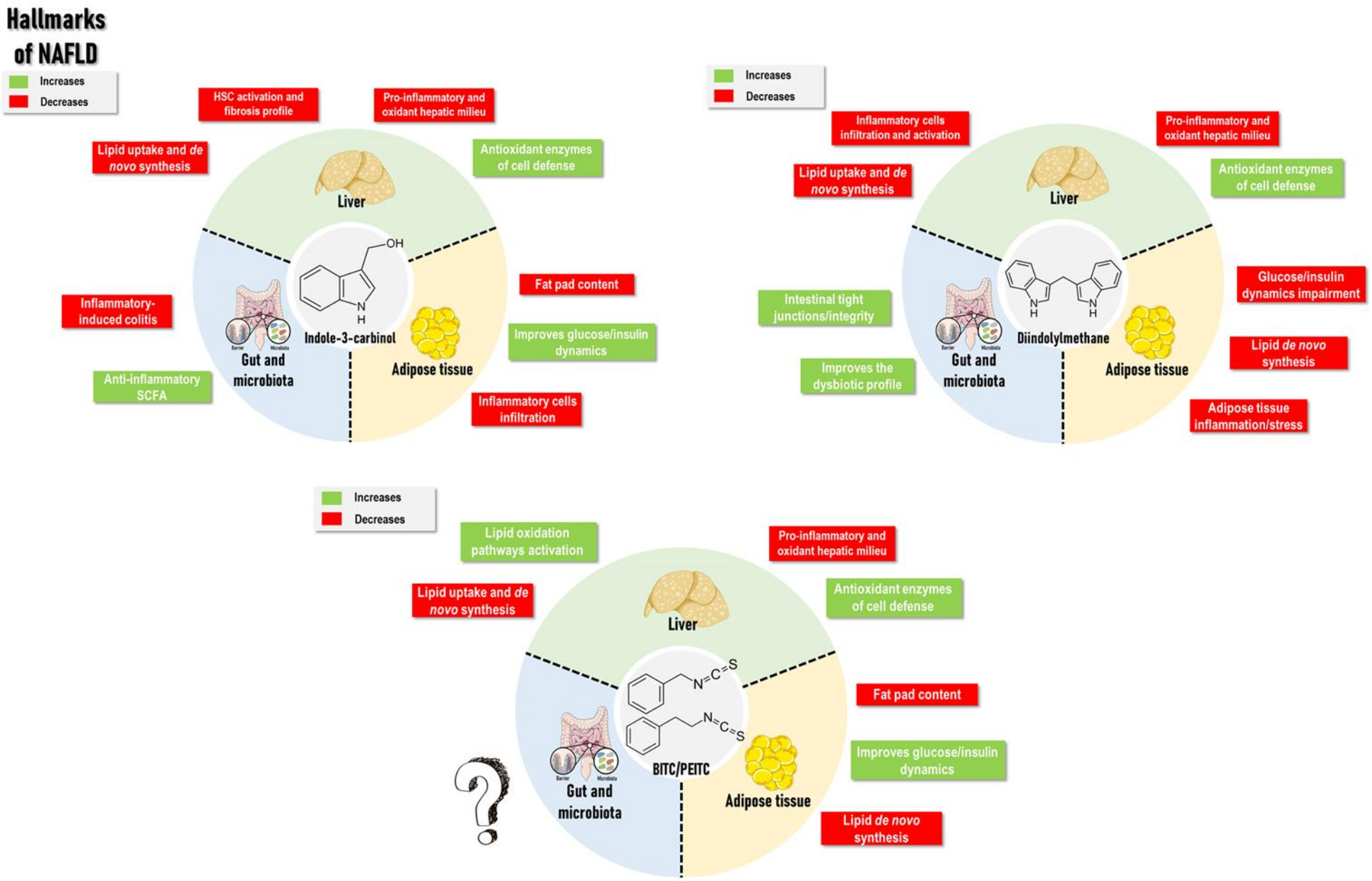

Figure 3. Effects of isothiocyanates (ITC) from *Brassicaceae* family on the gut-liver-adipose axis.

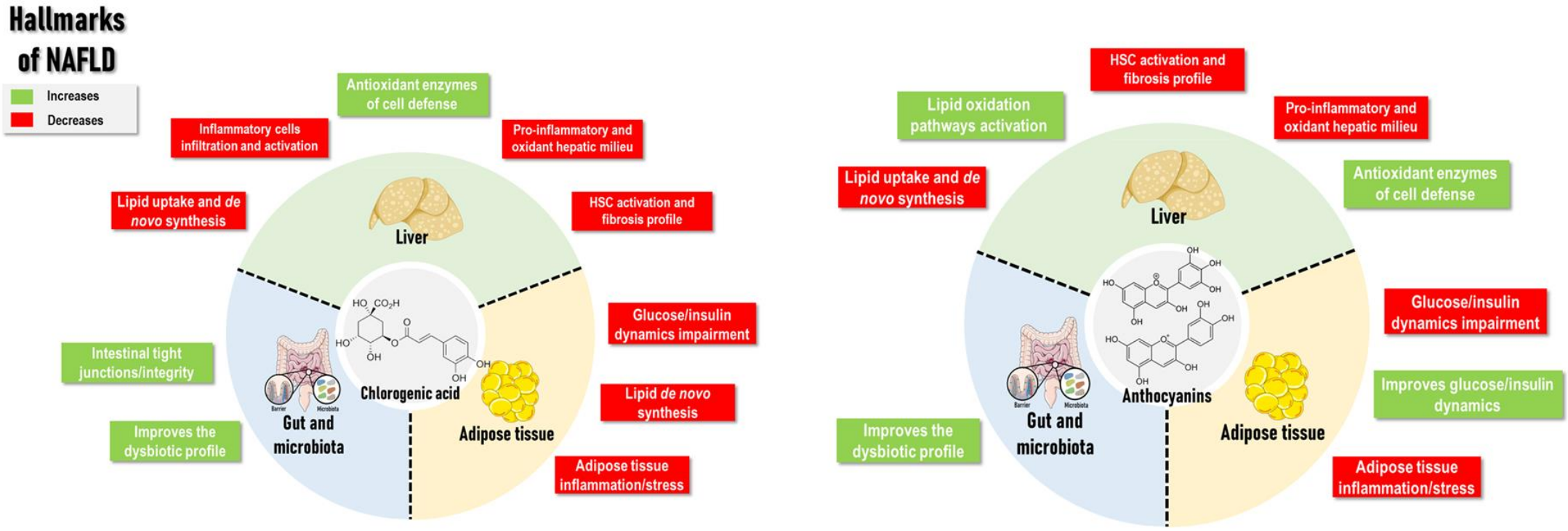

Figure 4. Effects of polyphenols from *Brassicaceae* family on the gut-liver-adipose axis.

Table 1. Implications of isothiocyanates and phenolic compounds on *in vivo* NAFLD models

Study	*Animal*	*Protocol*	*Treatment (dose/period)*	*Outcomes*
87	Male C57BL/6N	HFD: 20% of fat (or 40% of kcal derivative from fat) and 1% of cholesterol, for 10 weeks.	I3C (0.1% wt./wt.) was added to the chow.	• Restored the serum triglyceride and total cholesterol levels; • Restored the protein levels of SIRT1, LXRα, SREBP-1c, FAS, and pAMPK;
88	Male C57BL/6N	HFD: 20% of fat (or 40% of kcal) and 1% of cholesterol, for 10 weeks.	I3C (0.1% wt/wt) was added to chow.	• Reduced the visceral fat-pad weight content (epididymal, retroperitoneal, mesenteric, and peritoneal). • Alleviated the HOMA-IR index.
89	Male C57BL/6	DIO: ~30.6% of fat (or 61.2% of Kcal), for 12 weeks.	I3C (5mg/Kg of b.wt.) i.p. injections (3x/week for 12 weeks).	• Alleviated the blood glucose concentration and restored the glucose tolerance profile. • Reduced the number of $F4/80^+$ cells in the epididymal AT.
84	Male C57BL/6J	Lieber-DeCarli diet (5% vol./vol.), for 10 days.	I3C (40mg/Kg of b.wt.) daily oral gavages (10 days).	• Reduced the levels of 4-HNE and MDA; • Restored the GSH levels.
90	BALB/c and C57BL/6	2,4,6-trinitrobenzene sulfonic acid-induced colitis	I3C (40mg/Kg of b.wt.) i.p. injections.	• Increased the levels of butyrate-producer bacteria; • Restored the microbiota profile.
91	Male C57BL/6 (8 weeks old)	CCl_4-induced acute liver injury: 1:1 solution of oil-diluted CCl_4.	I3C (50.0 or 100 mg/Kg of b.wt.) oral gavages (3 days) (pre-treatment).	• Reduced the ALT and AST levels; • Reduced the number of activated Kupffer cells.
92	Female C57BL/6	MCD: methionine and choline aminoacids deficiency, for 8 weeks.	DIM (20.0 or 40.0 mg/Kg of b.wt.) (2x/week, for 8 weeks).	• Reduced the hepatic damage and the steatotic profile; • Increases the Treg/Th17 ratio.
93	Male C57BL/6J	HFD: ~34.1% of fat, for 10 weeks.	DIM (10mg/Kg of b.wt.).	• Improved the glucose and insulin plasma levels; • Reduced the levels of hepatic TBARS and lipid peroxides; • Increased the enzymatic activity of SOD, CAT, and GPx.
94	Male FVB mice (6-8 weeks old)	CCl_4-induced acute liver injury: 10% solution of oil-diluted CCl_4.	DIM (2.5, 5.0, 10.0 mg/Kg of b.wt., s.i.) (pre-treatment).	• Reduced the hepatic MDA levels; • Enhanced the protein levels of Nrf2.
95	Male C57BL/6N	HFD: 60% of Kcal derivative from fat, for 12 weeks	DIM (10.0 or 50.0 mg/Kg of b.wt.) was added to the chow added to chow.	• Inhibited body weight gain; • Inhibited the epididymal fat weight gain. • Reduced the epididymal fat pad weight;
96	Male C57BL/6 (4 weeks old)	HFCD: 60.0% of Kcal derivative from fat and 1% of cholesterol (wt./wt.), for 13 weeks.	PEITC (30.0 or 75.0 mg/Kg of b.wt.).	• Restored the serum levels of total cholesterol, TG, and LDL; • Reversed the IR profile and restored the serum levels of glucose and insulin; • Reduced the protein levels of CD36 and p65 NF-κB;

97	Male C57BL/6J (4 weeks old)	HFD: 60% of Kcal derivative from fat, for 18 weeks.	BITC (0.05 or 0.1% of wt./wt.) was added to the chow.	• Enhanced the protein levels of PPARγ, LXRα, and ABCA1. • Suppressed body weight gain and reduced the epididymal fat pad weight; • Alleviated the total cholesterol, TG, and NEFA levels; • Reduced the protein levels of SREBP-1c, FAS, LXRα, and ACC.
98	Male ICR mice (4 weeks old)	HFD: 21% of fat (or 37% of Kcal derivative from fat), for 8 weeks.	CGA (0.2g/Kg wt./wt.) was added to chow.	• Reduced epididymal and perirenal fat weight; • Inhibited the activity of FAS, ACAT, and HMG-CoA. • Restored β-oxidation activity.
99	Male ICR (5-6 weeks old)	HFD: 18.4% of fat, for 6 weeks.	CGA (15.0% wt./wt.) was added to the chow.	• Restored the *Firmicutes*/*Bacteroidetes* ratio. • Restored occludin and ZO-1 levels; • Reduced the protein levels of TLR4, TNF-α, and NF-κB;
100	Male C57BL/6 (6 weeks old)	HFD: 10% of fat and 2% of cholesterol (~x% of Kcal derivative from fat).	CGA (60 mg/Kg b.wt.), for 12 weeks (daily oral administrations).	• Restored the normal abundance of *Escherichia coli*, *Enterococcus*. and *Bifidobacterium* bacteria.
101	Male Sprague-Dawley rats.	CCl_4-induced fibrosis: 40% ol-diluted solution i.p. (3.0mL/Kg of b.wt.; 2x/week), for 8 weeks.	CGA (60 mg/Kg b.wt.), for 8 weeks (daily intragastric injections).	• Reduced the HSC activation and hepatic fibrosis; • Reduced the MDA levels, while enhancing the SOD, CAT, and GSH levels. • Increased the Nrf2 and reduced the CYP2E1 protein levels.
102	Male C57BL/6 (5 weeks old)	WD: 30% of fat (~60% of Kcal derivative from fat) and fructose-added water (4% wt./wt.), for 12 weeks.	Bilberry anthocyanins (2.0% wt./wt.) were added to the chow.	• Reduced the hepatic TBARS levels; • Induced the protein expression of Nrf2; • Restored the adequate *Firmicutes/Bacteroidetes* ratio.
103	Male C57BL/6 (8 weeks old)	CCl_4-induced acute liver injury: i.p. of 20% oil-diluted solution, for 1 week.	Cyanidin-3-glucoside (100.0, 200.0, 400.0 mg/Kg b.wt.), daily intragastric adminsitrations, for 1 week.	• Reduced the levels of apoptosis of hepatocytes; • Reduced the levels of oxidative stress markers; • Enhanced the protein levels of Nrf2.
104	Male C57BL/6J and C57BL/6J$^{db/db}$ (5 weeks old)	HFD: 58% of Kcal derivative from fat, for 17 weeks.	Cyanidin-3-glucoside (0.2% wt./wt.) was added to chow, for 5 weeks.	• Inhibited the IR profile on both HFD-induced and *db/db* mice; • Reduced the number of F4/80$^+$ cells on both HFD-induced and *db/db* mice; • Reduced the hepatic expression of *Mcp-1*, *Il6*, and *Tnfa*.

Abbreviations: 4-HNE: 4-hydroxynonenal; ABCA1: ATP-binding cassette transporter; ACC: acetyl-CoA carboxylase; ACAT: acetyl-CoA acetyltransferase; ALT: alanine aminotransferase; AST: aspartate aminotransferase; BITC: benzyl isothiocyanate; CAT: catalase; CCl_4: carbon tetrachloride; CGA: chlorogenic acid; CYP2E1: cytochrome P450 family 2 subfamily E member 1; DIM: diindolylmethane; DIO: diet-induced obesity;

FA: fatty acid; FAS: fatty acid synthase; GPx: glutathione peroxidase; GSH: gluthathione; HFD: high-fat diet; HFCD: high-fat-cholesterol diet; HOMA-IR: homeostatic assessment index of insulin resistance; HSC: hepatic stellate cells; I3C: indole-3-carbinol; Il6: interleukin-6; IR: insulin resistance; LDL: low density lipoprotein; LXR-α: liver X receptor α; MDA: malondialdehyde; MCD: methionine and choline deficient diet; Mcp1: monocyte chemoattractant protein-1; NEFA: non-esterifed fatty acid; NF-κB (p65): nuclear factor kappa B; Nrf2: nuclear factor-erythroid 2-related factor 2; pAMPK:: phosphorylated AMP-activated protein kinase; PPARγ: peroxisome proliferator-activated receptor gamma; SIRT-1: sirtuin-1; SOD: superoxide dismutase; SREBP-1c: sterol regulator element-binding protein-1c; TBARS: thiobarbituric acid reactive substances; TG: triglycerides; TLR4: toll-like receptor 4; Tnfa: tumor necrosis factor α; ZO-1: zonula occludens-1.

Table 2. Implications of isothiocyanates and phenolic compounds on *in vitro* NAFLD models

Study	*Cell line*	*Cell origin*	*Treatment (concentration)*	*Outcomes*
[105]	HepG2	Human	I3C (50 µmol/L) for 24 hours.	• Decreased lipid synthesis and trafficking; • Inhibited lipogenic activity; • Reduced the mRNA levels of SREBP-1c and FASN.
[109]	HepG2	Human	I3C (2.0 or 10.0 µmol/L) for 72 hours.	• Induced Nrf2 translocations and phosphorylation; • Increased the mRNA levels of CAT, SOD, GR, and GPx.
[91]	3T3-L1	Mouse	I3C (6.25, 50.0, or 100.0 µmol/L) for 24 hours.	• Dose-dependent inhibition of lipid content in adipocytes and differentiation of preadipocytes.
[118]	RAW264.7, primary adipocytes, and 3T3-L1	Mouse, human, mouse, respectively	I3C (1.0, 10.0, or 100.0 µmol/L) for 24 hours.	• Dose-dependent reduction of iNOS mRNA levels (co-culture of RAW264.7 and primary adipocytes); • Reduced the concentration of medium IL-6 (co-culture of RAW264.7 and primary adipocytes); • Dose-dependent increase of PPARγ mRNA levels (co-culture of RAW264.7 and primary adipocytes); • Reduced the lipid content in 3T3-L1 cells.
[111]	RAW264.7	Mouse	I3C (25.0, 50.0 or 100.0 µmol/L) for 24 hours.	• Reduced the synthesis of IL-1β and IL-6; • Reduced the phosphorylation of the IFR3-IFN-β-STAT1/3 pathway.
[117]	RAW264.7	Mouse	DIM (5.0 or 10.0 µmol/L) for	• Reduced the phosphorylation of JNK/AP-1 pathway; • Reduced the activity of NF-κB; • Reduced the protein levels of TNF-α, IL-6, and IL-1β.
[119]	Caco-2	Human	DIM (5.0, 10.0, 20.0, and 40.0 µmol/L), for 24 hours.	• Increased the protein levels of ZO-1 and occludin.
[95]	3T3-L1	Mouse	DIM (20.0, 40.0, and 60.0 µmol/L), for 6 days (pre-treatment)	• Inhibited the early stages of the differentiation process of pre-adipocytes; • Reduced the lipid content of adipocytes; • Inhibited lipogenesis-related proteins, like FAS and SREBP-1c.
[120]	HepG2	Human	PEITC (5.0 or 10.0 µmol/L).	• Increased Nrf2 mRNA levels;

[101]	HSC-T6	Rat	CGA (12.5, 25.0, and 50 µg/mL), for 24 hours.	• Reduced COX-2 mRNA levels; • Reduced p65 NF-κB biding to DNA and p65 NF-κB nuclear levels; • Especially the higher dose alleviated the PDGF-induced collagen and ROS synthesis; • Reduced the ROS-mediated p-38 and p-ERK protein levels.
[121]	RAW264.7	Mouse	CGA (12.5, 25.0, and 37.5 µg/mL), 2, 4, 6, and 8 hours.	• Inhibited the prostaglandin E_2 releasing; • Suppressed the NF-κB and JNK activation; • Reduced the mRNA levels of COX-2.
[122]	HepG2	Human	Delphinidin (10.0, 20.0, 40.0 µmol/L) for 24 hours, or pre-treatment, for 2 hours.	• Upregulated the Nrf2/HO-1 pathway; • Reduced the H_2O_2-associated oxidative stress.
[103]	HepG2	Human	Cyanidin-3-glucoside (10.0, 20.0, and 40.0 µmol/L), for 6 hours (pre-treatment).	• Reduced the H_2O_2-induced apoptosis; • Restored the levels of apoptosis-related proteins (cleaved caspase-3 and BAX).

Abbreviations: AP-1: BAX: Bcl2- associated X protein; CAT: catalase; CGA: chlorogenic acid; COX-2: cyclooxygenase-2; DIM: diindolylmethane; FAS: fatty acid synthase; GPx: glutathione peroxidase; GR: glutathione reductase; H_2O_2: hydrogen peroxide; HO-1: heme oxygenase-1; I3C: indole-3-carbinol; IFR-3: interferon regulatory factor-3; IL-1β: interleukin-1β; IL-6: interleukin-6; INF-β: interferon-β; JNK: c-Jun N-terminal kinase; NF-κB (p65): nuclear factor kappa B; Nrf2: nuclear factor-erythroid 2-related factor 2; pERK: phosphorylated extracellular signal-regulated kinase; PDGF: platelet-derived growth factor; PEITC: phenethyl isothiocyanate; PPARγ: peroxisome proliferator-activated receptor gamma; PTEIC: phenethyl isothiocyanate; ROS: reactive oxygen species; SOD: superoxide dismutase; SREBP-1c: sterol regulator element-binding protein-1c; STAT1: signal transducer and activator of transcription 1; STAT3: signal transducer and activator of transcription 3; TNF-α: tumoral necrosis factor-α; ZO-1: zonula occludens-1.

Chapter 2

Establishment of a murine model of NASH: outcomes in different mice strains

Abstract

During the 20th century, the worldwide population faced dietary shifts and lifestyle-related changes, contributing to the emerging of nonalcoholic fatty liver disease (NAFLD) and its most severe form, nonalcoholic steatohepatitis (NASH). Although several efforts, there are no effective therapies for NAFLD/NASH patients, becoming urgent the development of a reliable experimental model that resembles the main aspects of the corresponding human disease. For that, we established a fast-inducing hybrid model (diet- and chemically-induced) of fibrosis-associated NASH in two different mice strains (C57BL/6J and BALB/c) by associating a western diet protocol (WD) to weekly-increased doses of carbon tetrachloride [CCl_4, 0.25-1.50µL/g of body weight (b.wt.)], for 8 weeks. Additionally, we assessed whether maintaining mice on the WD protocol (additional 6 weeks) would keep NASH traits, after the CCl_4 protocol ceasing. Only in the C57BL/6J strain, the hybrid protocol caused glucose intolerance, while both strains featured increased relative liver weight ($p<0.0001$) Besides, the WD+CCl4 groups featured an increased NAS grading and a microvesicular steatosis profile ($p<0.0001$). The hybrid protocol caused extensive fibrosis ($p<0.0001$), enhanced the α-smooth muscle actin (α-SMA) levels ($p<0.0001$), and increased the number of $Ki67^+$ ($p<0.0001$), $CD68^+$ ($p<0.0001$), and $casp3^+$ ($p<0.0001$) cells in the liver, while increased the number of CD68+ cells in the adipose tissue of both strains ($p=0.0432$ and $p=0.0004$, respectively). Of note, only BALB/c featured adipocytes hypertrophy ($p<0.0001$) with an increase in mast cells ($p=0.0083$). We also observed reduced levels of Nrf2 in both strains ($p<0.0001$), while only C57BL/6J mice featured increased levels of NF-κB ($p=0.005$), besides a divergent metabolomic profile between mice strains, suggesting a strain-dependent susceptibility to the hybrid model of NASH.

Introduction

1. Introduction

Recently, it has been reported that non-alcoholic fatty liver disease (NAFLD), which comprises a wide spectrum of chronic liver disease, ranging from hepatic steatosis (NAFL) to non-alcoholic steatohepatitis (NASH), affects almost 25% of the worldwide population and has become the leading cause of chronic liver disease, whereas it is also projected to become the leading cause of liver transplantations in the USA [1–3]. On the other hand, NASH features as the most severe form of NAFLD, affecting around 5% of the global population, and has been appointed as a leading cause of cirrhosis, while in the UK ~35% of hepatocellular carcinoma patients has been attested as NAFLD-related cases [4,5]. In parallel, it is predicted that NAFLD-related annual medical care cost for the government healthcare system is about $103 bi and €35 bi in the USA and Europe, respectively. In addition, NAFLD-related deaths in industrialized countries should double in the period 2016-2030, suggesting an urgent need of discovering new preclinical approaches and potentially effective therapies for patients [6–8]. Thus, enabling the investigation of pivotal steps of NAFLD emergence and progression.

For that purpose, several *in vivo* and *in vitro* experimental model has been designed, in order to mimic some of the NAFLD hallmarks, especially the gut-liver-adipose axis-related disorders, featuring impaired lipid, carbohydrate, and microbiota metabolism [9]. Seeking a “real-life” inducing protocol, Asgharpour *et al*. [10] established the diet-induced animal model of NAFLD (DIAMOND), in which animals were fed a western diet protocol [WD, high-fat chow associated with a high-sugar solution (HSS, 23.1 and 18.9 g/L of fructose and glucose, respectively)] for drinking, for 8-52 weeks, in order to induce NAFLD. Of note, NASH occurrence was observed after a long period of protocol (only after 52 weeks). On the other hand, NASH emergence in C57BL/6J mice can be accelerated by associating the WD to intraperitoneal injections (i.p.) of carbon tetrachloride [(CCl_4, 0.32μg/g of body weight (b.wt.), 1x week, for 12 weeks], establishing a short-period model of NASH [11]. The CCl_4 is a well-known hepatotoxin frequently used in hepatic chronic diseases models as an inducer of hepatic fibrosis and promoter of hepatocarcinogenesis

[12]. This molecule is metabolized by the hepatic microsomal system, especially by the CYP2E1, which converts the CCl_4 into CCl_3* radical, a reactive molecule that induces lipid peroxidation of hepatocytes and further apoptosis and necrosis, establishing the pro-inflammatory milieu in which NAFLD is susceptible to emerge and progress to NASH [11,13]. Indeed, a combined protocol of WD and CCl_4 induced lipid deposition, lobular inflammation, and extensive fibrosis, as well as high transcriptomic resemblance in comparison to NASH patients, although metabolic disorders were not observed [11]. Then, still urgent to establish an adequate experimental model that resembles traits of the corresponding disease in a short-period of protocol, in order to unravel the morphological and molecular aspects related to NASH, as well as discover new potential preclinical strategies.

Thus, our paper aimed at establishing a fibrosis-associated NASH hybrid protocol (diet- and chemically-induced), evaluating: (1) which mice strain is more susceptible to the hybrid protocol (C57BL/6J or BALB/c), (2) the unravel a molecular mechanism associated with NASH development, and (3) determine the hepatic metabolomic profile of mice submitted to the hybrid protocol of NASH.

Materials and methods

2. Experimental design

Male C57BL/6J and BALB/c mice were fed a WD protocol [chow enriched with fat/sucrose (200g/Kg or ~37.5 and ~17% of total calories; Pragsoluções Biociências, Brazil) and a HSS for drinking [55/45% weight/weight (w/w) proportion of d-fructose/d-glucose or 23.1 and 18.9g/L diluted in filtered water, respectively; Dinâmica, Brazil], or a basal diet [normocaloric chow (Nuvilab CR-1, Nuvital, Brazil) and tap water for drinking], for 8 or 14 weeks (Figure 1). The nutritional composition is available in Table 1. Additionally, CCl_4 and WD+CCl_4 groups received weekly-increased intraperitoneal (i.p.)

Table 1. Nutritional composition of the basal and hyperlipidic chows.

Dietary nutrients	Basal chow	Hyperlipidic chow
Protein (g)	220	235
Corn starch (g)	554	202
Sucrose (g)	-	202
Soy oil (g)	40	-
Corn oil (g)	-	50
Lard (g)	-	200
Fibers (g)	70	50
Mineral mix (g)	90	90
Vitamin mix (g)	10	10
Total (g)	1000	1000
Total (kcal/g)	3456	4806

Nutritional composition of the hypercaloric chow used in the western diet protocol.

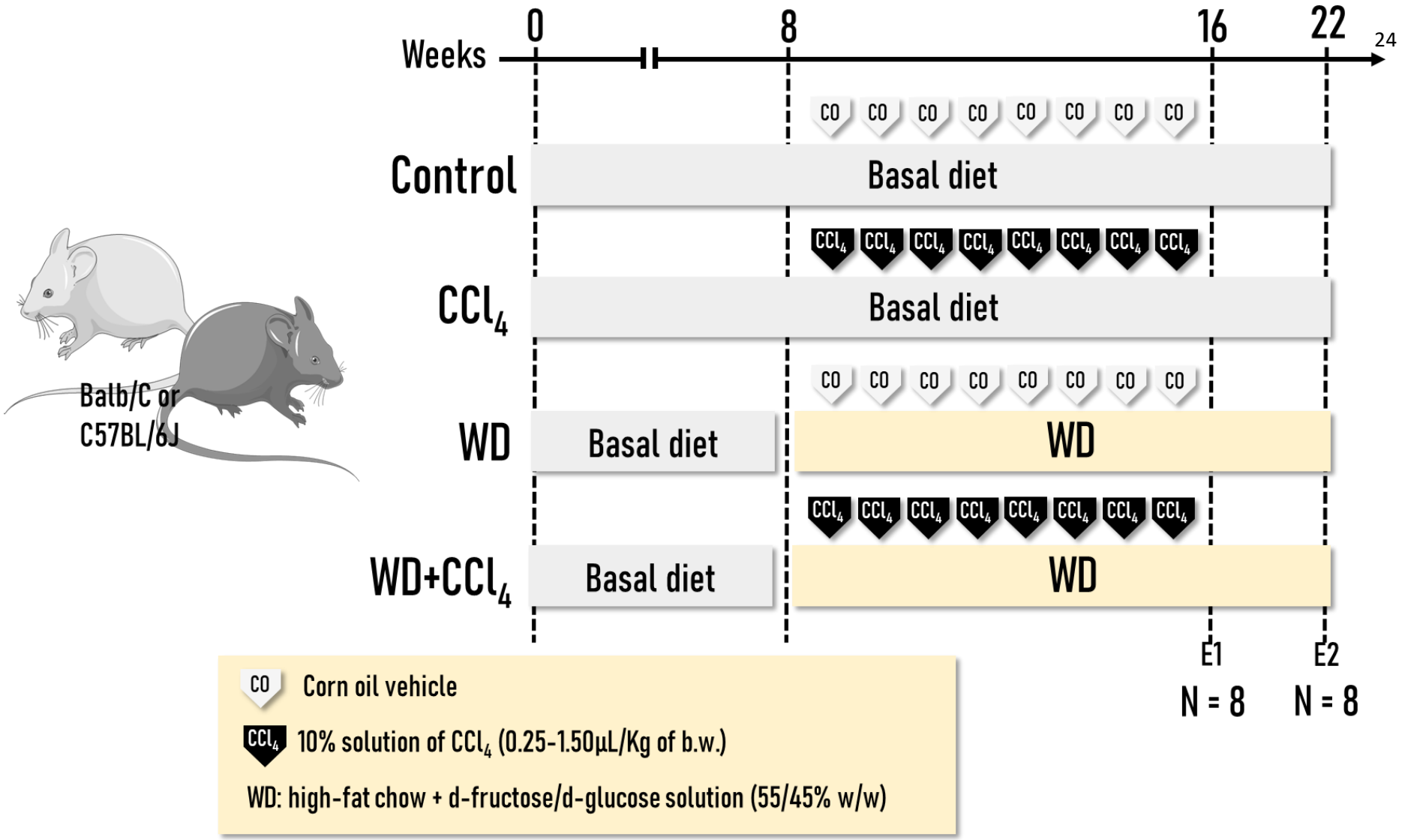

Figure 1. **Experimental design.** Hybrid-induced model of non-alcoholic steatohepatitis (NASH) protocol in male C57BL/6J or BALB/c mice. Control [standard chow and 3x weekly intraperitoneal (i.p.) injections of corn oil vehicle]; carbon tetrachloride [CCl_4, 3x weekly i.p. injections of 10% corn oil solution of CCl_4, with doses of 0.25µL/g of body weight (b.w.) increased utmost of 1.50 µL/g b.w.]; western diet [WD, chow enriched with fat (20%) and sucrose (20%) and 3x weekly i.p. injections of corn oil vehicle]; WD+CCl4 (chow enriched with fat (20%) and sucrose (20%) and 3x weekly i.p injections of 10% corn oil solution of CCl_4, with doses of 0.25µL/g b.w. increased utmost of 1.50 µL/g b.w.); n = 5-6 (control and WD) or 7-9 (CCl4 and WD+CCl_4). CO: corn oil; CCl_4: carbontetrachloride; E1: first euthanasia timepoint; E2: second euthanasia timepoint; WD: western diet. Representative images were acquired from Servier Medical Art (smart.servier.com).

injections of a 10% diluted oil solution of CCl_4 (0.25-1.50µL/g of body weight (b.w.), 3x/week) protocol, for 8 weeks, while control and WD groups received corn oil vehicle, as previously established by our group [12]. Animals were fasted for 12 hours and then euthanized by exsanguination under ketamine/xylazine anesthesia (100/16mg/Kg/b.w. i.p.) after 8 (first euthanasia, E1, N = 8 animals/group) or 14 weeks (second euthanasia, E2, N = 8 animals/group). At E1, the euthanasia occurred 48 hours after the last i.p. injection of CCl_4. The blood was collected in heparinized syringes from cardiac puncture, centrifuge (1503xg, 15 min.), and serum samples were collected and stored in -80ºC for further analysis. At the necropsy, the liver was removed, weighted, and then liver samples from the left lobe and adipose tissue (AT) were collected and fixed in 10% formalin or snap-frozen into liquid nitrogen for further storage at -80ºC. Additional liver samples from left and medial lobes and AT (epididymal, EAT, retroperitoneal, and intestinal) samples were collected and stored at -80ºC for biochemical and molecular analysis. The animals were obtained from the School of Veterinary Medicine and Animal Science of the University of São Paulo (FMVZ, USP, São Paulo-SP, Brazil) and kept in Botucatu Medical School of the São Paulo State University (FMB, UNESP, São Paulo – SP, Brazil) in a room with continuous ventilation, relative humidity (45-65%), controlled temperature (20-24ºC) and light/dark cycle 12:12 hours, with *ad libitum* offering of chow and water. Body weight and food/water consumption were recorded once a week during the experimental period. This experiment was performed under Botucatu Medical School/UNESP Ethics Committee on Use of Animals (CEUA) approval (Protocol number 1343/2020), and animals received human care according to the “Guide for the Care and Use of Laboratory Animals” [14].

2. Glucose tolerance test

Four days before the euthanasia, mice were fasted for 12 hours and submitted to a glucose tolerance test (GTT). Mice were weighted and blood samples were collected from the caudal vein, in order to measure the glucose level in an automatic glucometer (Accu-Chek, Roche, Germany). Further, animals received an i.p. injection of a water-diluted d-glucose solution (2 g/Kg b.w.) (Dinâmica, Brazil). Glucose levels were measured following 30, 60, 90, and 120 min. after the injection [15].

3. Histological analysis

The liver samples from the left lobe and the EAT fixed in 10% formalin were embedded in paraffin. Then, 5-8µm thick sections were obtained and disposed on regular or polarized glass slides, and further, liver sections were stained with Hematoxylin & Eosin (H&E) or Sirius Red, while EAT sections were stained with Toluidine Blue (0.05%, pH 4.0). Additionally, liver and EAT sections were submitted to immunohistochemistry assay. Also, 10µm thick liver sections were obtained from snap-frozen (-80ºC) samples embedded in Optimal Cutting Temperature medium (Tissue-Trek, USA) for Oil Red staining (Sigma Aldrich, USA).

3.1Evaluation of Non-alcoholic Fatty Liver Diseases Activity Score and Fibrosis

The liver sections stained with H&E were used for evaluating the NAFLD Activity Score (NAS), according to previously established criteria [16], while sections stained with Oil Red were used to evaluate lipid deposits. Photomicrographs of 10 randomly-selected fields/animal (200× magnification, software CellSense, Olympus Corporation, Japan). Photomicrographs of 5 randomly selected fields/animal sections stained with Oil Red were acquired for morphometric analysis to evaluate the lipid deposit (%) in the liver sections. Similarly, photomicrographs of 10 randomly selected fields/animals were acquired to perform the morphometric analysis to evaluate the total area filled with collagen deposit (%) in the liver from sections stained with Sirius Red.

3.2 Morphometric analysis of adipocytes and mast cells counting

Five-micron thickness EAT sections, stained with H&E and toluidine blue (Sigma Aldrich, USA), were used for evaluating the number/mm² of adipocytes and its occupied area (%), and mastocytes infiltration (number of mastocytes/mm²), respectively, as established previously [17]. For that, photomicrographs of 10 randomly selected fields were acquired (200x magnification, software CellSense, Olympus Corporation, Japan) and analyzed by the software ImageJ (NIH, USA). For adipocyte analysis, the extension Adiposoft, from Image J (NIH, USA) was used.

3.3 Immunohistochemistry

Semiquantitative analysis of immunoreactivities for Ki67 (*i.e.,* a marker for cellular proliferation), CD68 (*i.e.,* a marker of macrophages), α-smooth muscle actin (α-SMA) (*i.e.,* a marker of active hepatic stellate cells, HSC), and cleaved caspase-3 (casp3) (i.e., a marker of apoptotic cells) were performed in liver sections. In EAT sections, the immunohistochemistry reactions to CD68 were performed. deparaffinated five-micron sections in silane-covered slides were submitted to antigen retrieval in 0.01M citrate buffer (pH 6.0, 120ºC, 5 min) in a Pascal Pressure Chamber (Dako Cytomation, Denmark). Then, a blockade of endogenous peroxidase and nonspecific bindings with 10% H_2O_2 in phosphate-buffered saline (PBS) (15 min.), followed by treatment with skim milk (60 min.) and overnight incubation in a humidified chamber (4ºC) with Ki67 (MA5-14520, 1:200 dilution, ThermoFisher, USA), CD68 (ab125212, 1:1000 dilution, Abcam, UK), α-SMA (ab124964, 1:500 dilution, Abcam, UK), and cleaved caspase-3 (5A1E, 1:50, dilution, Cell Signaling, USA) antibodies diluted in 1% bovine serum albumin solution were performed. After three wash-steps with PBS (5 min. each), slides were incubated with a single step horseradish peroxidase (HRP)-polymer (EasyPath - Erviegas, Brazil) (20 min). Reactions were visualized with 3´3-diaminobenzidine (DAB) chromogen (Sigma–Aldrich, USA) and counterstained with Harris hematoxylin.

Photomicrographs of 10 randomly-selected fields/animal (200x magnification, software CellSense, Olympus Corporation, Japan) from liver sections immunostained for α-SMA were acquired and % positive area marker was performed with software Leica Qwin (Leica Biosystems, Germany), by calculating the total area filled by α-SMA (%). Similarly, CD68, Ki67 (in the liver and EAT), and casp3 analysis were performed by acquiring photomicrographs of 10 randomly selected fields/animal (200x magnification, software CellSense, Olympus Corporation, Japan). Then, the mean number of CD68 positive macrophages and Ki67 and cleaved caspase-3 positive ($Ki67^+$ and $casp3^+$, respectively) hepatocytes were expressed by area analyzed (mm^2) using the software ImageJ (NIH, USA).

4. Protein extraction and western blotting

Liver samples from the left lobe (~100mg) and stored in -80ºC were homogenized in RIPA buffer (Cell Signaling, USA) with the addition of 1.0% of a protease inhibitor cocktail (Sigma Aldrich, USA), in a

proportion of 30mg of tissue/100µL of buffer for the following pulverizing step with a Polytron mixer (Thermo Fisher Scientific, USA) (25,000 rpm, 10 seg.). After that, the samples were stored at 4ºC for 2 hours, and then, centrifuged (10,000g, 4ºC, 30 min.). The supernatant was collected for further protein quantification, by the Bradford assay. For the western blotting essays, 10µL of the liver homogenate (total protein concentration of 7µg/µL) were mixed to the same volume of Laemmli buffer (2.5mM Tris, 2.0% SDS, 10.0% glycerol, 0.01% of bromophenol blue, and 5.0% of 2-mercaptoethanol, and heated (95ºC, 5 min.). Then, samples were submitted to an electrophoresis run in 10.0% SDS-PAGE gel and transferred to a nitrocellulose membrane (Bio-Rad Laboratories, USA) for immunodetection. Membranes were submitted to a blockage of non-specific protein binding in a 5.0% skim milk solution diluted in tris-tween solution (TBS-T, 1M tris, 5M NaCl, pH 7.2, 500µL tween-20) for 1 hour. After the blockage, 3 washing steps (5 min.) were done, and membranes were overnight incubated with anti-Nrf2 (PA5-27282, ~95-110 kDa, 1:1000, Thermo Scientific, USA), anti-NF-κB (p65) (sc-372, 65 kDa, 1:1000, Santa Cruz, Biotechnology, USA) antibodies and anti-β-actin (endogenous control, sc- 1615, ~43kDa, 1:1000, Santa Cruz Biotechnology, USA) diluted in TBS-T. After that, 5 washing steps were done, and membranes were incubated with anti-rabbit (ab7621, 1:3000, Abcam, UK) and anti-goat (ab 97110, 1:3000, Abcam, UK) secondary antibodies for 2 hours. Membranes were exposed to ECL Clarity Max (Bio-Rad Laboratories, USA) for immunodetection in a G:BOX Chemi System (Syngen, UK), with the software GeneSys (Syngen, UK). The quantification step was done in the software ImageJ (NIH, USA), and the interest protein expression was normalized by the endogenous control expression.

5. **Metabolomic analysis**

Hepatic samples (~200mg) stored at -80ºC were used for the global metabolite identification, by adding chloroform/methanol/distilled water (1:2:1 proportion) and a ceramic grinding sphere for tissue preparation. Then, a FastPrep (MP Biomedicals, USA) was used for tissue grinding and homogenization (1 min.), followed by a centrifuge process (1500g, 15 min., 4ºC) for hydroalcoholic phase acquirement. Samples were concentrated in a SpeedVac Vacuum Concentrator (Thermo Fisher Scientific, USA)

overnight and then, stored at -80ºC. Following, samples were analyzed by a nuclear magnetic resonance (NMR) assay (NMR 500/54 Premium Shielded, Agilent Technologies, USA), in order to identify the metabolomic profile of samples. Finally, a partial least square discriminant analysis (PLS-DA), followed by the variable importance in projection (VIP) score determination (only VIP score $\geq$ 1.5 were considered).

6. Statistical analysis

The GTT data were used to draw a glycemic curve and the area under the curve (AUC) was measured, and analyzed by two-way ANOVA, while the score data were evaluated by the non-parametrical Kruskal-Wallis test and a *post hoc* Tukey's test. The metabolomic profile was analyzed by the PLS-DA, followed by the VIP score determination. The other collected data were analyzed by one-way ANOVA or Kruskal-Wallis, followed by a *post hoc* Tukey's test. Differences were considered significant when $p<0.05$. Data were presented as mean± standard deviation (S.D.) or box plot and were analyzed with the software GraphPad Prism 6.01 (GraphPad, USA)

Results

7. General findings

In both mice strains, the WD-receiving groups displayed decreased chow consumption and enhanced HSS consumption (Figure 2), compared to the control and CCl_4 groups. Otherwise, the CCl_4-receiving groups featured reduced final body weight compared to the WD group at E1 ($p<0.0001$ and $p=0.029$, respectively), (Table 2) [12]. Indeed, ceasing the CCl_4 protocol enables the body weight reestablishment, as observed at E2 groups (Table 2), a CCl_4-dependent effect of hepatotoxicity and weight loss. At the necropsy, we observed that the liver of all mice fed WD showed a yellowish aspect, at both E1 and E2 timepoint, whereas a rough surface aspect was observed in CCl_4-receiving groups at E1, compared to the smooth characteristic observed in control groups (Figure 3).

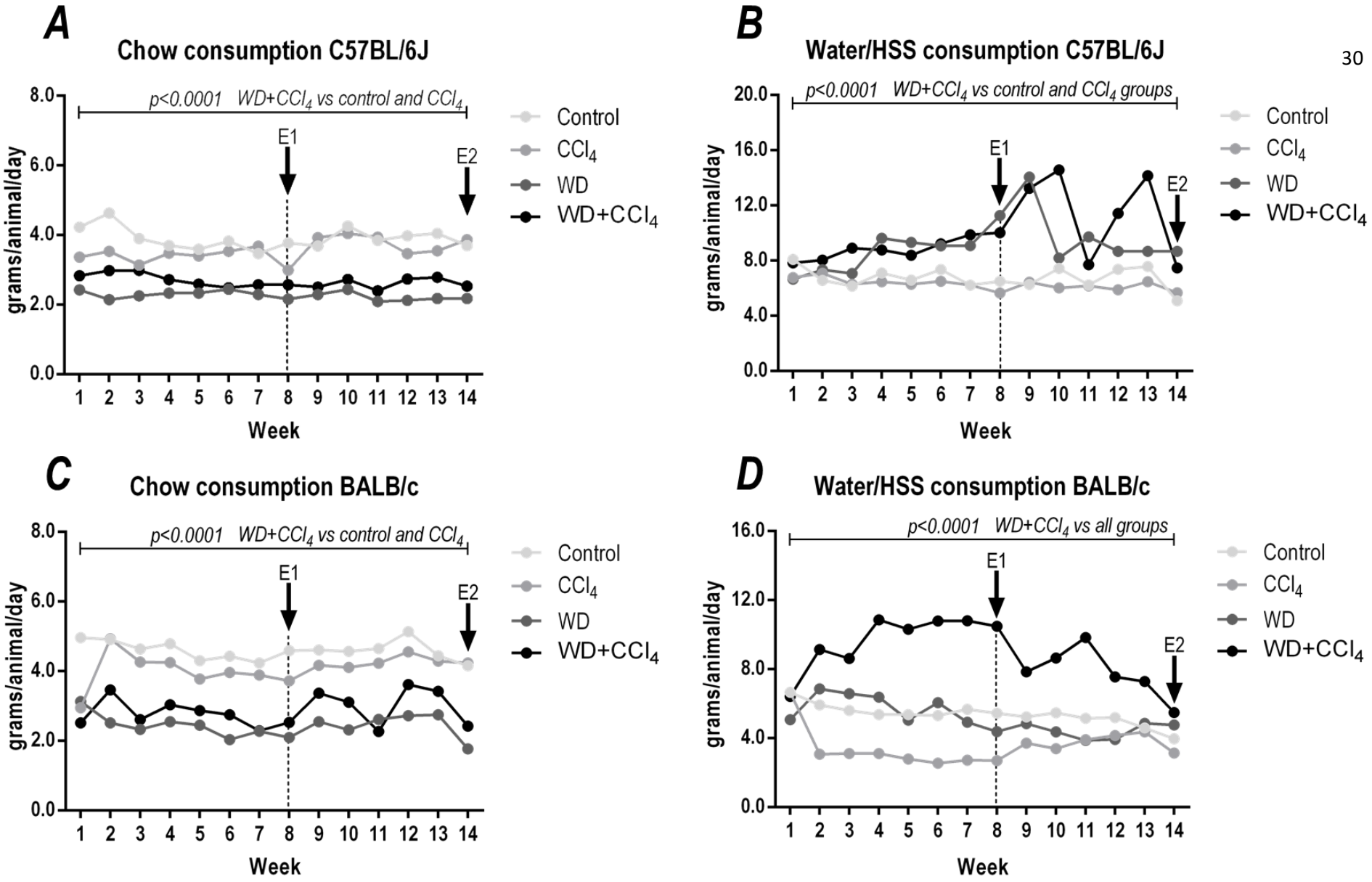

Figure 2. Effects of the hybrid protocol of NASH over chow and HSS consumption in C57BL/6J and BALB/c mice. **(A, B, C, and D)** Animals were weighted and their chow and HSS consumption was measured 1x/week, during 14 weeks. Control [standard chow and 3x weekly intraperitoneal (i.p.) injections of corn oil vehicle]; carbon tetrachloride [CCl_4, 3x weekly i.p. injections of 10% corn oil solution of CCl_4, with doses of 0.25µL/g of body weight (b.w.) increased utmost of 1.50 µL/g b.w.]; western diet [WD, chow enriched with fat (20%) and sucrose (20%) and 3x weekly i.p. injections of corn oil vehicle]; WD+CCl4 (chow enriched with fat (20%) and sucrose (20%) and 3x weekly i.p injections of 10% corn oil solution of CCl_4, with doses of 0.25µL/g b.w. increased utmost of 1.50 µL/g b.w.); n = 5-6 (control and WD) or 7-9 (CCl4 and WD+CCl_4). E1: first euthanasia timepoint; E2: second euthanasia timepoint.The data are expressed in mean±standard deviation, and were analyzed by One-Way ANOVA, and Tukey pos-hoc test.

Table 2. Effects of hybrid NASH model on final body weight, and absolute and relative liver and fat weights of C57BL/6J or BALB/c mice.

Parameters	C57BL/6J							
	E1				E2			
	Control	CCl_4	WD	WD+CCl_4	Control	CCl_4	WD	WD+CCl_4
Final body weight (g)	26.6 ± 2.50^{ac}	22.5 ± 1.50^{b}	29.4 ± 3.00^{a}	26.2 ± 1.60^{c}	28.4 ± 2.20	25.9 ± 2.80	26.0 ± 3.10	28.2 ± 1.20
Absolute liver weight (g)	1.07 ± 0.09^{ab}	1.15 ± 0.12^{a}	0.95 ± 0.13^{b}	1.10 ± 0.11^{ab}	1.08 ± 0.12^{a}	1.13 ± 0.15^{a}	0.80 ± 0.05^{b}	0.99 ± 0.11^{a}
Relative liver weight (%)	3.85 ± 0.28^{c}	5.09 ± 0.51^{a}	3.23 ± 0.36^{c}	4.20 ± 0.28^{b}	3.82 ± 0.44b	4.38 ± 0.28^{a}	3.08 ± 0.26^{c}	3.52 ± 0.37^{bc}
Total fat weight (g)*	0.35 ± 0.10^{b}	0.36 ± 0.05	1.05 ± 0.46^{a}	0.58 ± 0.18^{b}	0.52 ± 0.09^{b}	0.33 ± 0.08^{b}	1.15 ± 0.46^{a}	0.59 ± 0.21^{b}
Relative total fat weight (%)	1.34 ± 0.41^{b}	1.59 ± 0.23^{b}	3.54 ± 1.32^{a}	2.24 ± 0.77^{b}	1.84 ± 0.35^{b}	1.26 ± 0.24^{b}	4.31 ± 1.24^{a}	2.08 ± 0.71^{b}
Absolute epididymal fat weight (g)	0.11 ± 0.05^{b}	0.12 ± 0.03^{b}	0.47 ± 0.26^{a}	0.26 ± 0.11^{b}	0.23 ± 0.04^{bc}	0.10 ± 0.04^{c}	0.61 ± 0.23^{a}	0.28 ± 0.11^{b}
Absolute retroperitoneal fat weight (g)	0.03 ± 0.03^{b}	0.06 ± 0.01^{b}	0.28 ± 0.12^{a}	0.11 ± 0.06^{b}	0.08 ± 0.03^{b}	0.06 ± 0.03^{b}	0.30 ± 0.17^{a}	0.14 ± 0.06^{b}
Absolute intestinal fat weight (g)	0.21 ± 0.03^{b}	0.17 ± 0.05^{b}	0.31 ± 0.12^{a}	0.20 ± 0.05^{b}	0.21 ± 0.03	0.17 ± 0.04	0.23 ± 0.07	0.16 ± 0.05
	BALB/c							
	E1				E2			
	Control	CCl_4	WD	WD+CCl_4	Control	CCl_4	WD	WD+CCl_4
Final body weight (g)	28.2 ± 1.10^{a}	25.3 ± 1.20^{b}	28.9 ± 1.10^{a}	25.0 ± 2.00^{b}	30.0 ± 1.40^{ab}	27.2 ± 2.30^{b}	31.2 ± 2.90^{a}	30.4 ± 1.60^{a}
Absolute liver weight (g)	1.25 ± 0.10^{b}	1.59 ± 0.15^{a}	1.19 ± 1.10^{b}	1.43 ± 0.27^{a}	1.21 ± 0.08^{ab}	1.23 ± 0.17^{ab}	1.12 ± 0.11^{b}	1.40 ± 0.18^{a}
Relative liver weight (%)	4.43 ± 0.40^{b}	6.30 ± 0.57^{a}	4.12 ± 0.27^{b}	5.73 ± 0.87^{a}	4.04 ± 0.26^{b}	4.50 ± 0.33^{a}	3.58 ± 0.13^{b}	4.60 ± 0.44^{a}
Total fat weight (g)*	0.53 ± 0.18^{b}	0.32 ± 0.08^{c}	1.10 ± 0.25^{a}	0.27 ± 0.13^{c}	0.51 ± 0.17^{b}	0.28 ± 0.08^{b}	1.61 ± 0.47^{a}	0.57 ± 0.25^{b}
Relative total fat weight (%)	1.87 ± 0.64^{b}	1.24 ± 0.30^{bc}	3.77 ± 0.74^{a}	1.05 ± 0.45^{c}	1.72 ± 0.60^{b}	1.04 ± 0.24^{b}	5.10 ± 1.11^{a}	1.86 ± 0.79^{b}
Absolute epididymal fat weight (g)	0.24 ± 0.12^{b}	0.11 ± 0.07^{b}	0.59 ± 0.12^{a}	0.13 ± 0.09^{b}	0.27 ± 0.06^{b}	0.08 ± 0.04^{b}	0.09 ± 0.29^{a}	0.27 ± 0.15^{b}
Absolute retroperitoneal fat weight (g)	0.04 ± 0.0^{b}	0.03 ± 0.02^{b}	0.13 ± 0.06^{a}	0.03 ± 0.01^{b}	0.05 ± 0.02^{bc}	0.02 ± 0.02^{c}	0.28 ± 0.07^{a}	0.08 ± 0.06^{b}
Absolute intestinal fat weight (g)	0.25 ± 0.07^{b}	0.18 ± 0.04^{bc}	0.37 ± 0.09^{a}	0.12 ± 0.05^{c}	0.25 ± 0.07^{b}	0.18 ± 0.04^{bc}	0.37 ± 0.09^{a}	0.17 ± 0.05^{c}

Data are mean ± S.D. n = 5-6 (control and WD) or 8-10 (CCl_4 and WD+CCl_4) mice/group. *Sum of absolute epididymal, retroperitoneal and intestinal fat weights. Different letters correspond to statistical differences among groups by ANOVA and *post hoc* Tukey test ($p<0.05$), and the statistical tests were made between timepoints of the same strain. Control [standard chow and 3x weekly intraperitoneal (i.p.) injections of corn oil vehicle]; carbon tetrachloride [CCl_4, 3x weekly i.p. injections of 10% corn oil solution of CCl_4, with doses of 0.25µL/g of body weight (b.w.) increased utmost of 1.50 µL/g b.w.]; western diet [WD, chow enriched with fat (20%) and sucrose (20%) and 3x weekly i.p. injections of corn oil vehicle]; WD+CCl4 (chow enriched with fat (20%) and sucrose (20%) and 3x weekly i.p injections of 10% corn oil solution of CCl_4, with doses of 0.25µL/g b.w. increased utmost of 1.50 µL/g b.w.); n = 5-6 (control and WD) or 7-9 (CCl4 and WD+CCl_4).

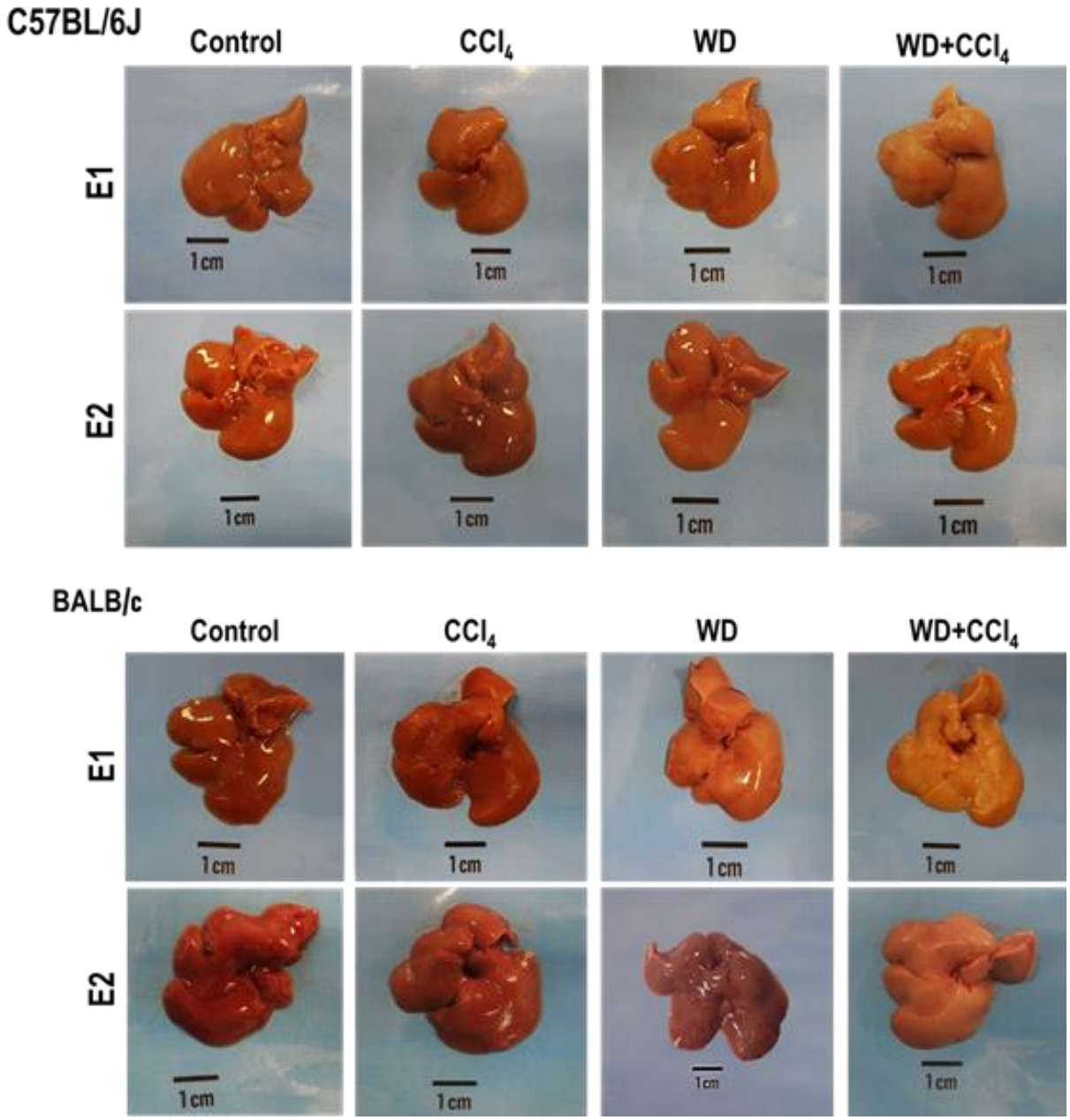

Figure 3. Effects of hybrid model of NASH on the hepatic macroscopic overview in C57BL/6J and BALB/c mice. Macroscopic overview. Control [standard chow and 3x weekly intraperitoneal (i.p.) injections of corn oil vehicle]; carbon tetrachloride [CCl_4, 3x weekly i.p. injections of 10% corn oil solution of CCl_4, with doses of 0.25µL/g of body weight (b.w.) increased utmost of 1.50 µL/g b.w.]; western diet [WD, chow enriched with fat (20%) and sucrose (20%) and 3x weekly i.p. injections of corn oil vehicle]; WD+CCl4 (chow enriched with fat (20%) and sucrose (20%) and 3x weekly i.p injections of 10% corn oil solution of CCl_4, with doses of 0.25µL/g b.w. increased utmost of 1.50 µL/g b.w.); n = 5-6 (control and WD) or 7-9 (CCl4 and WD+CCl_4). E1: first euthanasia timepoint; E2: second euthanasia timepoint.

Accordingly, the CCl_4 administration increased the total and relative weight of the liver ($p<0.0001$) (Table 2), and only WD groups featured increased total (sum of the AT weight) and relative fat weight ($p<0.0001$) at both timepoints and strains (Table 2). In these terms, the hybrid protocol of NASH contributed to the establishment of the macroscopic aspects observed in the liver of the WD+CCl_4 group.

8. The hybrid protocol induces a strain-dependent glucose intolerance profile

At E1, in the C57BL/6J strain, the WD and WD+CCl_4 groups featured a higher AUC and a rising trend compared to control and CCl_4 groups (~23.9 and 36,1%, respectively), with a higher glucose level at 60 and 90 min. ($p<0.0001$) (Figure 4). Conversely, in the BALB/c strain, only WD mice displayed a higher AUC among the groups, marked by an increased glucose level at 30 and 60 min. ($p=0.0122$) (Figure 4). At the E2 timepoint, there was no difference in the AUC among groups of the C57BL/6J mice. Differently, ceasing the CCl_4 protocol lead BALB/c mice to develop a glucose intolerance profile, compared to the control group. Data suggest that the induction of glucose intolerance by the hybrid protocol acts in a strain-dependent manner, probably due to C57BL/6J high susceptibility to metabolic disorders, during the hybrid protocol of NASH [18].

9. The hybrid protocol enhances NAS grading

Although hepatocellular hypertrophy was not observed, after 8 weeks of hybrid protocol, C57BL/6J and BALB/c mice featured an extensive microvesicular steatosis profile and fibrosis, besides the frequent occurrence of centrilobular inflammation, lobular inflammation, and hepatocellular ballooning (Figure 5). Additionally, we observed a similar grading of inflammatory foci in both strains ($p=0.0001$ and $p=0.0012$, respectively) (Table 3) (Figure 6), but only C57BL/6J mice featured a rising trend of the microvesicular steatosis grade compared to the WD group (Table 3) (Figure 6), while BALB/c mice displayed a similar grading to the strain-corresponding WD group ($p=0.0013$) (Table 3) (Figure 6). Accordingly, in both strains, WD+CCl_4 groups displayed enhanced NAS final grade compared to control and WD groups counterparts ($p<0.0001$ and $p=0.0004$, respectively) (Table 3) (Figure 6). Moreover, the CCl_4 protocol induces the frequent occurrence of hepatocellular ballooning only in C57BL/6J mice ($p=0.0001$) (Table 3) (Figure 6).

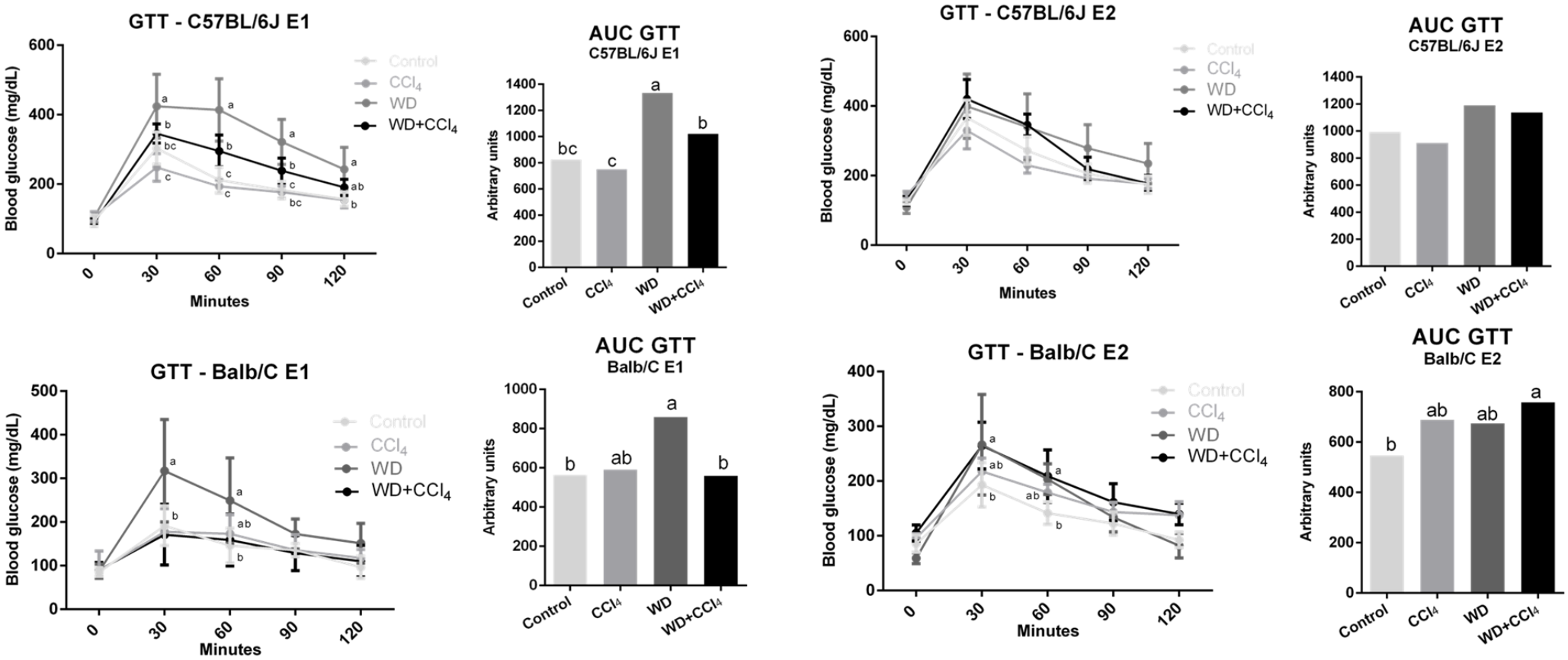

Figure 4. Effects of hybrid model of NASH in the glucose tolerance test (GTT) of C57BL/6J and BALB/c mice. The blood glucose levels were measured in different timepoints (0, 30, 60, 90, and 120 min.) by a glucometer and the area under the curve was measured and plotted. Different letters correspond to significative differences among the groups in each timepoint or total AUC. The data were analyzed by Two-way ANOVA and *pos hoc* Kruskal-Wallis test. Control [standard chow and 3x weekly intraperitoneal (i.p.) injections of corn oil vehicle]; carbon tetrachloride [CCl_4, 3x weekly i.p. injections of 10% corn oil solution of CCl_4, with doses of 0.25µL/g of body weight (b.w.) increased utmost of 1.50 µL/g b.w.]; western diet [WD, chow enriched with fat (20%) and sucrose (20%) and 3x weekly i.p. injections of corn oil vehicle]; WD+CCl4 (chow enriched with fat (20%) and sucrose (20%) and 3x weekly i.p injections of 10% corn oil solution of CCl_4, with doses of 0.25µL/g b.w. increased utmost of 1.50 µL/g b.w.); n = 5-6 (control and WD) or 7-9 (CCl_4 and WD+CCl_4). E1: first euthanasia timepoint; E2: second euthanasia timepoint.

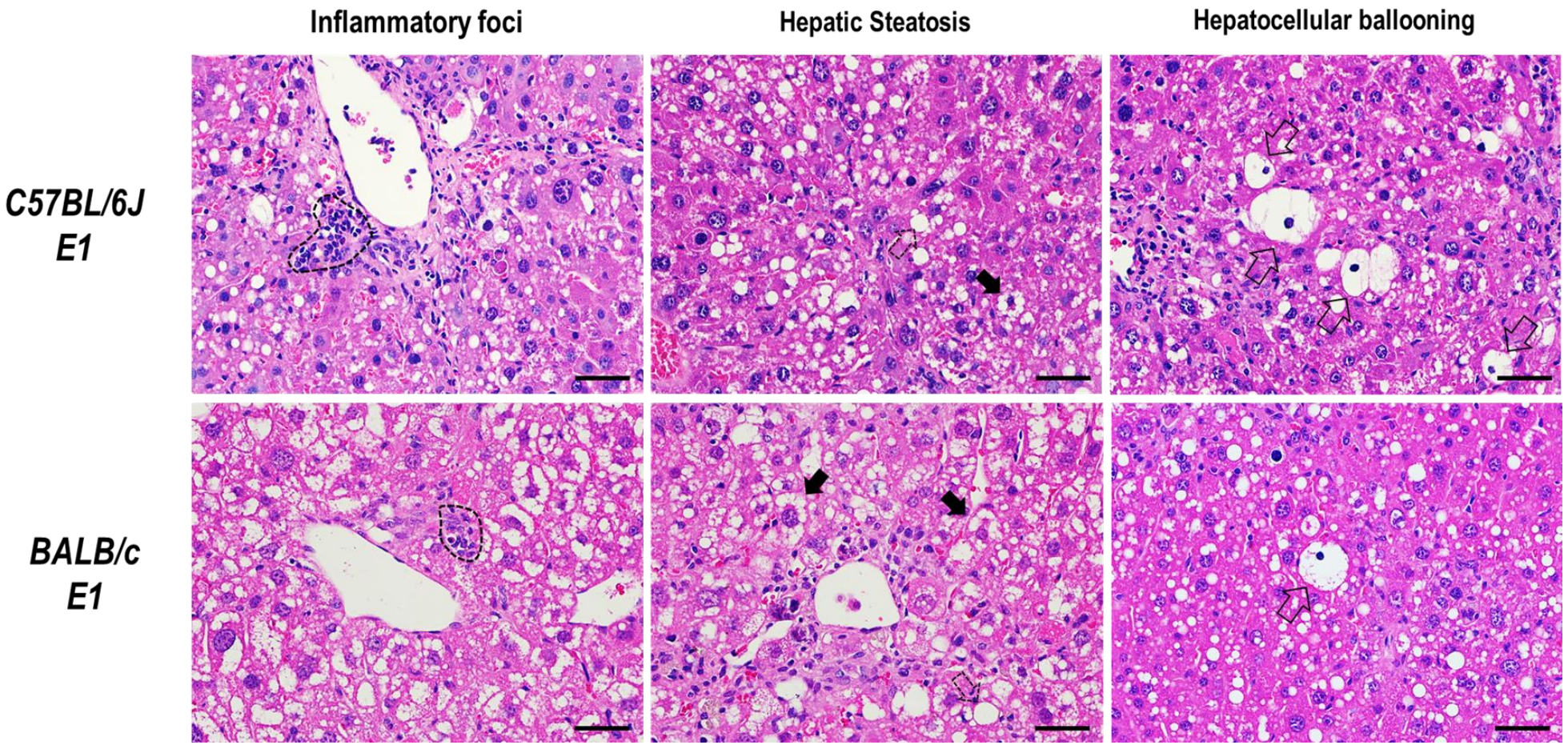

Figure 5. Effects of hybrid model of NASH in C57BL/6J and BALB/c mice. Representative photomicrographs (40x objective, scale bar=20µm) of morphologic features considered in NAS analysis in C57BL/6J or BALB/c mice, stained with hematoxilin and eosin (H&E). Dotted outlines indicating inflammatory foci, filled arrows indicates microvesicular steatosis, dotted arrow indicates macrovesicular steatosis, and unfilled arrows indicates hepatocellular ballooning. Control [standard chow and 3x weekly intraperitoneal (i.p.) injections of corn oil vehicle]; carbon tetrachloride [CCl_4, 3x weekly i.p. injections of 10% corn oil solution of CCl_4, with doses of 0.25µL/g of body weight (b.w.) increased utmost of 1.50 µL/g b.w.]; western diet [WD, chow enriched with fat (20%) and sucrose (20%) and 3x weekly i.p. injections of corn oil vehicle]; WD+CCl4 (chow enriched with fat (20%) and sucrose (20%) and 3x weekly i.p injections of 10% corn oil solution of CCl_4, with doses of 0.25µL/g b.w. increased utmost of 1.50 µL/g b.w.); n = 5-6 (control and WD) or 7-9 (CCl_4 and WD+CCl_4).

Table 3. Effects of the hybrid model of NASH on nonalcoholic fatty liver disease activity score (NAS, sum of macrovesicular and microvesicular steatosis, hepatocellular hypertrophy, and inflammatory foci scores) and hepatocellular ballooning in C57BL/6J and BALB/c mice.

Parameters	*C57BL/6J*							
	E1				*E2*			
	Control	*CCl_4*	*WD*	*WD+CCl_4*	*Control*	*CCl_4*	*WD*	*WD+CCl_4*
Macrovesicular steatosis (0-3)	0 (0;0)	0 (0;0)	0 (0;0)	0 (0;0)	0 (0;0)	0 (0;0)	0 (0;0)	0 (0;0)
Microvesicular steatosis (0-3)	0 (0;0)^{b}	0 (0;0)^{b}	0 (1.0;1.0)^{ab}	2.0 (2.0;2.0) ^{a}	0 (0;0)^{b}	0 (0;0)^{b}	1.3 (1.0;1.9)^{a}	1.0 (0.0;1.0)^{ab}
Hepatocellular hypertrophy (0-3)	0 (0;0)	0 (0;0)	0 (0;0)	0 (0;0)	0 (0;0)	0 (0;0)	0 (0;0)	0 (0;0)
Inflammatory foci (0-3)	0 (0;0)^{b}	2.0 (1.8;2.0)^{a}	0 (0;0)^{b}	1.5 (1.0;2.0)^{a}	0 (0;0)	1.0 (0.8;1.0)	0.3 (0.0;0.5)	0.5 (0.4;1.0)
Hepatocellular ballooning*	0 ± 0^{b}	3.2 ± 1.6^{a}	0 ± 0^{b}	2.9 ± 1.8^{a}	0 ± 0	0 ± 0	0 ± 0	0 ± 0
NAFLD activity score (0-12)	0 (0;0)^{b}	2.0 (2.0;2.8)^{a}	0 (0;0.8)^{b}	2.8 (2.0;4.7)^{a}	0 (0;0)^{b}	1.0 (0.8;1.0)^{ab}	1.8 (1.5;2.3)^{a}	1.3 (0.8;1,7)^{ab}
	BALB/c							
	E1				*E2*			
	Control	*CCl_4*	*WD*	*WD+CCl_4*	*Control*	*CCl_4*	*WD*	*WD+CCl_4*
Macrovesicular steatosis (0-3)	0 (0;0)^{b}	0 (0;0)^{b}	0.3 (0;0.5)^{a}	0 (0;0.5)^{b}	0 (0;0)^{b}	0 (0;0)^{b}	1.0 (0.6;1.8)^{a}	0 (0;1.0)^{b}
Microvesicular steatosis (0-3)	1.0 (1.0;1.0)^{b}	0 (1.0;1.0)^{b}	3.0 (3.0;3.0)^{a}	3.0 (3.0;3.0)^{a}	0 (0;0)^{b}	0 (0;0)^{b}	1.0 (0.6; 1.0)^{a}	0.3 (0;1.0)^{ab}
Hepatocellular hypertrophy (0-3)	0 (0;0)	0 (0;0)	0 (0;0)	0 (0;0)	0 (0;0)	0 (0;0)	0 (0;0)	0 (0;0)
Inflammatory foci (0-3)	0 (0;0)^{b}	1,3 (0.8;1.5)^{a}	0 (0;0)^{b}	0.5 (0.5;1.0)^{ab}	0 (0;0)	0 (0;0)	0 (0;0)	0.0 (0.0;0.5)
Hepatocellular ballooning*	0.0 ± 0.0	0.3 ± 0.0	0.00 ± 0.00	0.6 ± 0.8	0.0 ± 0.00	0.0 ± 0.0	0.0 ± 0.0	0.0 ± 0.0
NAFLD activity score (0-12)	0 (0;0)^{b}	1.5 (0;1.5)^{ab}	1.3 (1.0;1.5)^{ab}	4 (4.0;4.0)^{a}	0 (0;0)^{b}	0 (0;0)^{b}	2.5 (1.3;3.0)^{a}	0.8 (0.4;1.6)^{ab}

Table 2. Parameters were analyzed by Kruskall-Wallis and post-hoc Dunn's test, or One-Way ANOVA and post-hoc Tukey's test, and data were expressed as median and first and third quartile, or mean $\pm$ standard deviation (S.D) (*), respectively, according to mice strain and timepoint. The data were analyzed by Two-way ANOVA and *pos hoc* Kruskal-Wallis test. Control [standard chow and 3x weekly intraperitoneal (i.p.) injections of corn oil vehicle]; carbon tetrachloride [CCl_4, 3x weekly i.p. injections of 10% corn oil solution of CCl_4, with doses of 0.25µL/g of body weight (b.w.) increased utmost of 1.50 µL/g b.w.]; western diet [WD, chow enriched with fat (20%) and sucrose (20%) and 3x weekly i.p. injections of corn oil vehicle]; WD+CCl4 (chow enriched with fat (20%) and sucrose (20%) and 3x weekly i.p injections of 10% corn oil solution of CCl_4, with doses of 0.25µL/g b.w. increased utmost of 1.50 µL/g b.w.); n = 5-6 (control and WD) or 7-9 (CCl_4 and WD+CCl_4).

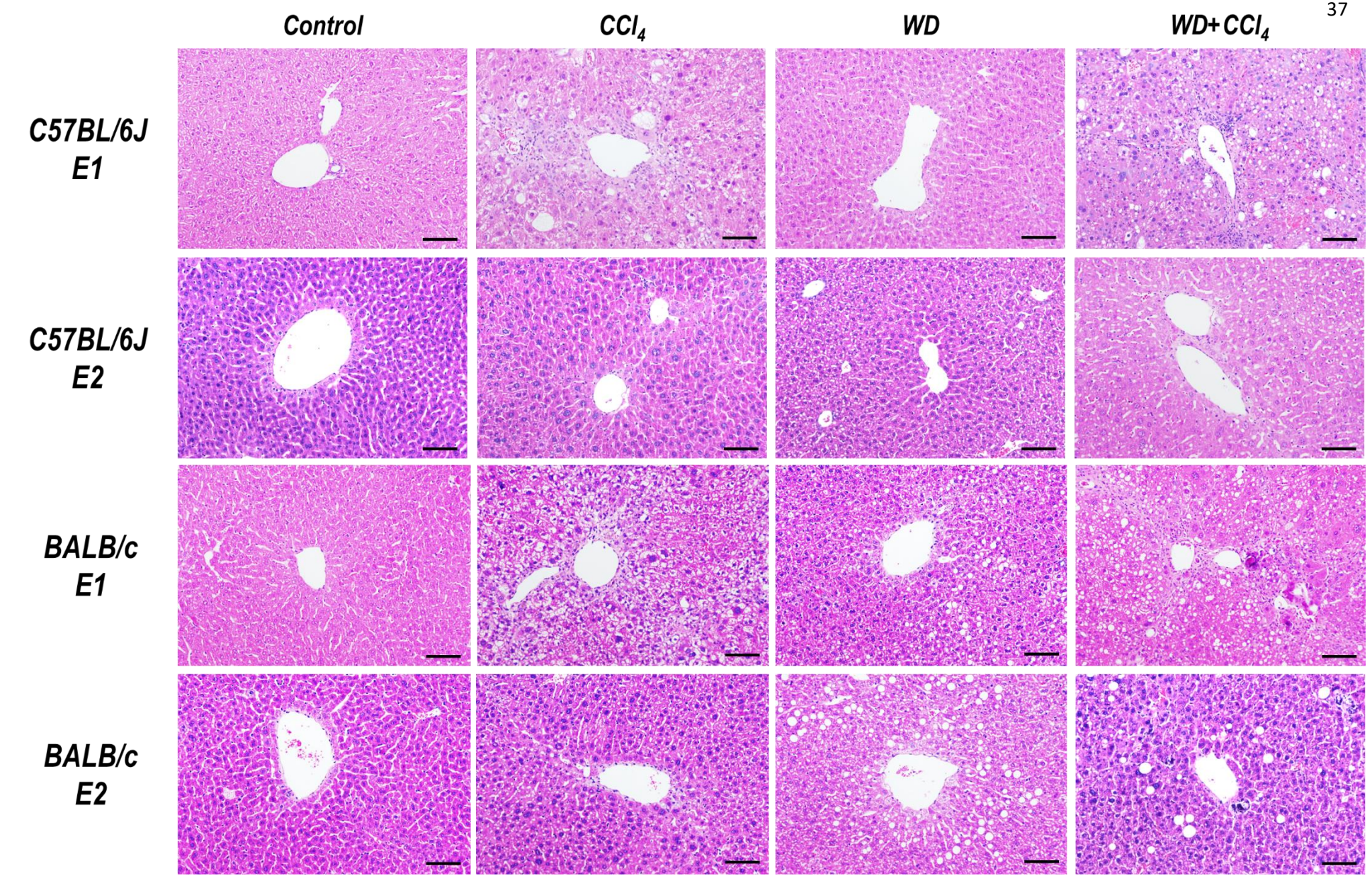

Figure 6. Effects of hybrid model of NASH in C57BL/6J and BALB/c mice. Representative photomicrographs (20x objective, scale bar=50µm) of C57BL/6J and BALB/c mice sections stained with hematoxilin and eosin (H&E). Control [standard chow and 3x weekly intraperitoneal (i.p.) injections of corn oil vehicle]; carbon tetrachloride [CCl_4, 3x weekly i.p. injections of 10% corn oil solution of CCl_4, with doses of 0.25µL/g of body weight (b.w.) increased utmost of 1.50 µL/g b.w.]; western diet [WD, chow enriched with fat (20%) and sucrose (20%) and 3x weekly i.p. injections of corn oil vehicle]; WD+CCl4 (chow enriched with fat (20%) and sucrose (20%) and 3x weekly i.p injections of 10% corn oil solution of CCl_4, with doses of 0.25µL/g b.w. increased utmost of 1.50 µL/g b.w.); n = 5-6 (control and WD) or 7-9 (CCl_4 and WD+CCl_4).

Although mild microvesicular steatosis was still observed in the WD+CCl_4 at E2 of both strains (p=0.002 and p=0.0024, respectively) (Table 3) (Figure 6), the inflammatory foci grading and the occurrence of hepatocellular ballooning strikingly decreased after ceasing the Cl_4 protocol, and a difference among groups was not observed. Hence, the NAS grading in the WD+CCl_4E2 groups of both strains also decreased and was similar to WD and CCl_4 groups (p=0.003 and p=0.0018, respectively) (Table 3) (Figure 6), suggesting that the CCl_4 exerts remarkable activity as an accelerator of NASH establishment and progression when combined with the WD protocol.

10. The hybrid protocol enhances lipid and collagen deposition and HSC activation

Since the WD protocol failed to maintain the morphological aspects of NASH at the E2 timepoint, only the E1 timepoint (both strains) was chosen for assessing the lipid deposit. The WD+CCl_4 group of C57BL/6J strain featured a moderate/severe steatosis profile, while a severe steatosis profile was observed in both WD+CCl_4 and WD BALB/c mice. Accordingly, the analysis of oil red-stained sections confirmed the effects observed in H&E-stained sections, by assessing that the NASH-inducing protocol enhanced the lipid deposit in C57BL/6J mice ($p<0.0001$), but not in BALB/c mice since both WD+CCl_4 and WD groups featured similar levels of lipid droplets in the hepatic parenchyma ($p<0.0001$) (Figure 7). In parallel, we observed that the hybrid protocol enhances the deposit of collagen independently of mice strain ($p<0.0001$) at E1 (Figures 8 and 9). Surprisingly, after ceasing the CCl_4, only the WD+CCl_4 group of BALB/c mice displayed an enhanced deposit of collagen compared to other groups ($p<0.0001$) (Figure 9), in contrast to C57BL/6J mice, whose WD+CCl_4 and CCl_4 groups of C57BL/6J mice featured similar levels of collagen deposition ($p<0.0001$) (Figure 8).

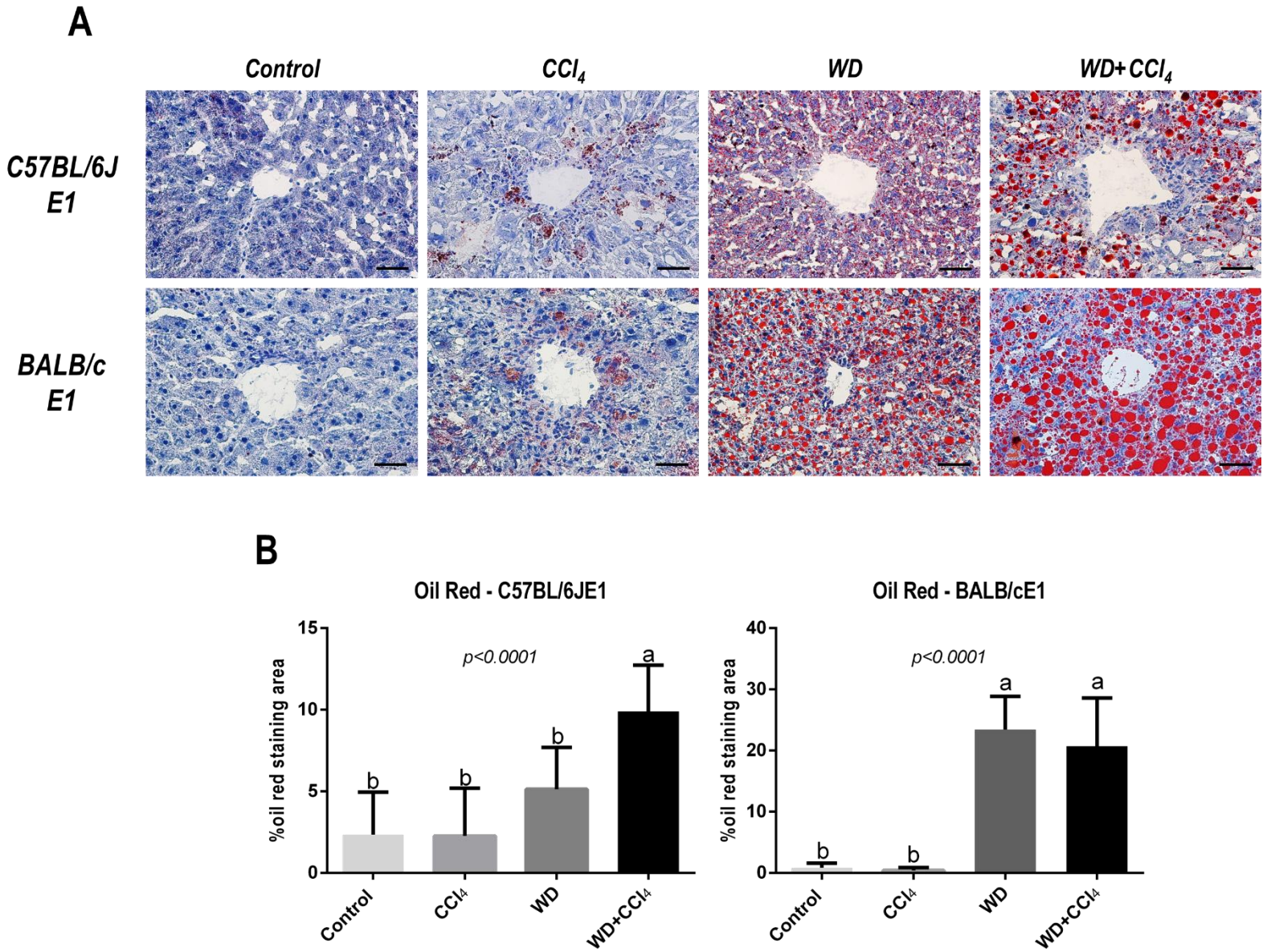

Figure 7. Effects of hybrid model of NASH over the lipid deposition in C57BL/6J and BALB/c mice. **(A)** Representative photomicrographs (20x objective, scale bar=50µm) of sections stained with oil red-O solution. **(B)** Semiquantitative analysis of lipid deposition (% of oil red staining area) in hepatic sections of C57BL/6J and BALB/c mice. Different letters correspond to statistical differences among groups. Data were analyzed by One-way ANOVA and *pos hoc* Tukey test, and it were considered statistically different when p<0.05. Control [standard chow and 3x weekly intraperitoneal (i.p.) injections of corn oil vehicle]; carbon tetrachloride [CCl_4, 3x weekly i.p. injections of 10% corn oil solution of CCl_4, with doses of 0.25µL/g of body weight (b.w.) increased utmost of 1.50 µL/g b.w.]; western diet [WD, chow enriched with fat (20%) and sucrose (20%) and 3x weekly i.p. injections of corn oil vehicle]; WD+CCl4 (chow enriched with fat (20%) and sucrose (20%) and 3x weekly i.p injections of 10% corn oil solution of CCl_4, with doses of 0.25µL/g b.w. increased utmost of 1.50 µL/g b.w.); n = 6 (control and WD) or 6 (CCl_4 and WD+CCl_4).

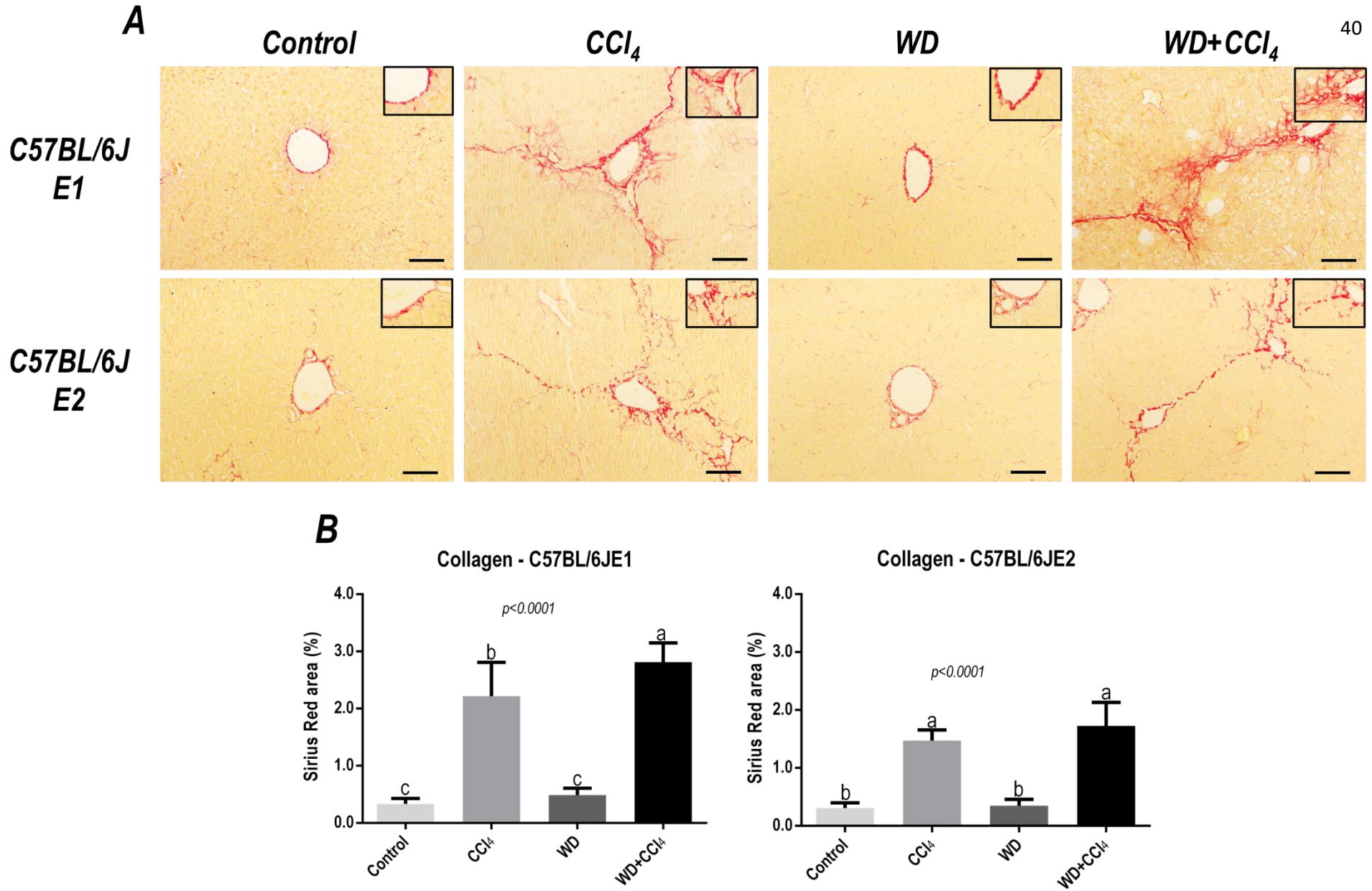

Figure 8. Effects of hybrid model of NASH over the collagen deposition in C57BL/6J mice. **(A)** Representative photomicrographs (20x objective, scale bar=50µm) of sections stained with sirius red. **(B)** Semiquantitative analysis of collagen deposition (% of sirius red area) in hepatic sections of C57BL/6J mice. Different letters correspond to statistical differences among groups. Data were analyzed by One-way ANOVA and *pos hoc* Tukey test, and it were considered statistically different when $p<0.05$. Control [standard chow and 3x weekly intraperitoneal (i.p.) injections of corn oil vehicle]; carbon tetrachloride [CCl_4, 3x weekly i.p. injections of 10% corn oil solution of CCl_4, with doses of 0.25µL/g of body weight (b.w.) increased utmost of 1.50 µL/g b.w.]; western diet [WD, chow enriched with fat (20%) and sucrose (20%) and 3x weekly i.p. injections of corn oil vehicle]; WD+CCl4 (chow enriched with fat (20%) and sucrose (20%) and 3x weekly i.p injections of 10% corn oil solution of CCl_4, with doses of 0.25µL/g b.w. increased utmost of 1.50 µL/g b.w.); n = 5-6 (control and WD) or 7-9 (CCl_4 and WD+CCl_4).

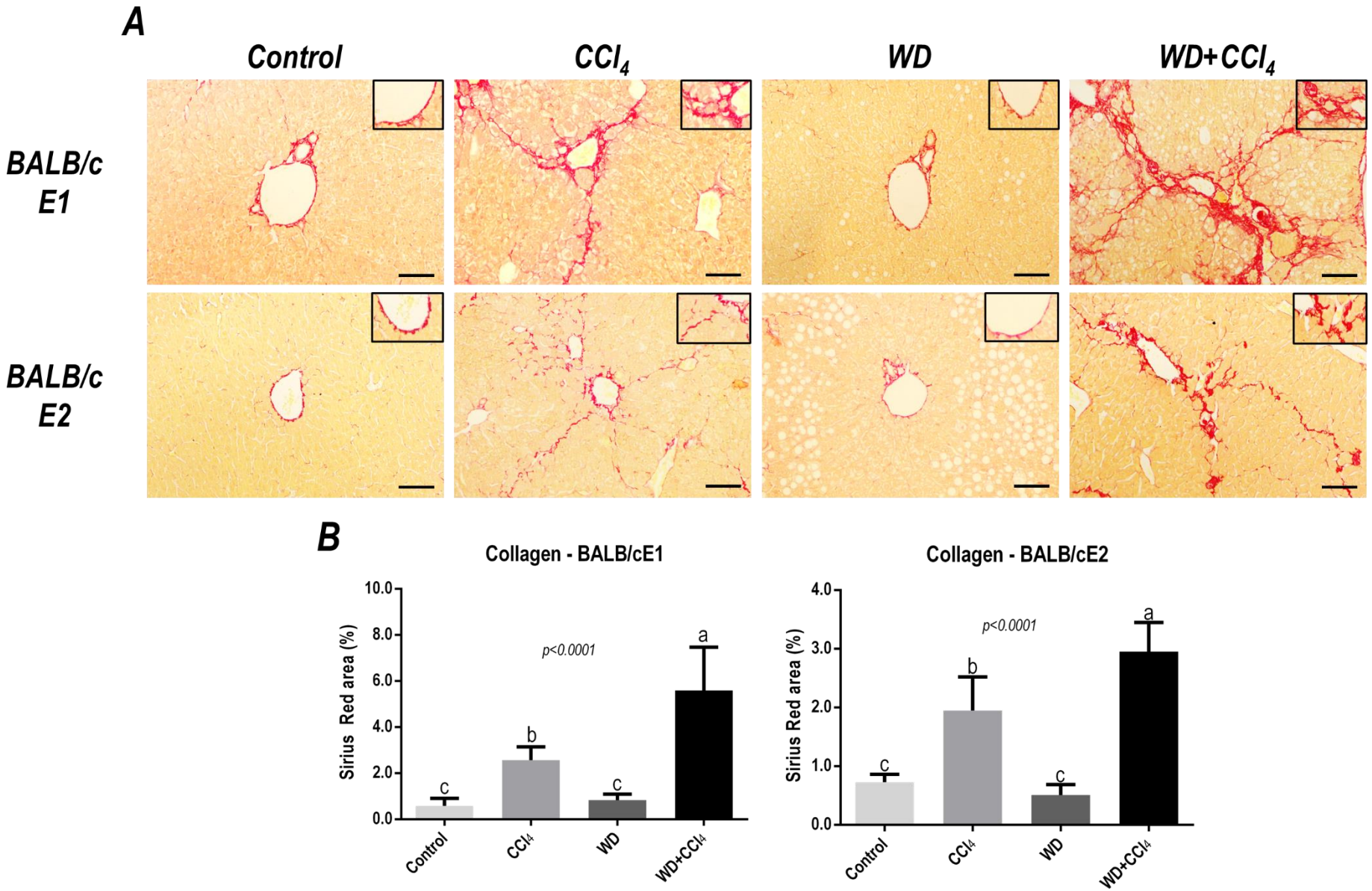

Figure 9. Effects of hybrid model of NASH over the collagen deposition in BALB/c mice. **(A)** Representative photomicrographs (20x objective, scale bar=50µm) of sections stained with sirius red. **(B)** Semiquantitative analysis of collagen deposition (% of sirius red area) in hepatic sections of BALB/c mice. Different letters correspond to statistical differences among groups. Data were analyzed by One-way ANOVA and *pos hoc* Tukey test, and it were considered statistically different when $p<0.05$. Control [standard chow and 3x weekly intraperitoneal (i.p.) injections of corn oil vehicle]; carbon tetrachloride [CCl_4, 3x weekly i.p. injections of 10% corn oil solution of CCl_4, with doses of 0.25µL/g of body weight (b.w.) increased utmost of 1.50 µL/g b.w.]; western diet [WD, chow enriched with fat (20%) and sucrose (20%) and 3x weekly i.p. injections of corn oil vehicle]; WD+CCl4 (chow enriched with fat (20%) and sucrose (20%) and 3x weekly i.p injections of 10% corn oil solution of CCl_4, with doses of 0.25µL/g b.w. increased utmost of 1.50 µL/g b.w.); n = 5-6 (control and WD) or 7-9 (CCl_4 and WD+CCl_4).

In order to understand the underlying mechanism related to collagen synthesis and further deposition, we assessed the immunoreactivity for α-SMA, indicative of HSC activation. In agreement with the sirius red data, we observed that the hybrid protocol of NASH enhanced the levels of α-smooth muscle actin (α-SMA) independently of the mice strain ($p<0.0001$) (Figures 10 and 11). Additionally, after ceasing the CCl_4 protocol, the C57BL/6J WD+CCl_4 mice maintained the increased levels of α-SMA ($p<0.0001$) (Figure 10), while the BALB/c WD+CCl_4 group featured a rising trend compared to other groups ($p=0.0009$) (Figure 11). Taken together, we provide evidence that the hybrid protocol enhances the activation of HSC, due to both the lipotoxicity and hepatocellular injuries caused by lipid accumulation and CCl_4-induced lipid peroxidation, leading to enhanced collagen deposition.

11. The hybrid protocol enhances the number of Ki67$^+$, casp3$^+$, and CD68$^+$ cells

We observed that the CCl_4-induced groups increased the number of Ki67+ cells in C57BL/6J ($p<0.0001$) (Figure 12), whereas the hybrid protocol enhanced the number of Ki67+ cells in the hepatic parenchyma of BALB/c mice ($p<0.0001$) (Figure 13). Conversely, after ceasing the CCl_4 protocol, only C57BL/6J mice featured an increased number of Ki67$^+$ cells ($p<0.0001$) (Figure 12). Additionally, after 8 weeks of protocol, the CCl_4-receiving groups of C57BL/6J mice showed an increased number of casp3+ cells ($p<0.0001$) (Figure 14), whereas the hybrid protocol enhanced the number of casp3+ cells in BALB/c mice ($p<0.0001$) (Figure 15). Surprisingly, after the stopping CCl_4 protocol, an increased number of casp3+ cells were still observed in CCl_4 and WD+CCl_4 groups in both strains ($p=0.0007$ and $p=0.0003$, respectively) (Figures 14 and 15). Moreover, the hepatic resident macrophages, or Kupffer cells (KC), and monocyte-derived macrophages (MDM) have been suggested as pivotal cells involved in the steatosis transition to NASH, due to its capacity to exert pro-oxidant/inflammatory activities.

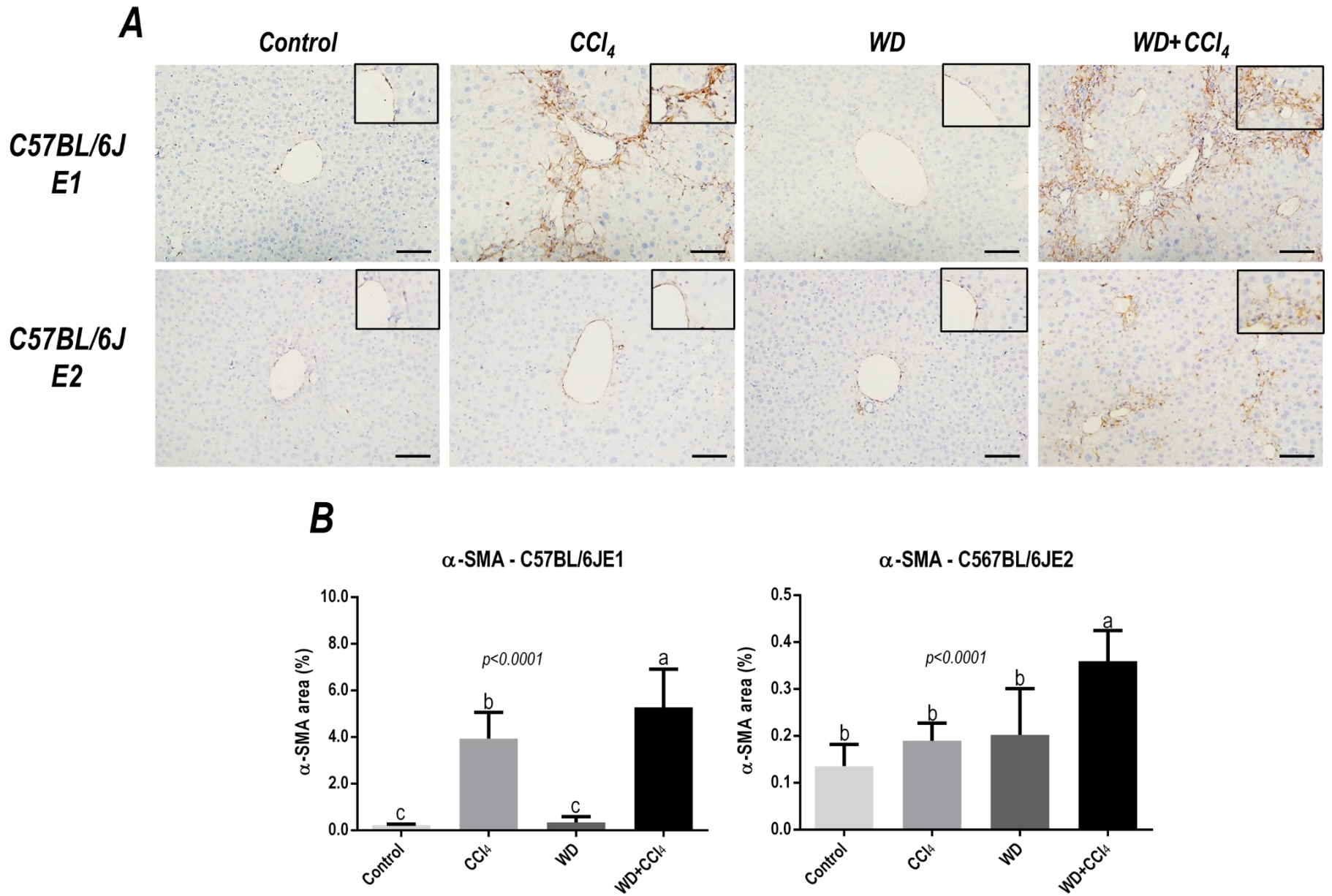

Figure 10. Effects of hybrid model of NASH over the α-smooth muscle actin (α-SMA) expression in C57BL/6J mice. **(A)** Representative photomicrographs (20x objective, scale bar=50µm) of sections immunoreacted for α-smooth muscle actin (α-SMA). **(B)** Semiquantitative analysis of α-SMA expression (% of α-SMA area) in hepatic sections of C57BL/6J mice. Different letters correspond to statistical differences among groups. Data were analyzed by One-way ANOVA and *pos hoc* Tukey test, and it were considered statistically different when p<0.05. Control [standard chow and 3x weekly intraperitoneal (i.p.) injections of corn oil vehicle]; carbon tetrachloride [CCl_4, 3x weekly i.p. injections of 10% corn oil solution of CCl_4, with doses of 0.25µL/g of body weight (b.w.) increased utmost of 1.50 µL/g b.w.]; western diet [WD, chow enriched with fat (20%) and sucrose (20%) and 3x weekly i.p. injections of corn oil vehicle]; WD+CCl4 (chow enriched with fat (20%) and sucrose (20%) and 3x weekly i.p injections of 10% corn oil solution of CCl_4, with doses of 0.25µL/g b.w. increased utmost of 1.50 µL/g b.w.); n = 5-6 (control and WD) or 7-9 (CCl_4 and WD+CCl_4).

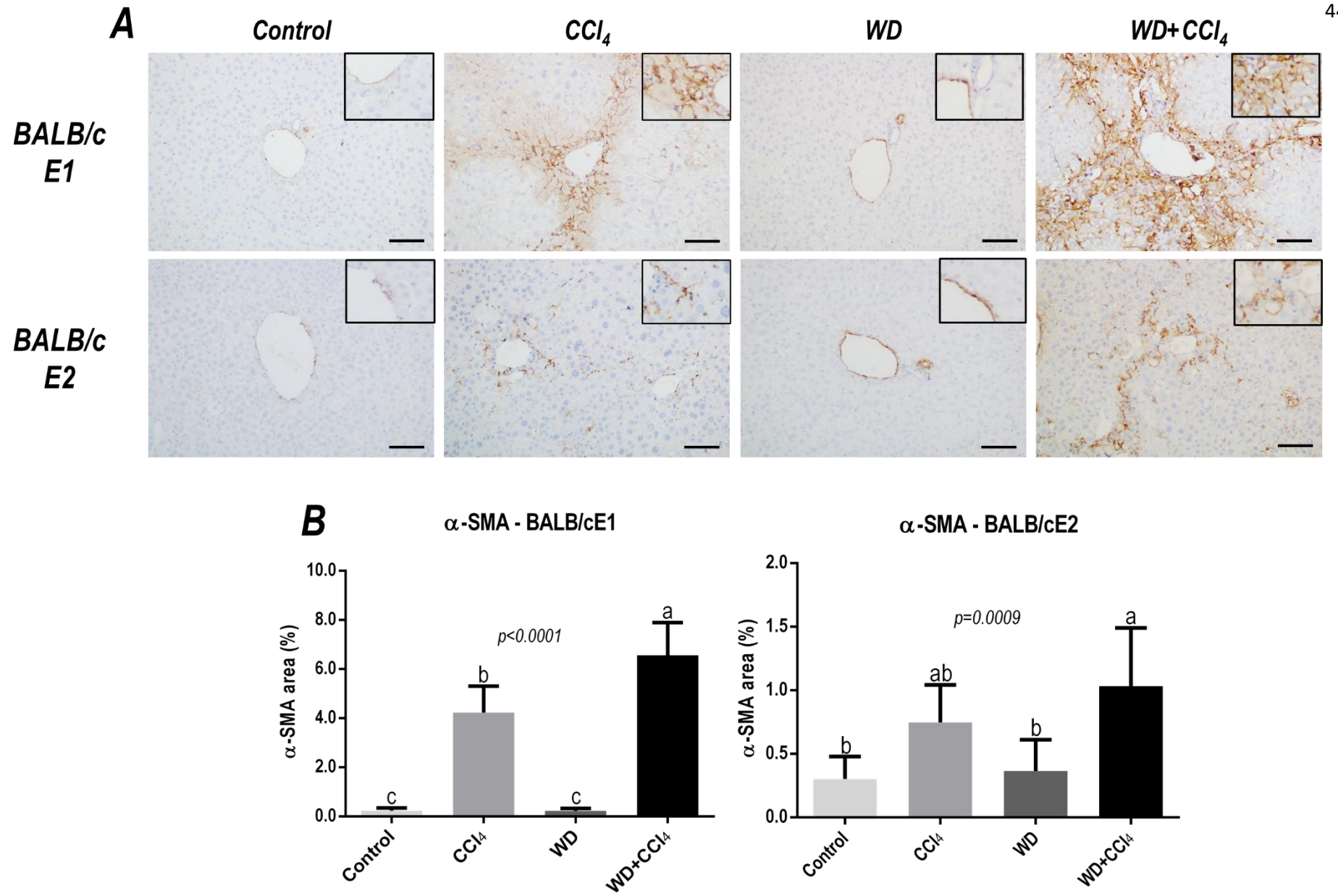

Figure 11. Effects of hybrid model of NASH over the α-smooth muscle actin (α-SMA) expression in BALB/c mice. **(A)** Representative photomicrographs (20x objective, scale bar=50µm) of sections immunoreacted for α-smooth muscle actin (α-SMA). **(B)** Semiquantitative analysis of α-SMA expression (% of α-SMA area) in hepatic sections of BALB/c mice. Different letters correspond to statistical differences among groups. Data were analyzed by One-way ANOVA and *pos hoc* Tukey test, and it were considered statistically different when $p<0.05$. Control [standard chow and 3x weekly intraperitoneal (i.p.) injections of corn oil vehicle]; carbon tetrachloride [CCl_4, 3x weekly i.p. injections of 10% corn oil solution of CCl_4, with doses of 0.25µL/g of body weight (b.w.) increased utmost of 1.50 µL/g b.w.]; western diet [WD, chow enriched with fat (20%) and sucrose (20%) and 3x weekly i.p. injections of corn oil vehicle]; WD+CCl4 (chow enriched with fat (20%) and sucrose (20%) and 3x weekly i.p injections of 10% corn oil solution of CCl_4, with doses of 0.25µL/g b.w. increased utmost of 1.50 µL/g b.w.); n = 5-6 (control and WD) or 7-9 (CCl_4 and WD+CCl_4).

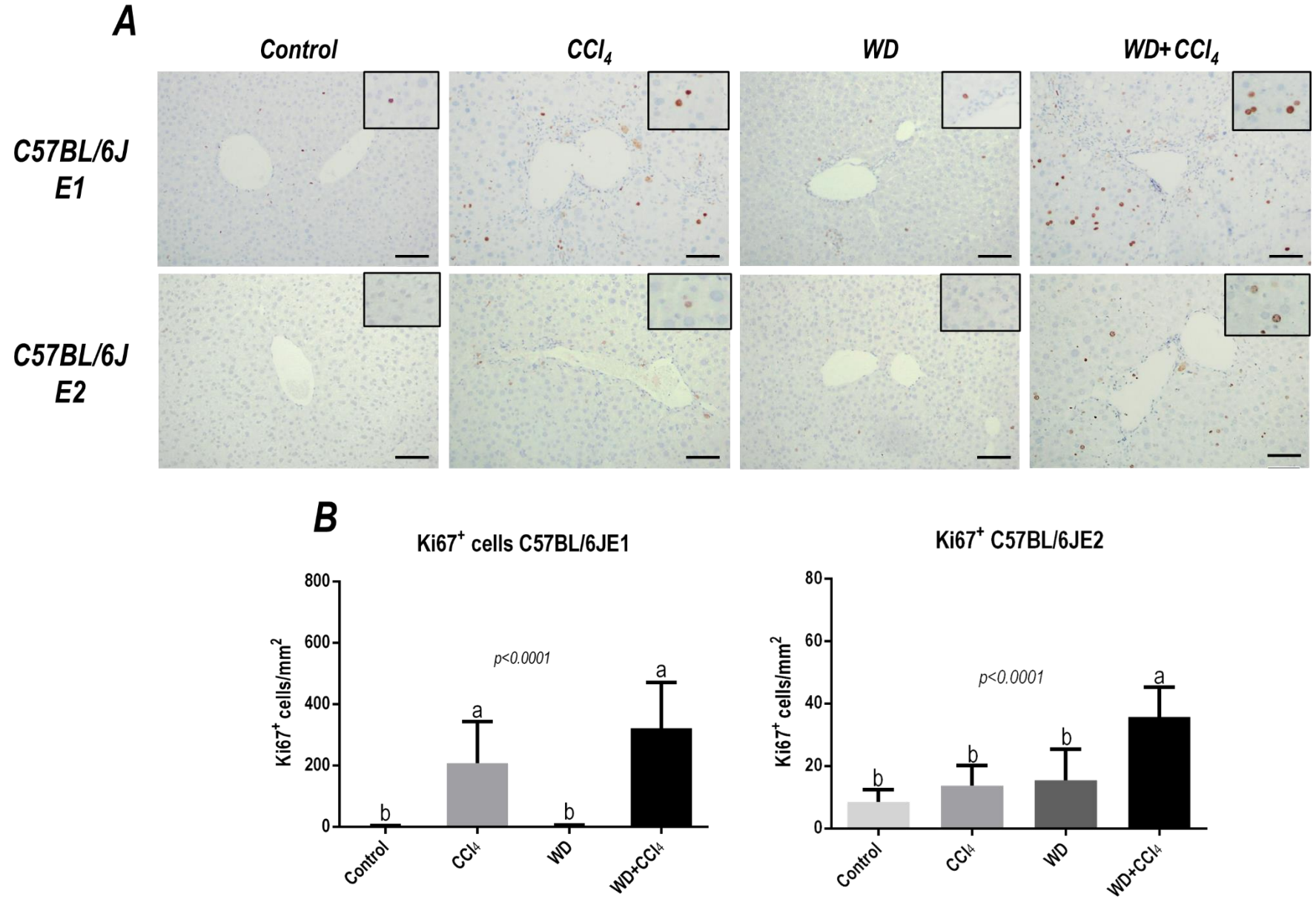

Figure 12. Effects of hybrid model of NASH over the number of hepatic Ki67+ cells in C57BL/6J mice. **(A)** Representative photomicrographs (20x objective, scale bar=50µm) of sections immunoreacted for Ki67+. **(B)** Semiquantitative analysis of the number of Ki67+ cells in hepatic sections of C57BL/6J mice. Different letters correspond to statistical differences among groups. Data were analyzed by One-way ANOVA and *pos hoc* Tukey test, and it were considered statistically different when p<0.05. Control [standard chow and 3x weekly intraperitoneal (i.p.) injections of corn oil vehicle]; carbon tetrachloride [CCl_4, 3x weekly i.p. injections of 10% corn oil solution of CCl_4, with doses of 0.25µL/g of body weight (b.w.) increased utmost of 1.50 µL/g b.w.]; western diet [WD, chow enriched with fat (20%) and sucrose (20%) and 3x weekly i.p. injections of corn oil vehicle]; WD+CCl_4 (chow enriched with fat (20%) and sucrose (20%) and 3x weekly i.p injections of 10% corn oil solution of CCl_4, with doses of 0.25µL/g b.w. increased utmost of 1.50 µL/g b.w.); n = 5-6 (control and WD) or 7-9 (CCl_4 and WD+CCl_4).

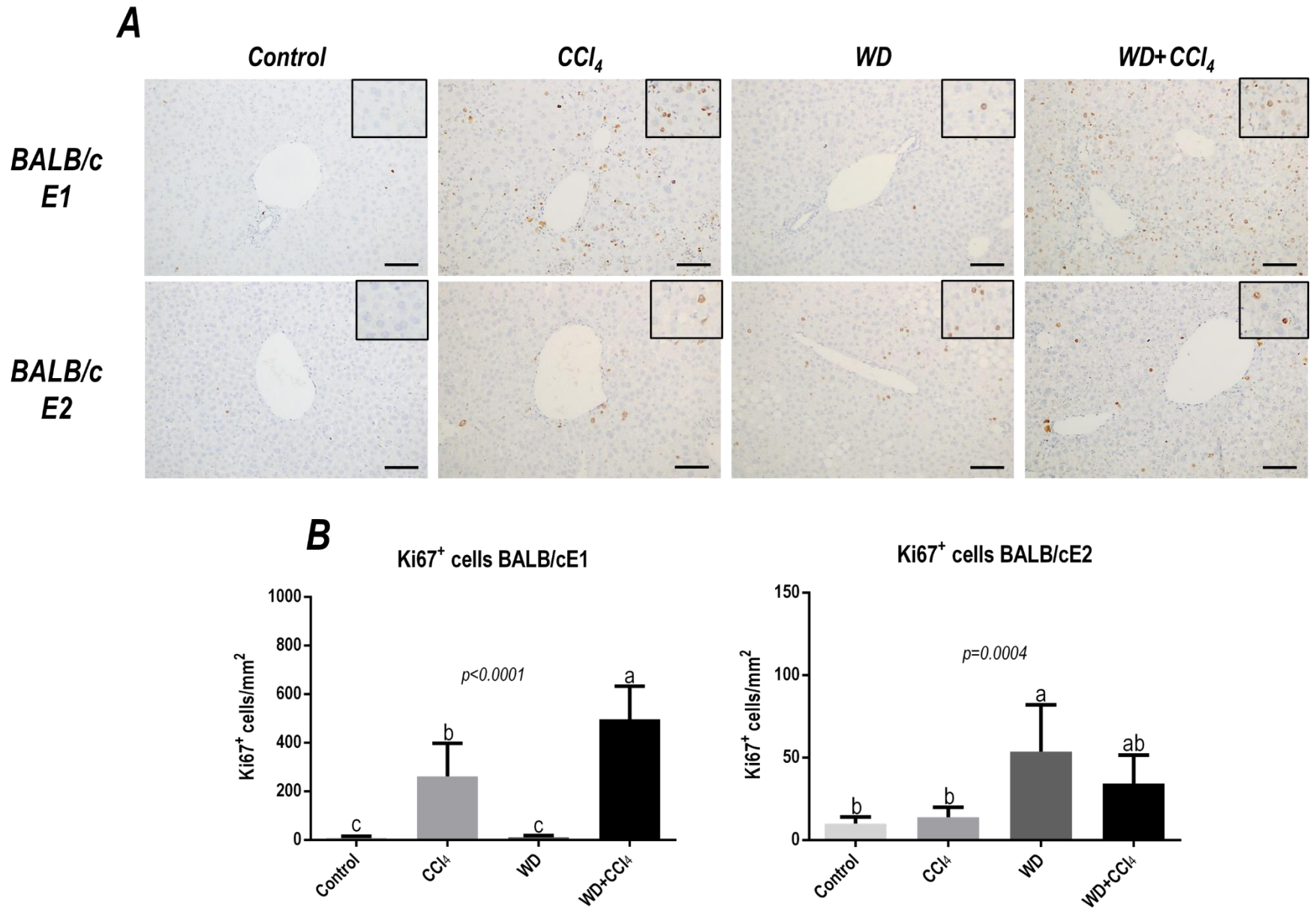

Figure 13. Effects of hybrid model of NASH over the number of hepatic Ki67⁺ cells in BALB/c mice. **(A)** Representative photomicrographs (20x objective, scale bar=50µm) of sections immunoreacted for Ki67⁺. **(B)** Semiquantitative analysis of the number of Ki67⁺ cells in hepatic sections of BALB/c mice. Different letters correspond to statistical differences among groups. Data were analyzed by One-way ANOVA and *pos hoc* Tukey test, and it were considered statistically different when $p<0.05$. Control [standard chow and 3x weekly intraperitoneal (i.p.) injections of corn oil vehicle]; carbon tetrachloride [CCl_4, 3x weekly i.p. injections of 10% corn oil solution of CCl_4, with doses of 0.25µL/g of body weight (b.w.) increased utmost of 1.50 µL/g b.w.]; western diet [WD, chow enriched with fat (20%) and sucrose (20%) and 3x weekly i.p. injections of corn oil vehicle]; WD+CCl4 (chow enriched with fat (20%) and sucrose (20%) and 3x weekly i.p injections of 10% corn oil solution of CCl_4, with doses of 0.25µL/g b.w. increased utmost of 1.50 µL/g b.w.); n = 5-6 (control and WD) or 7-9 (CCl_4 and WD+CCl_4).

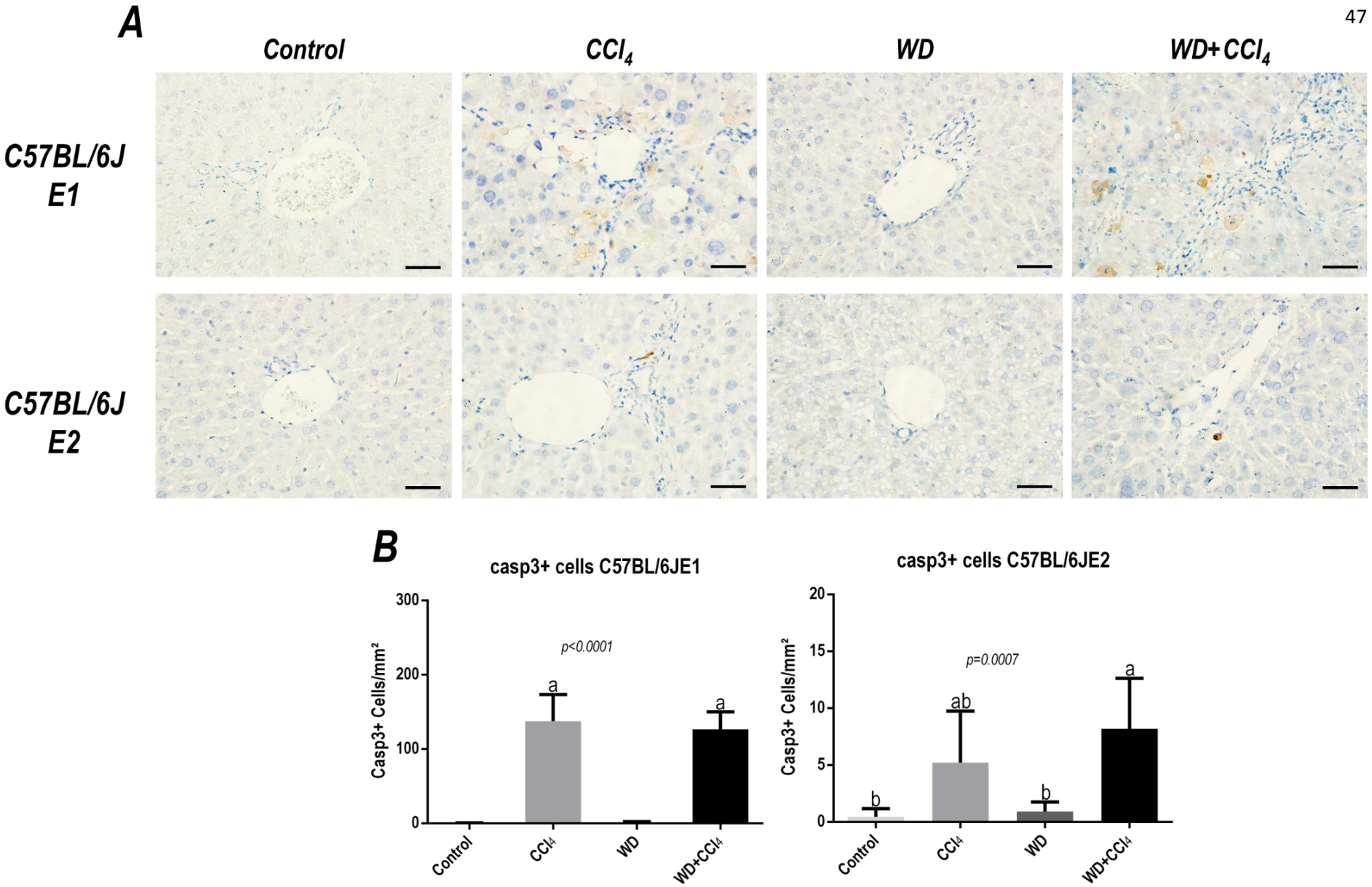

Figure 14. Effects of hybrid model of NASH over the number of hepatic casp3⁺ cells in C57BL/6J mice. **(A)** Representative photomicrographs (20x objective, scale bar=50µm) of sections immunoreacted for casp3⁺ .**(B)** Semiquantitative analysis of the number of casp3⁺ cells in hepatic sections of C57BL/6J mice. Different letters correspond to statistical differences among groups. Data were analyzed by One-way ANOVA and *pos hoc* Tukey test, and it were considered statistically different when $p<0.05$. Control [standard chow and 3x weekly intraperitoneal (i.p.) injections of corn oil vehicle]; carbon tetrachloride [CCl_4, 3x weekly i.p. injections of 10% corn oil solution of CCl_4, with doses of 0.25µL/g of body weight (b.w.) increased utmost of 1.50 µL/g b.w.]; western diet [WD, chow enriched with fat (20%) and sucrose (20%) and 3x weekly i.p. injections of corn oil vehicle]; WD+CCl4 (chow enriched with fat (20%) and sucrose (20%) and 3x weekly i.p injections of 10% corn oil solution of CCl_4, with doses of 0.25µL/g b.w. increased utmost of 1.50 µL/g b.w.); n = 5-6 (control and WD) or 7-9 (CCl_4 and WD+CCl_4).

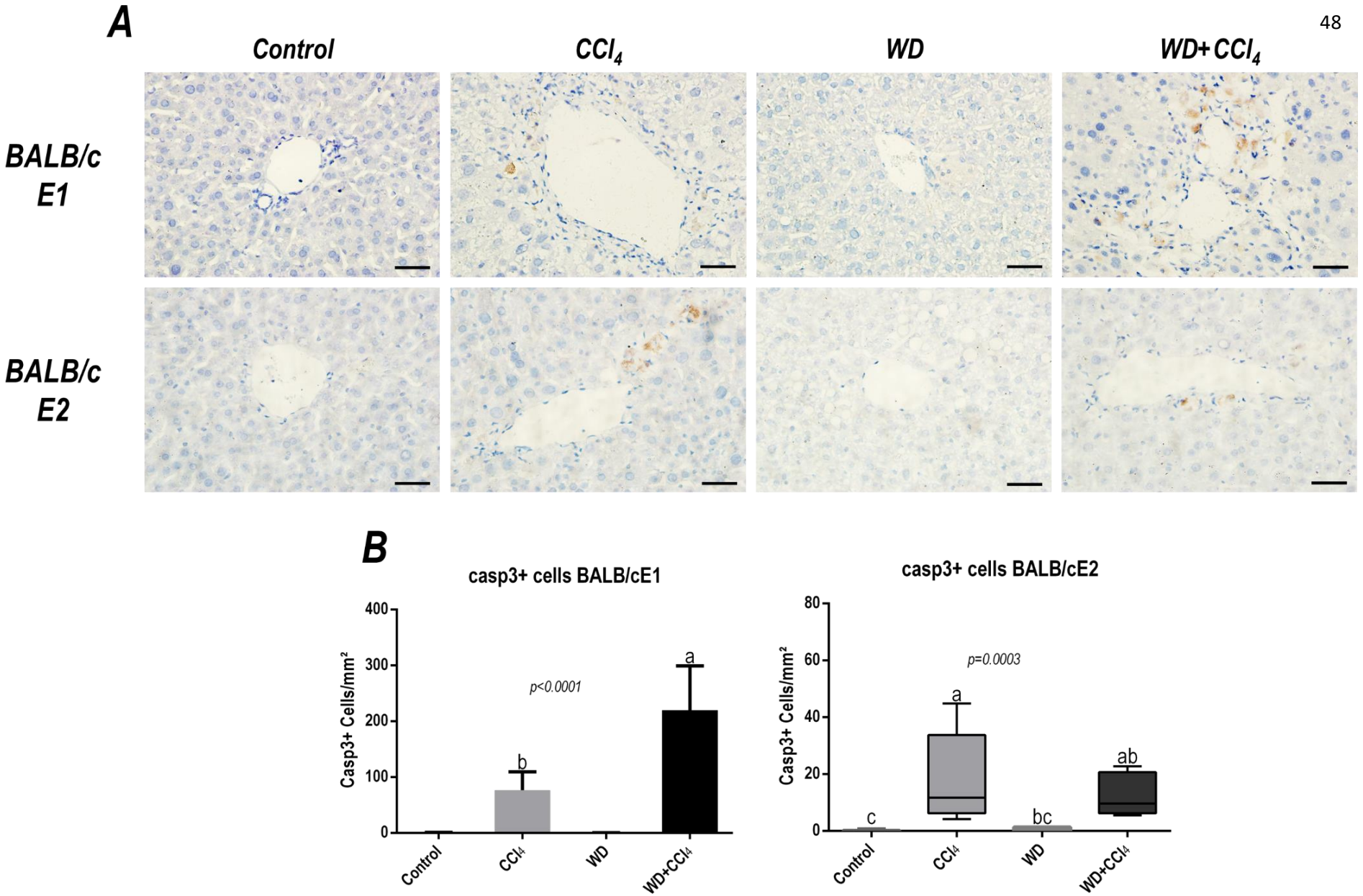

Figure 15. Effects of hybrid model of NASH over the number of hepatic casp3⁺ cells in BALB/c mice. **(A)** Representative photomicrographs (20x objective, scale bar=50µm) of sections immunoreacted for casp3⁺. **(B)** Semiquantitative analysis of the number of casp3⁺ cells in hepatic sections of BALB/c mice. Different letters correspond to statistical differences among groups. Data were analyzed by One-way ANOVA and *pos hoc* Tukey test, and it were considered statistically different when $p<0.05$. Control [standard chow and 3x weekly intraperitoneal (i.p.) injections of corn oil vehicle]; carbon tetrachloride [CCl_4, 3x weekly i.p. injections of 10% corn oil solution of CCl_4, with doses of 0.25µL/g of body weight (b.w.) increased utmost of 1.50 µL/g b.w.]; western diet [WD, chow enriched with fat (20%) and sucrose (20%) and 3x weekly i.p. injections of corn oil vehicle]; WD+CCl4 (chow enriched with fat (20%) and sucrose (20%) and 3x weekly i.p injections of 10% corn oil solution of CCl_4, with doses of 0.25µL/g b.w. increased utmost of 1.50 µL/g b.w.); n = 5-6 (control and WD) or 7-9 (CCl_4 and WD+CCl_4).

The hybrid protocol of NASH increased the number of CD68+ cells. Kinoshita *et al*. [19] described that the membrane receptor CD68 enables the identification of KC the fraction which exerts phagocytic and enhanced ROS-producing activity. Indeed, a strain-dependent response was observed, since, after 8 weeks of hybrid protocol, only C57BL/6J mice featured an enhanced number of hepatic $CD68^+$ cells ($p<0.0001$) (Figure 16), compared to other groups, while CCl_4-induced mice displayed an increased number of CD68+ cells in BALB/c mice ($p<0.0001$) (Figure 17). Surprisingly, after CCl_4-ceasing, WD+CCl_4 groups of both C57BL/6J and BALB/c mice still featured an increased number of $CD68^+$ cells compared to the respective control groups ($p=0.003$ and $p<0.0001$, respectively) (Figure 16 and 17). Thus, we suggest that the pro-oxidant and lipotoxic hepatic milieu modulates hepatocytes phenotypical profile, leading to the CD68+ cells recruitment, and triggering death-related pathways that might contribute to NASH establishment and progression.

12. The hybrid protocol enhances the hypertrophy of adipocytes and the number of $CD68^+$ and mast cells

Only in the WD+CCl_4 group of BALB/c mice ($p<0.0001$), we observed the occurrence of the hypertrophy of adipocytes, compared to the control group (Figures 18 and 19), suggesting different AT stress-induced responses between the strains. Additionally, the hybrid protocol enhanced the number of $CD68^+$ cells in both C57BL/6J and BALB/c mice ($p=0.0432$ and $p=0.0004$, respectively) (Figures 20 and 21), although only C57BL/6J mice still featured an increased number of CD68+ cells after CCl_4 ceasing ($p<0.0001$) (Figure 21). Although both strains featured higher levels of $CD68^+$ cells and hence, inflammation, only in BALB/c mice, the hybrid protocol enhanced the number of mast cells (MC) ($p=0.0083$) compared to other groups (Figures 22 and 23). After the CCl_4-ceasing, a higher number of MC was not observed in both strains.

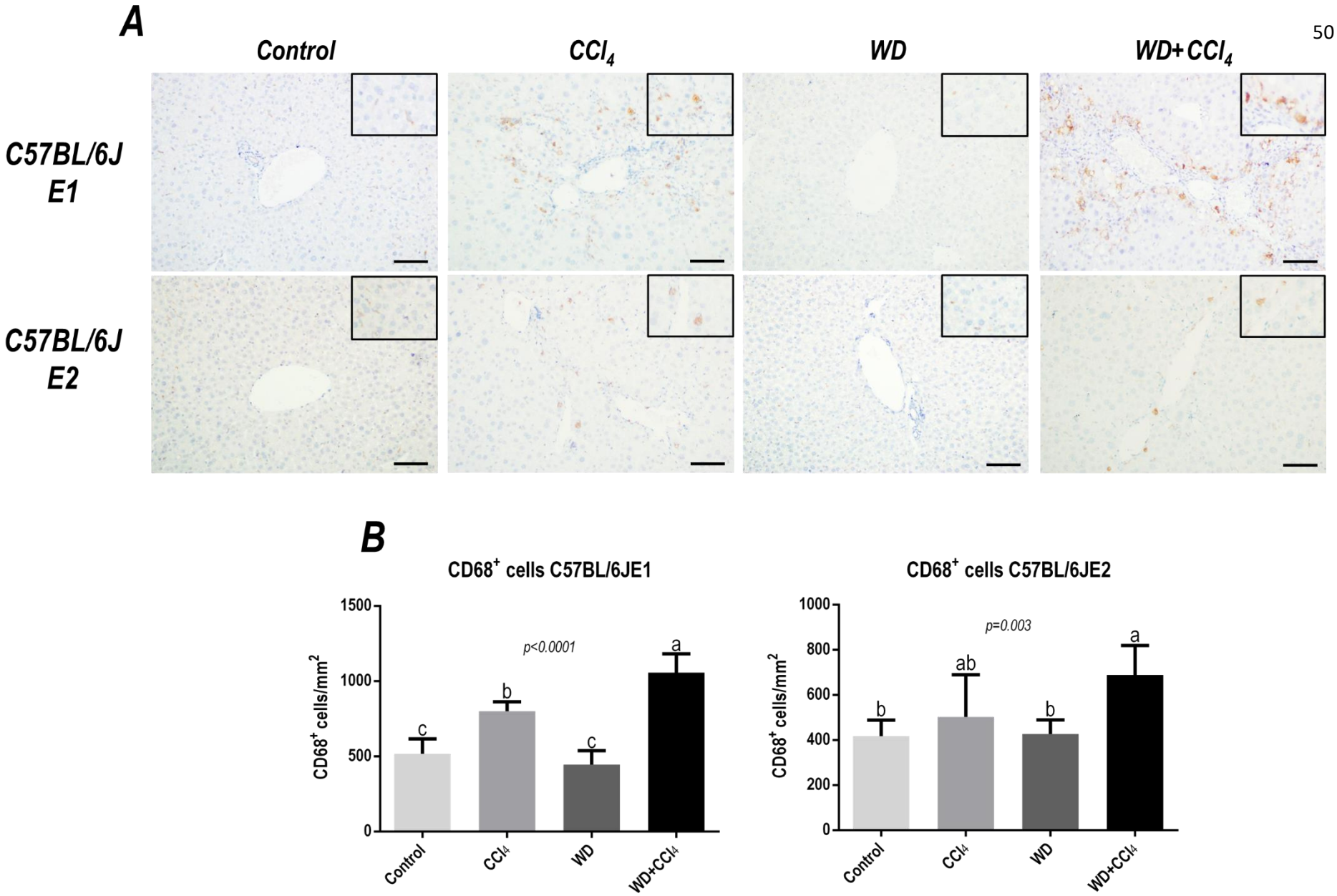

Figure 16. Effects of hybrid model of NASH over the number of hepatic CD68⁺ cells in C57BL/6J mice. **(A)** Representative photomicrographs (40x objective, scale bar=50µm) of sections immunoreacted for CD68⁺. **(B)** Semiquantitative analysis of the number of CD68⁺ cells in hepatic sections of C57BL/6J mice. Different letters correspond to statistical differences among groups. Data were analyzed by One-way ANOVA and *pos hoc* Tukey test, and it were considered statistically different when $p<0.05$. Control [standard chow and 3x weekly intraperitoneal (i.p.) injections of corn oil vehicle]; carbon tetrachloride [CCl_4, 3x weekly i.p. injections of 10% corn oil solution of CCl_4, with doses of 0.25µL/g of body weight (b.w.) increased utmost of 1.50 µL/g b.w.]; western diet [WD, chow enriched with fat (20%) and sucrose (20%) and 3x weekly i.p. injections of corn oil vehicle]; WD+CCl4 (chow enriched with fat (20%) and sucrose (20%) and 3x weekly i.p injections of 10% corn oil solution of CCl_4, with doses of 0.25µL/g b.w. increased utmost of 1.50 µL/g b.w.); n = 5-6 (control and WD) or 7-9 (CCl_4 and WD+CCl_4).

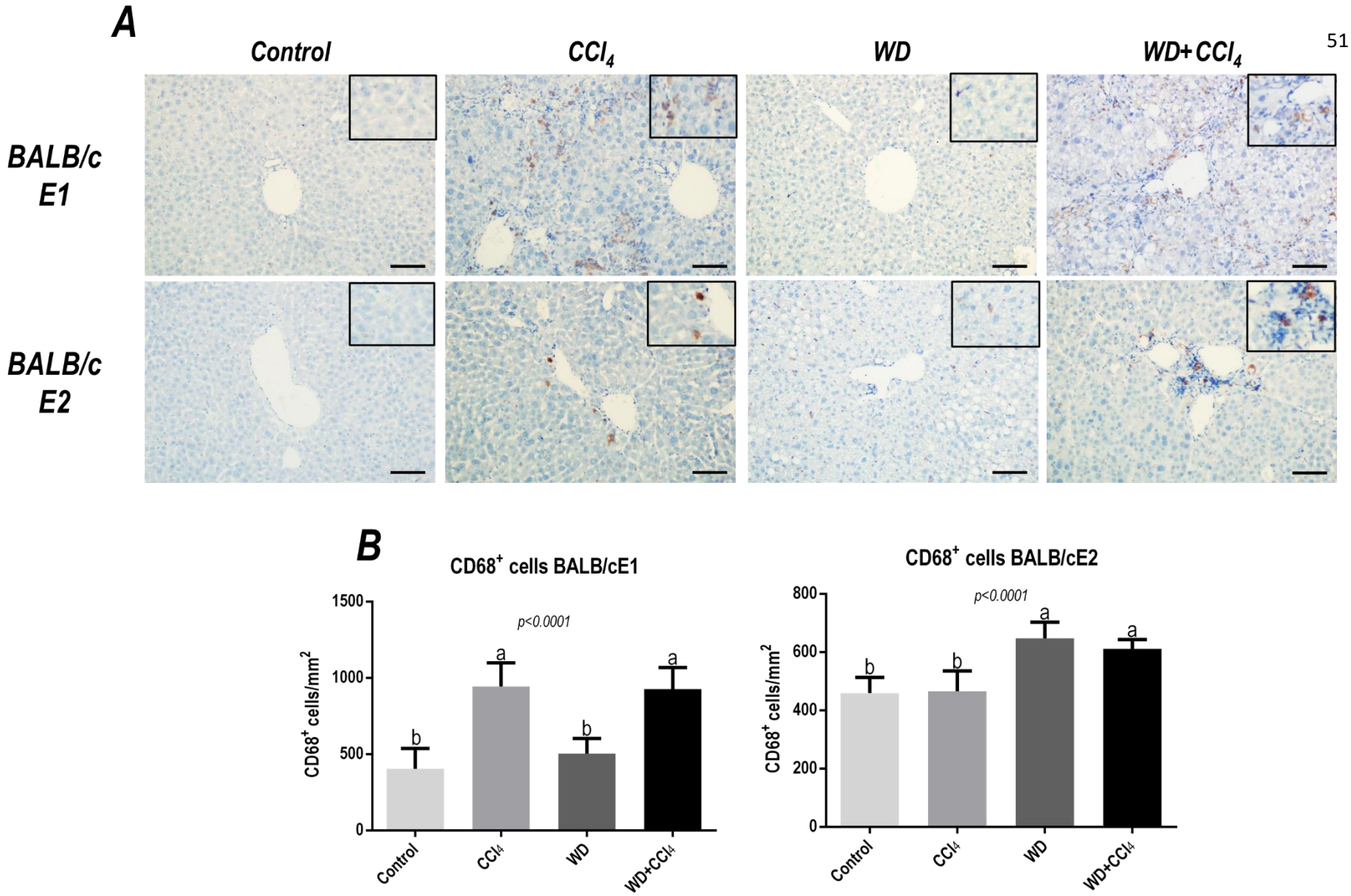

Figure 17. Effects of hybrid model of NASH over the number of hepatic CD68+ cells in BALB/c mice. **(A)** Representative photomicrographs (40x objective, scale bar=50µm) of sections immunoreacted for CD68+. **(B)** Semiquantitative analysis of the number of CD68+ cells in hepatic sections of BALB/c mice. Different letters correspond to statistical differences among groups. Data were analyzed by One-way ANOVA and *pos hoc* Tukey test, and it were considered statistically different when $p<0.05$. Control [standard chow and 3x weekly intraperitoneal (i.p.) injections of corn oil vehicle]; carbon tetrachloride [CCl_4, 3x weekly i.p. injections of 10% corn oil solution of CCl_4, with doses of 0.25µL/g of body weight (b.w.) increased utmost of 1.50 µL/g b.w.]; western diet [WD, chow enriched with fat (20%) and sucrose (20%) and 3x weekly i.p. injections of corn oil vehicle]; WD+CCl4 (chow enriched with fat (20%) and sucrose (20%) and 3x weekly i.p injections of 10% corn oil solution of CCl_4, with doses of 0.25µL/g b.w. increased utmost of 1.50 µL/g b.w.); n = 5-6 (control and WD) or 7-9 (CCl_4 and WD+CCl_4).

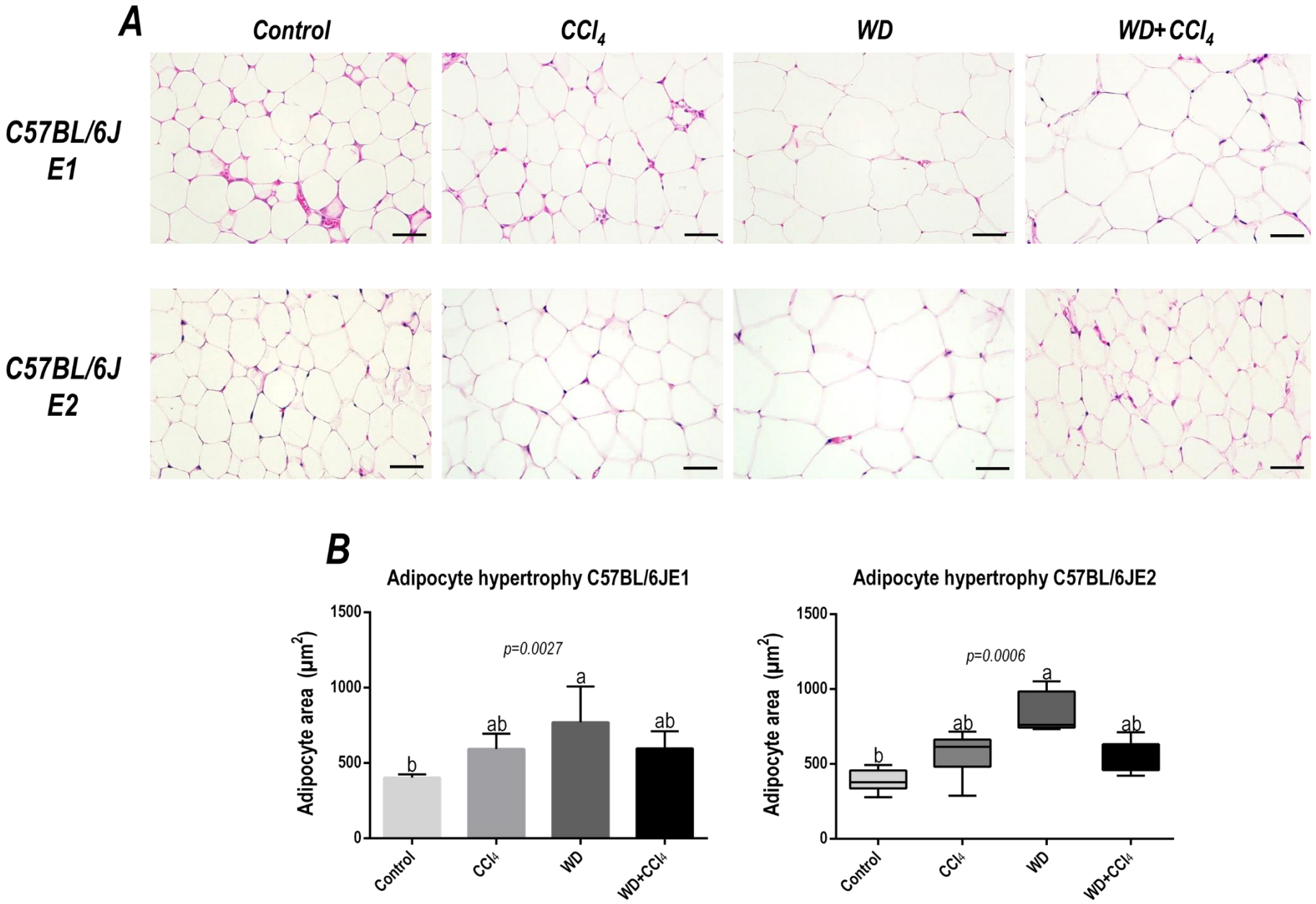

Figure 18. Effects of hybrid model of NASH over the hypertrophy of adipocytes in C57BL/6J mice. **(A)** Representative photomicrographs (20x objective, scale bar=50µm) of sections stained with H&E. **(B)** Semiquantitative morphometric analysis of the hypertrophy of adipocytes in C57BL/6JJ mice. Different letters correspond to statistical differences among groups. Data were analyzed by One-way ANOVA and *pos hoc* Tukey test, and it were considered statistically different when $p<0.05$. Control [standard chow and 3x weekly intraperitoneal (i.p.) injections of corn oil vehicle]; carbon tetrachloride [CCl_4, 3x weekly i.p. injections of 10% corn oil solution of CCl_4, with doses of 0.25µL/g of body weight (b.w.) increased utmost of 1.50 µL/g b.w.]; western diet [WD, chow enriched with fat (20%) and sucrose (20%) and 3x weekly i.p. injections of corn oil vehicle]; WD+CCl4 (chow enriched with fat (20%) and sucrose (20%) and 3x weekly i.p injections of 10% corn oil solution of CCl_4, with doses of 0.25µL/g b.w. increased utmost of 1.50 µL/g b.w.); n = 5-6 (control and WD) or 7-9 (CCl_4 and WD+CCl_4).

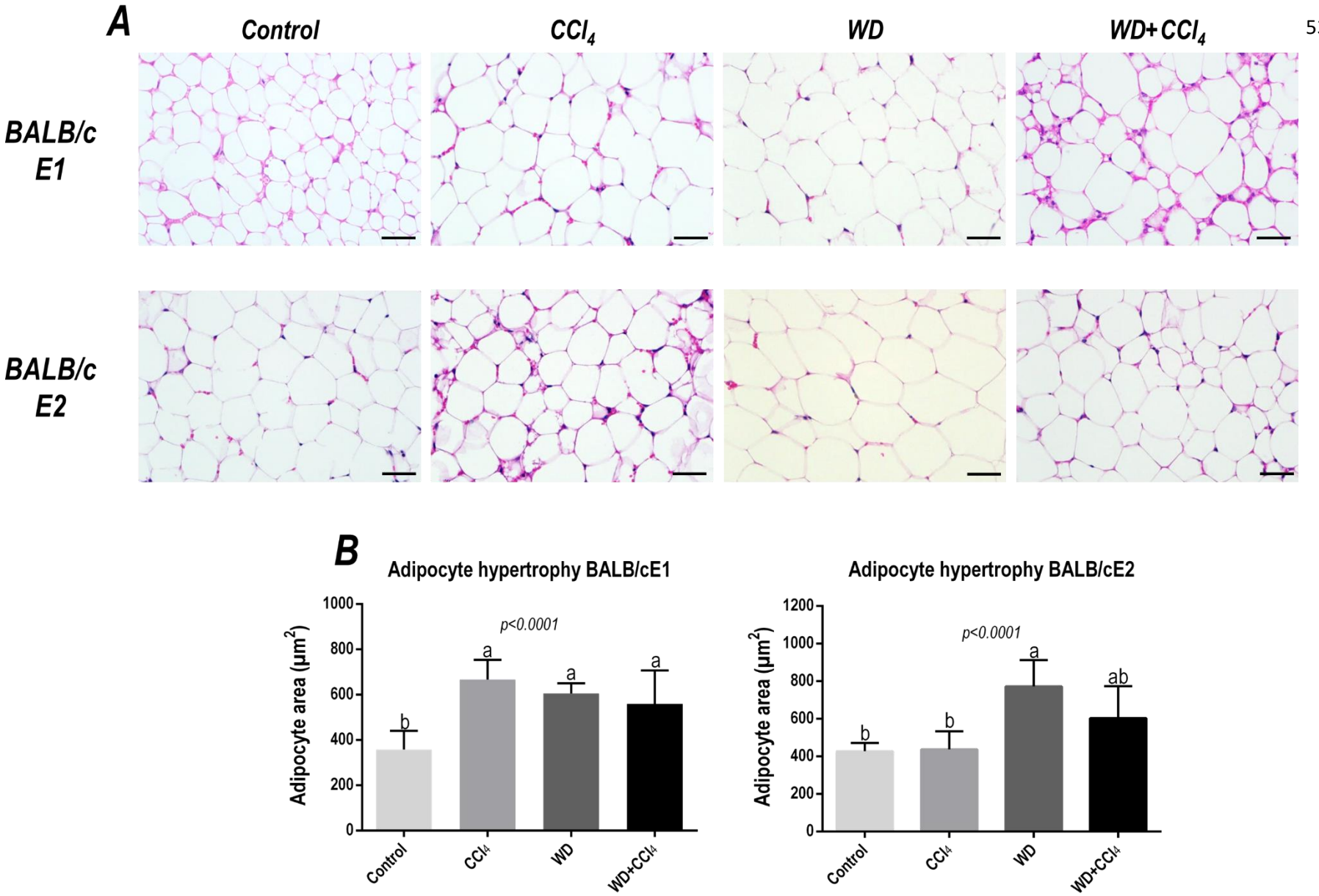

Figure 19. Effects of hybrid model of NASH over the hypertrophy of adipocytes in BALB/c mice. **(A)** Representative photomicrographs (20x objective, scale bar=50µm) of sections stained with H&E. **(B)** Semiquantitative morphometric analysis of the hypertrophy of adipocytes in BALB/c mice. Different letters correspond to statistical differences among groups. Data were analyzed by One-way ANOVA and *pos hoc* Tukey test, and it were considered statistically different when $p<0.05$. Control [standard chow and 3x weekly intraperitoneal (i.p.) injections of corn oil vehicle]; carbon tetrachloride [CCl_4, 3x weekly i.p. injections of 10% corn oil solution of CCl_4, with doses of 0.25µL/g of body weight (b.w.) increased utmost of 1.50 µL/g b.w.]; western diet [WD, chow enriched with fat (20%) and sucrose (20%) and 3x weekly i.p. injections of corn oil vehicle]; WD+CCl4 (chow enriched with fat (20%) and sucrose (20%) and 3x weekly i.p injections of 10% corn oil solution of CCl_4, with doses of 0.25µL/g b.w. increased utmost of 1.50 µL/g b.w.); n = 5-6 (control and WD) or 7-9 (CCl_4 and WD+CCl_4).

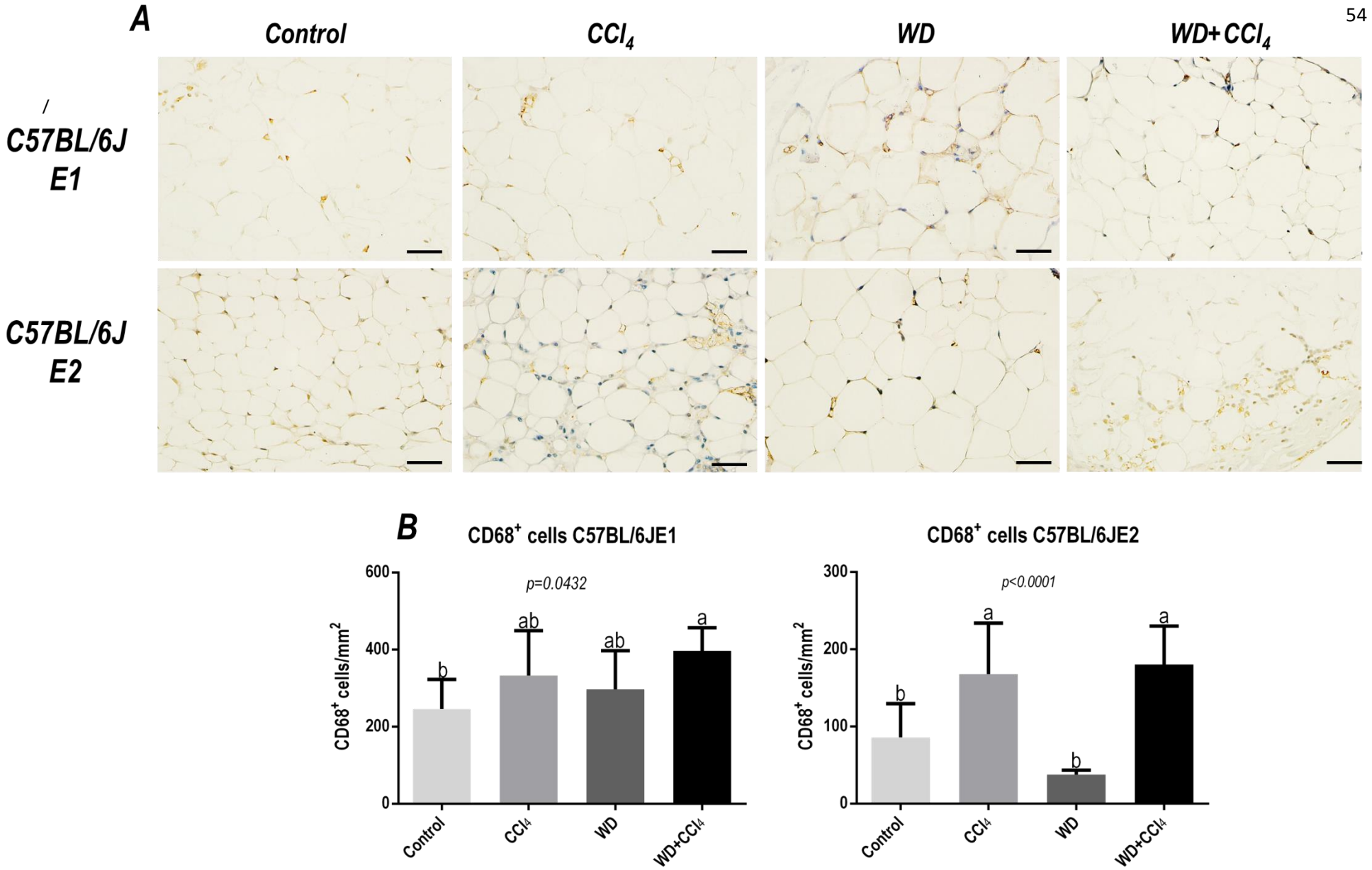

Figure 20. Effects of hybrid model of NASH over the number of hepatic CD68+ cells in C57BL/6J mice. **(A)** Representative photomicrographs (20x objective, scale bar=50µm) of immunoreacted sections for CD68. **(B)** Semiquantitative morphometric analysis of the hypertrophy of adipocytes in C57BL/6J mice. Different letters correspond to statistical differences among groups. Data were analyzed by One-way ANOVA and *pos hoc* Tukey test, and it were considered statistically different when $p<0.05$. Control [standard chow and 3x weekly intraperitoneal (i.p.) injections of corn oil vehicle]; carbon tetrachloride [CCl_4, 3x weekly i.p. injections of 10% corn oil solution of CCl_4, with doses of 0.25µL/g of body weight (b.w.) increased utmost of 1.50 µL/g b.w.]; western diet [WD, chow enriched with fat (20%) and sucrose (20%) and 3x weekly i.p. injections of corn oil vehicle]; WD+CCl4 (chow enriched with fat (20%) and sucrose (20%) and 3x weekly i.p injections of 10% corn oil solution of CCl_4, with doses of 0.25µL/g b.w. increased utmost of 1.50 µL/g b.w.); n = 5-6 (control and WD) or 7-9 (CCl_4 and WD+CCl_4).

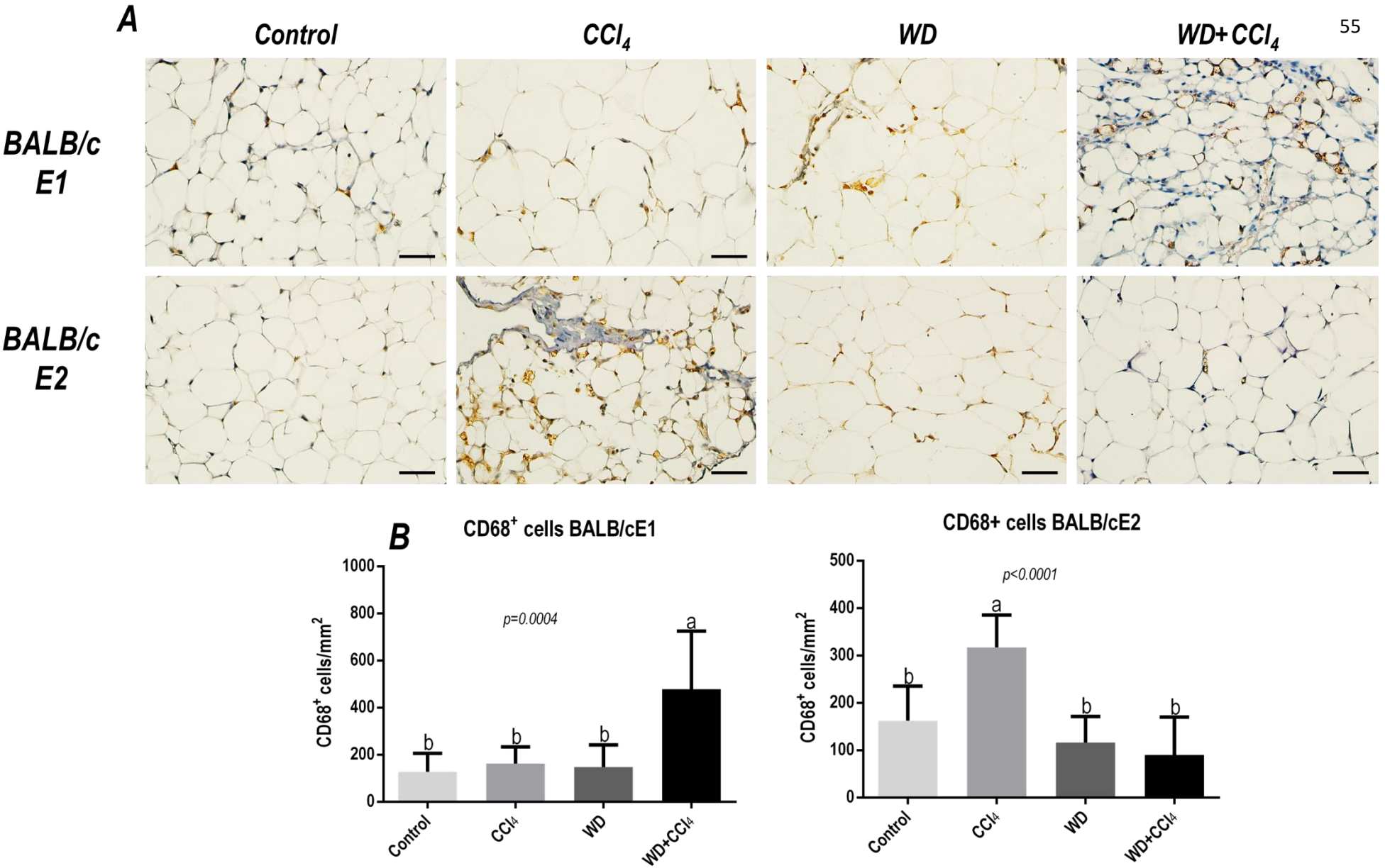

Figure 21. Effects of hybrid model of NASH over the number of hepatic CD68+ cells in BALB/c mice. **(A)** Representative photomicrographs (20x objective, scale bar=50µm) of immunoreacted sections for $CD68^+$ cells. **(B)** Semiquantitative morphometric analysis of the hypertrophy of adipocytes in BALB/c mice. Different letters correspond to statistical differences among groups. Data were analyzed by One-way ANOVA and *pos hoc* Tukey test, and it were considered statistically different when $p<0.05$. Control [standard chow and 3x weekly intraperitoneal (i.p.) injections of corn oil vehicle]; carbon tetrachloride [CCl_4, 3x weekly i.p. injections of 10% corn oil solution of CCl_4, with doses of 0.25µL/g of body weight (b.w.) increased utmost of 1.50 µL/g b.w.]; western diet [WD, chow enriched with fat (20%) and sucrose (20%) and 3x weekly i.p. injections of corn oil vehicle]; WD+CCl4 (chow enriched with fat (20%) and sucrose (20%) and 3x weekly i.p injections of 10% corn oil solution of CCl_4, with doses of 0.25µL/g b.w. increased utmost of 1.50 µL/g b.w.); n = 5-6 (control and WD) or 7-9 (CCl_4 and WD+CCl_4).

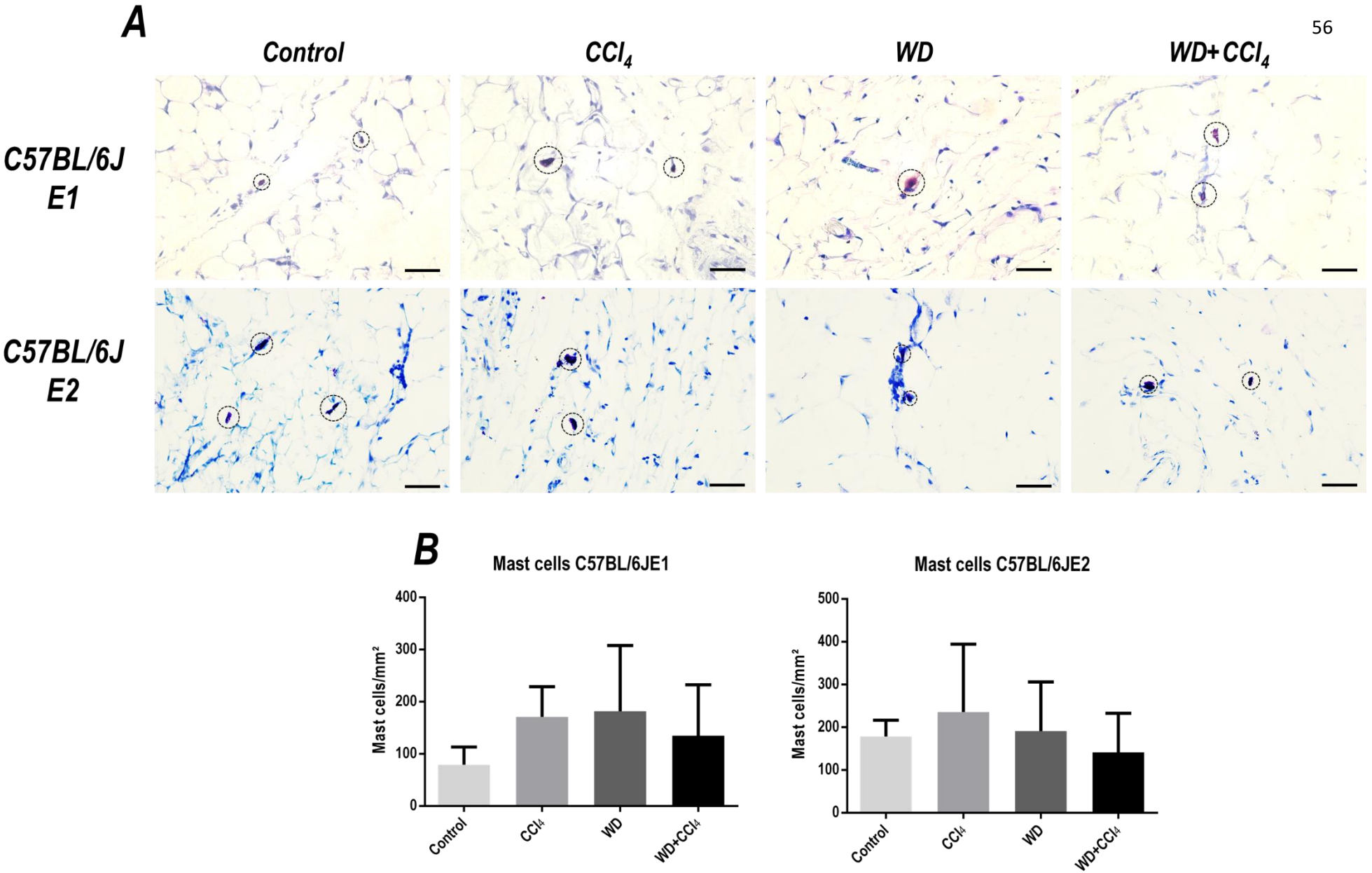

Figure 22. Effects of hybrid model of NASH over the number of mast cells in C57BL/6J mice. **(A)** Representative photomicrographs (20x objective, scale bar=50µm) of sections stained with toluidine blue. Dotted ciricles indicate the mast cells. **(B)** Semiquantitative morphometric analysis of the hypertrophy of adipocytes in C57BL/6J mice. Different letters correspond to statistical differences among groups. Data were analyzed by One-way ANOVA and *pos hoc* Tukey test, and it were considered statistically different when $p<0.05$. Control [standard chow and 3x weekly intraperitoneal (i.p.) injections of corn oil vehicle]; carbon tetrachloride [CCl_4, 3x weekly i.p. injections of 10% corn oil solution of CCl_4, with doses of 0.25µL/g of body weight (b.w.) increased utmost of 1.50 µL/g b.w.]; western diet [WD, chow enriched with fat (20%) and sucrose (20%) and 3x weekly i.p. injections of corn oil vehicle]; WD+CCl4 (chow enriched with fat (20%) and sucrose (20%) and 3x weekly i.p injections of 10% corn oil solution of CCl_4, with doses of 0.25µL/g b.w. increased utmost of 1.50 µL/g b.w.); n = 5-6 (control and WD) or 7-9 (CCl_4 and WD+CCl_4).

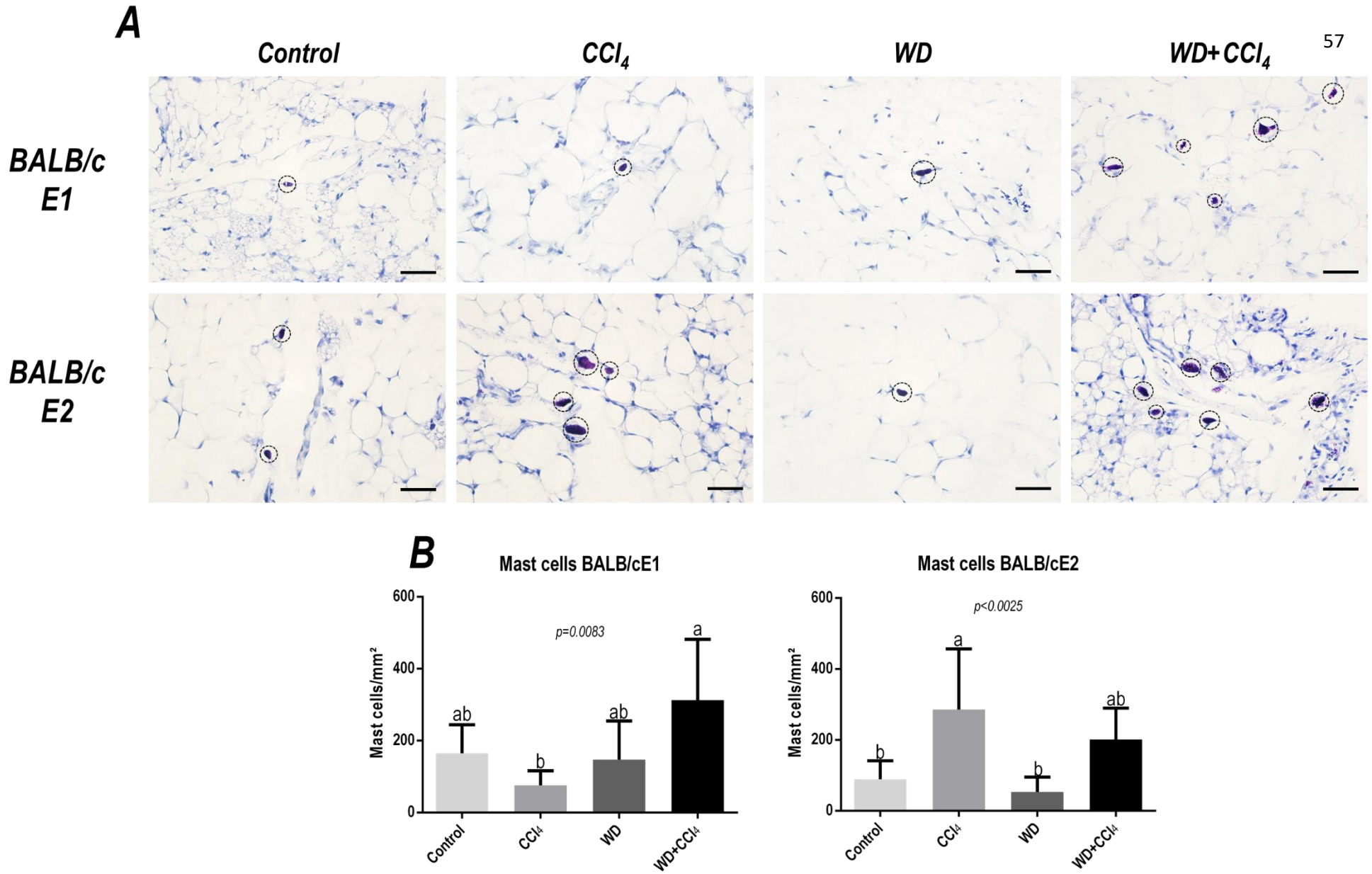

Figure 23. Effects of hybrid model of NASH over the number of mast cells in BALB/c mice. **(A)** Representative photomicrographs (20x objective, scale bar=50µm) of sections stained with toluidine blue. Dotted ciricles indicate the mast cells. **(B)** Semiquantitative morphometric analysis of the hypertrophy of adipocytes in BALB/c mice. Different letters correspond to statistical differences among groups. Data were analyzed by One-way ANOVA and *pos hoc* Tukey test, and it were considered statistically different when $p<0.05$. Control [standard chow and 3x weekly intraperitoneal (i.p.) injections of corn oil vehicle]; carbon tetrachloride [CCl_4, 3x weekly i.p. injections of 10% corn oil solution of CCl_4, with doses of 0.25µL/g of body weight (b.w.) increased utmost of 1.50 µL/g b.w.]; western diet [WD, chow enriched with fat (20%) and sucrose (20%) and 3x weekly i.p. injections of corn oil vehicle]; WD+CCl4 (chow enriched with fat (20%) and sucrose (20%) and 3x weekly i.p injections of 10% corn oil solution of CCl_4, with doses of 0.25µL/g b.w. increased utmost of 1.50 µL/g b.w.); n = 5-6 (control and WD) or 7-9 (CCl_4 and WD+CCl_4).

13. The hybrid protocol reduces the protein levels of Nrf2 but enhances NF-κB

Since our data suggest that the hybrid protocol, but not WD protocol maintenance after CCl_4-ceasing, demonstrates the morphological features observed in patients and other experimental models, we only assessed by western blotting the E1 timepoint. In both C57BL/6J and BALB/c mice, the hybrid protocol decreased the nuclear factor-erythroid 2-related factor 2 (Nrf2) levels ($p<0.0001$) (Figure 24). Additionally, we assessed the protein levels of the nuclear factor kappa B (NF-κB) (p65). Surprisingly, only C57BL/6J mice featured enhanced levels of NF-κB ($p=0.0050$) (~33% compared to the control group), while BALB/c mice do not, suggesting that exists a different response to the hybrid protocol according to mice strain.

14. The hybrid protocol of NASH modulates the hepatic metabolic profile

Considering the VIP score, the WD+CCl_4 group of C57BL/6J mice featured increased levels of valine and decreased levels of tyrosine (Figure 25). Conversely, the WD+CCl_4 BALB/c mice displayed increased levels of tyrosine, while decreased levels of lactate and inosine 5'-monophosphate (IMP), compared to control the corresponding group, was observed (Figure 26). Additionally, we established a comparative analysis among mice strain (between WD+CCl_4 groups, only) (Figure 27). By these terms, we observed that C57BL/6J mice showed increased levels of IMP whereas BALB/c mice featured enhanced levels of tyrosine, suggesting a strain-dependent response to the hybrid model of NASH.

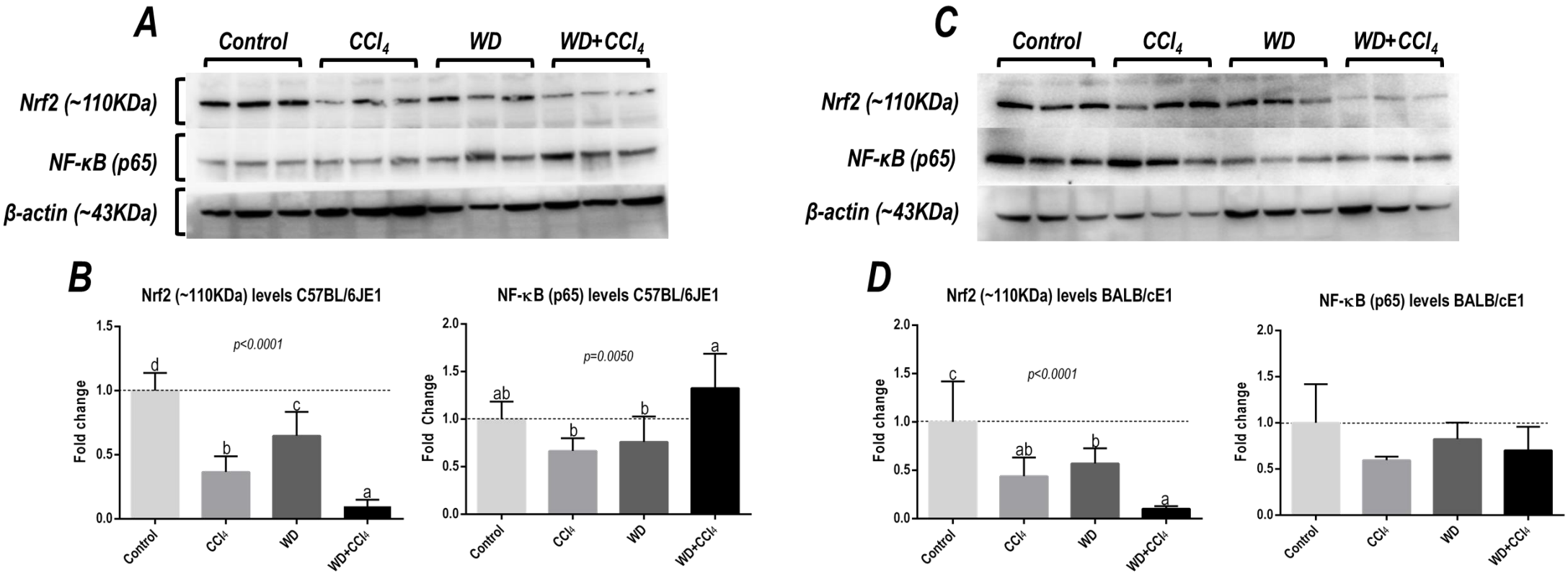

Figure 24. Effects of hybrid model of NASH on **(A)** the hepatic protein levels of Nrf2 (~110KDa) and NF-κB (p65) in C57BL/6J and **(C)** BALB/c mice. **(B)** Semiquantitative densitometric analysis of the protein levels of Nrf2 (~110KDa) and NF-κB (p65) in C57BL/6J and **(D)** in BALB/c mice. Different letters correspond to statistical differences among groups. Data were analyzed by One-way ANOVA and *pos hoc* Tukey test, and it were considered statistically different when $p<0.05$. Control [standard chow and 3x weekly intraperitoneal (i.p.) injections of corn oil vehicle]; carbon tetrachloride [CCl_4, 3x weekly i.p. injections of 10% corn oil solution of CCl_4, with doses of 0.25µL/g of body weight (b.w.) increased utmost of 1.50 µL/g b.w.]; western diet [WD, chow enriched with fat (20%) and sucrose (20%) and 3x weekly i.p. injections of corn oil vehicle]; WD+CCl4 (chow enriched with fat (20%) and sucrose (20%) and 3x weekly i.p injections of 10% corn oil solution of CCl_4, with doses of 0.25µL/g b.w. increased utmost of 1.50 µL/g b.w.); n = 5-6 (control and WD) or 7-9 (CCl_4 and WD+CCl_4).

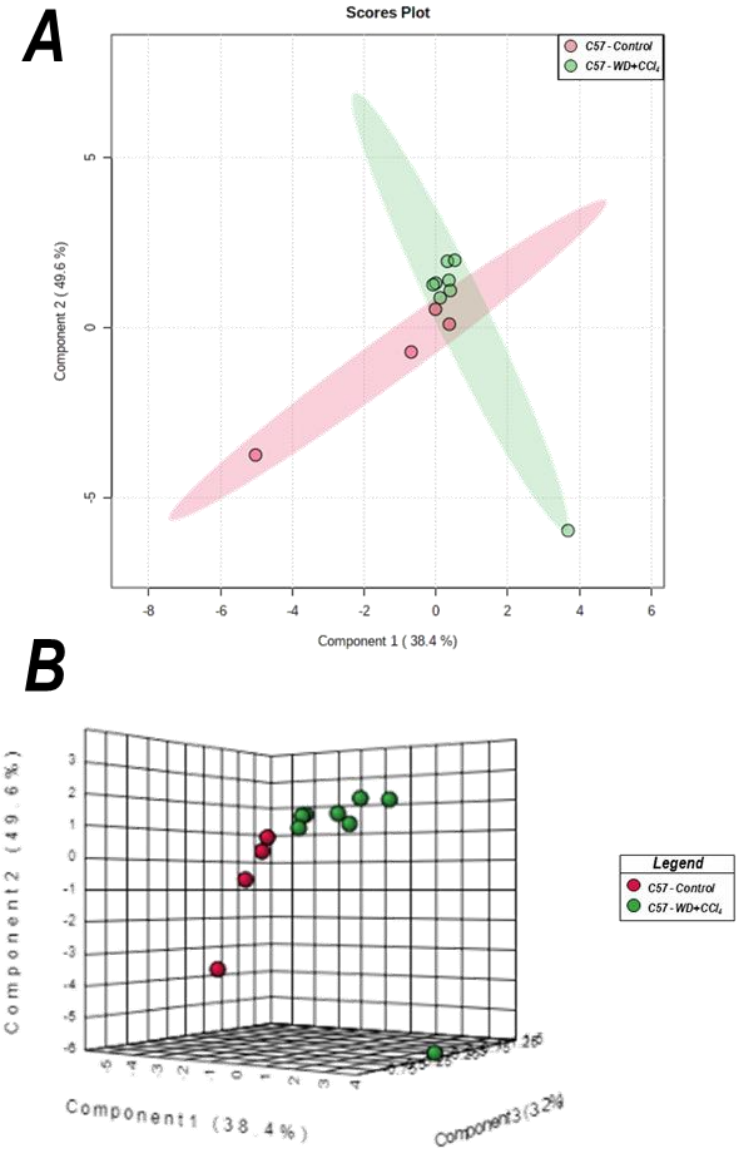

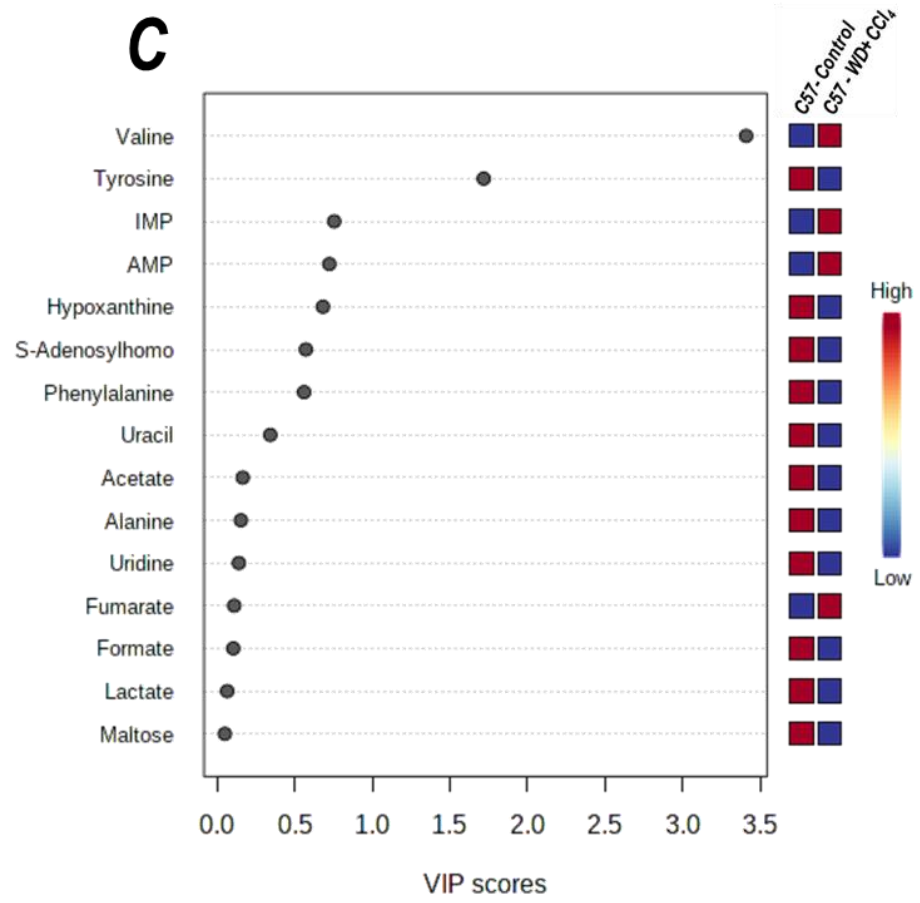

Figure 25. Effects of hybrid model of NASH on **(A)** the 2-D partial least squares-discriminant analysis (PLS-DA); **(B)** 3-D PLS-DA analysis; and **(C)** the identification of the metabolomic profile of C57BL/6J mice. Control (N=4) and WD+CCl_4 (N=9). Only VIP score $\geq$ 1.5 were considered for metabolomic data.

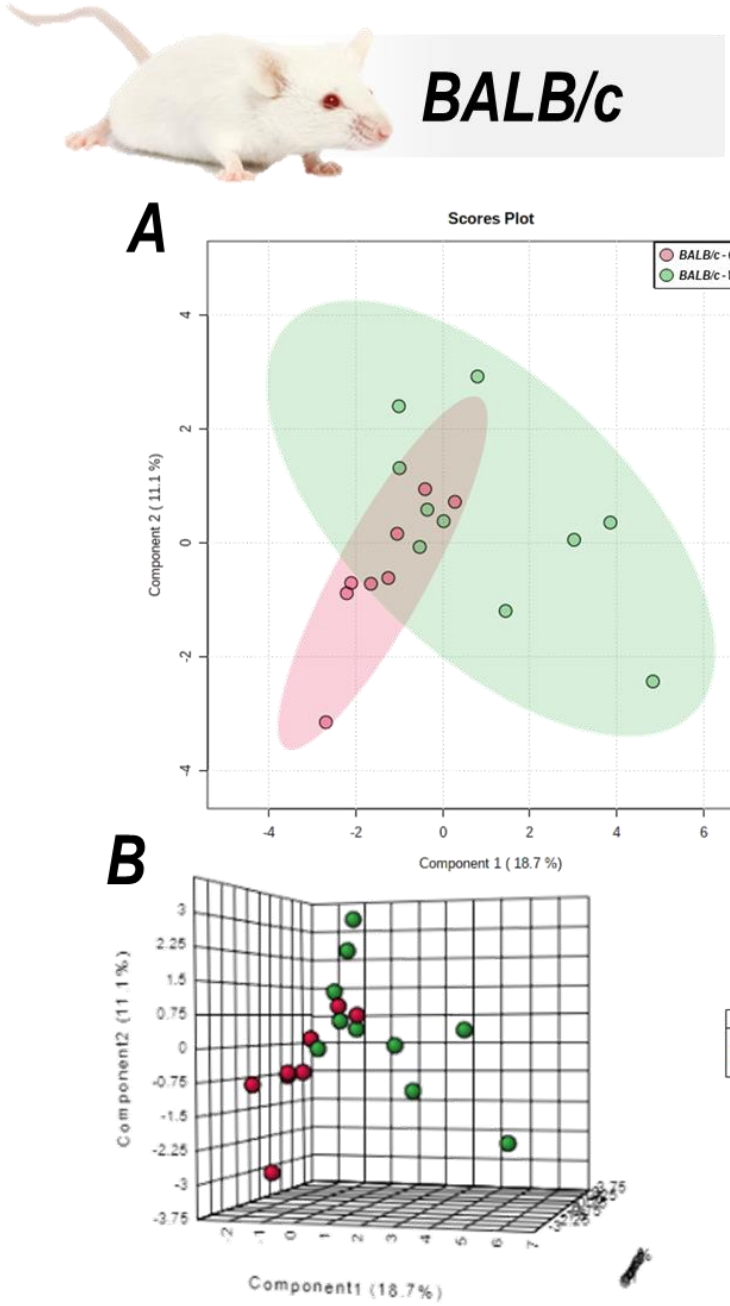

Figure 26. Effects of hybrid model of NASH on **(A)** the 2-D partial least squares-discriminant analysis (PLS-DA); **(B)** 3-D PLS-DA analysis; and **(C)** the identification of the metabolomic profile of C57BL/6J mice. Control (N=7) and WD+CCl_4 (N=10). Only VIP score $\geq$ 1.5 were considered for metabolomic data.

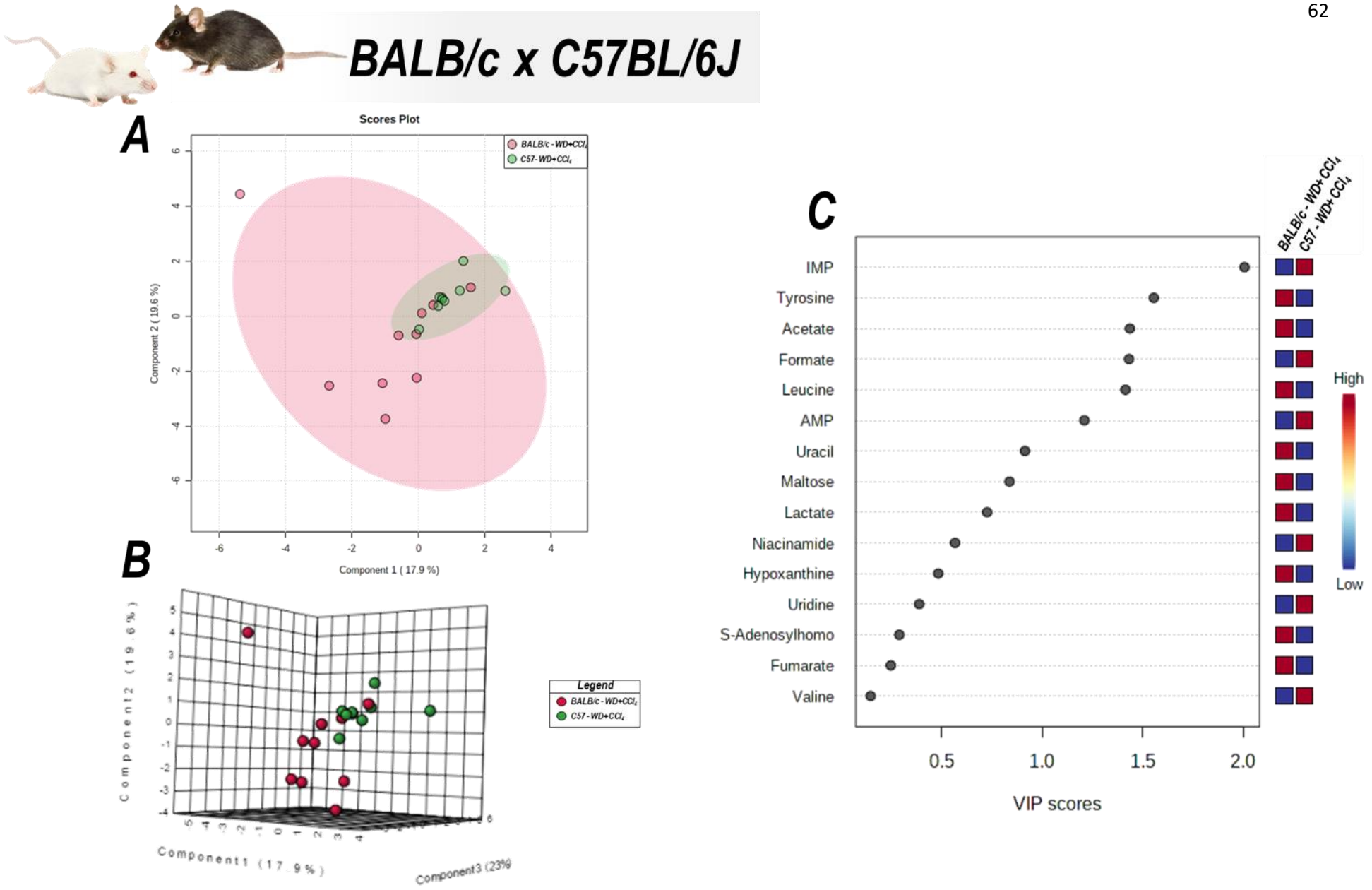

Figure 27. Comparative analysis of WD+CCl_4 groups, according to mice strain **(A)** the 2-D partial least squares-discriminant analysis (PLS-DA); **(B)** 3-D PLS-DA analysis; and **(C)** the identification of the metabolomic profile of C57BL/6J compared to BALB/c mice. WD+CCl_4 C57BL/6J: N=9; and WD+CCl_4 BALB/c: N=10. Only VIP score $\geq$ 1.5 were considered for metabolomic data.

Discussion

As previously described, mice were submitted to a hybrid protocol of NASH, in order to resemble morphologic, metabolic, and molecular traits of the corresponding disease of patients. For that, C57BL/6J and BALB/c mice were fed a WD diet, which induced a yellowish aspect of the liver. In addition, the liver of CCl_4-induced mice featured a rough surface aspect, suggesting that the CCl_4 protocol led to the development of hepatic scars, indicating the hepatic accumulation of collagen content. Additionally, at the E1 timepoint, WD+CCl_4 C57BL/6J mice featured an increasing trend of the GTT area under the curve, compared to the control group, suggesting a glucose intolerance trend, differently from the corresponding BALB/c strain group. The glucose intolerance and insulin resistance (IR) are widely observed in patients with NAFLD and NASH (~22.5 and 43.6%, respectively), contributing to the emergence of type II diabetes (T2D) and metabolic disorders (MS) by impairing the hepatic-adipose tissue axis lipid and carbohydrate metabolism [4,20]. The underlying molecular mechanisms associated with IR emergence remain not fully understood in murine models of high-fat-induced NASH, although there is evidence that the hepatic sterol regulatory element-binding protein (SREBP) 1c (SREBP-1c) plays a pivotal role in lipid metabolism impairment in hyperinsulinemic *LDRL*$^{-/-}$ mice, since AMPK phosphorylation blocks the SREBP-1c cleavage and nuclear translocation, and further its IR-promoting activity [21].

The CCl_4 is an hepatotoxin that is turned into trichloromethyl (CCl_3*) radical, due to the metabolization of CCl_4 in the microsomal system, in specific, by the CYP2E1. The CCl_3* radical, however, is an oxidant molecule that causes the lipid peroxidation of hepatocytes, further leading them to cellular death and triggering the intrinsic mechanisms for fibrosis progression and extracellular matrix deposition, and lipid metabolism impairment, hence, increasing the relative liver weight and causing the observed rough surface aspect [13,22]. Indeed, the hybrid protocol induced the morphological traits of NASH, at E1 timepoint but not E2, like mild/severe microvesicular steatosis and inflammatory foci occurrence, although hepatocellular ballooning was restrained to C57BL/6J mice, whereas after the CCl_4 protocol ceasing only an NAFL profile was observed. Thus, we suggest only the hybrid protocol (WD+CCl_4) at E1 timepoint, in

both strains, were able to establish a fast-induced model of fibrosing NASH that mimics the corresponding disease on patients, and, hence, were considered in further molecular analysis.

A strain-dependent response to the hybrid protocol of NASH was observed, since only C57BL/6J strain featured enhanced lipid content and hepatocellular ballooning occurrence, compared to other groups, whereas WD-fed mice of BALB/c strain featured similar levels of hepatic lipid content. These parameters are consistent with the increased NAS grading observed in WD+CCl_4 groups. In general, hepatic lipid accumulation occurs by the following mechanisms: **(1)** excessive influx of fatty acids, in special the saturated fatty acids (SFA); **(2)** decrease of the oxidation levels of fatty acids; **(3)** enhanced *de novo* synthesis of SFA; **(4)** impairment of the exportation mechanisms of fatty acids [20]. In addition, it has been reported that palmitate and lysophosphatidylcholine (LPC, main intracellular metabolite of palmitate)-treated Huh7 cells release extracellular vesicles (EV), which act as a communication mediator among hepatocytes and hepatic milieu cells, by a pro-apoptotic-dependent mechanism, suggesting that the exposure of hepatocytes to SFA alters its phenotypical aspect. In line with these, LPC and WD-induced C57BL/6J-isolated hepatocytes feature up-regulation of interleukin (IL)-1β (IL-1β) and IL-6 genes, and macrophage activation capacity, promoting an interplay among lipotoxicity of hepatocytes, EV releasing, and establishment of a hepatic pro-inflammatory microenvironment in which NASH is susceptible to progress [23].

The lipid-induced sublethal injuries of hepatocytes cause mitochondrial-related disorders that impair the oxidative dynamics of fatty acid and further accumulation of its byproducts, leading to the synthesis of reactive species of oxygen (ROS). However, it is also observed that mice featuring NASH presented a ~2-fold activity of the citric acid cycle, probably contributing to the electron leakage and oxidative stress [24]. It is also reported that C57BL/6J mice fed an atherogenic diet (high-fat chow with the addition of cholesterol), for 24 weeks, displayed increased levels of SREBP-1c and fatty acid synthase (FAS) mRNA, master regulators of fatty acid synthesis, as well as decreased levels of peroxisome proliferator-activated receptor α (PPARα) indicates the compromising of the hepatic antioxidant capacity

[25]. Taken together, the lipid accumulation and further disturbance of the metabolic/signaling profile of hepatocytes establish a feedback cycle between lipid accumulation and oxidative stress-mediated by the inflammatory response, in agreement with the NAS grading morphological aspects.

The WD+CCl_4 mice of both strains displayed extensive fibrosis and enhanced levels of collagen content compared to other groups, as well as the hybrid protocol induced the extensive activation of HSC, by increasing the hepatic α-SMA levels, whereas a strain-dependent response was observed regarding the number of $Ki67^+$ and $casp3^+$ hepatocytes and hepatic CD68+ cells. Several studies reported that CCl_4 is an hepatotoxin commonly used in experimental models to mimic the natural burden of extensive fibrosis and inflammation, in which the development of chronic liver diseases, like NASH and hepatocellular carcinoma, occurs [11,12,26]. On the other hand, Wobser et al. [27] described that the activation of HSC also occurs when exposed to a conditioned medium in which primary human hepatocytes were previously exposed to palmitate (0.1-0.4mM), increasing the levels of α-SMA, matrix metalloproteinase-2 (MMP-2), and transforming growth β (TGF-β) mRNA, indicative of HSC activation and liver fibrosis. In those terms, HSC are activated in the context of NAFL and induce collagen deposition in the liver. Thus, we suggest that the association of WD to the CCl_4 accelerates the progression of fibrosis due to the combination of the lipotoxic hepatic milieu associated with the injuries caused by the CCl_4, which is mostly related to the lipotoxicity and lipid peroxidation-inducing activity, promoting oxidative stress and inflammation.

The sublethal injuries caused by palmitate promotes the synthesis of ROS, due to the impairment of mitochondrial energy metabolism and electron leakage, increasing the levels of cell cycle markers (CDK4, CDK6, cyclin D1, cyclin D2, and cyclin D3) associated with the progression of the cell cycle progression in a MAPK/Akt-dependent mechanism [28]. In parallel, CCl_4 metabolism is mostly related to CYP2E1 activity, which exerts a remarkable relevance to the clearance of hepatic xenobiotics [13]. The CYP2E1 overexpression and uncoupling, however, is related to the synthesis of ROS, by producing H_2O_2, as a consequence of O_2 reduction, and lipid peroxidation, contributing to the death of hepatocytes and NASH progression [29]. Indeed, CYP2E1-null mice fed a high-fat diet (~60% of energy-derived calories)

featured decreased levels of lipid peroxidation, protein carbonylation, and oxidative stress compared to wild-type mice [30]. Additionally, the SFA-induced persistent stress causes profound changes in the genic profile of hepatocytes, leading ultimately to the activation of necrosis/apoptosis signaling pathways and the inflammatory response [20]. Several studies indicate that the exposure of hepatocytes to SFA induces the activation of death pathways, by inducing mitochondrial metabolism impairment and endoplasmic reticulum stress (ERS) [31–33]. During steatosis to NASH transition, it is observed that the overload of fatty acids in the mitochondria increases the bioavailability of acetyl-CoA and enhances the oxidative flux and further activation of the tricarboxylic acid cycle (TAC) [34]. As a consequence of the mitochondrial metabolism remodeling, the incomplete oxidation of fatty acids leads to the accumulation of cytotoxic metabolites (e.g.: ceramides and diacylglycerols), which triggers the inflammation and death signaling pathways [24]. Therefore, CCl_4-induced hepatocellular apoptosis/necrosis acts synergically to the lipid-mediated lipotoxicity, by inducing the ROS synthesis, lipid peroxidation, and following hepatocellular death, suggesting that the hybrid protocol of NASH increases the number of $Ki67^+$, in a compensatory manner, and $casp3^+$ cells, by establishing a sublethal pro-oxidant/inflammatory hepatic microenvironment.

The pro-oxidant and inflammatory hepatic milieu also contributes for the monocyte and resident macropahges recruitment and activation [35]. Lipotoxically-induced hepatocytes display a differential profile of EV content (high mRNA levels of IL-1β and IL-6) and releasing levels in a death receptor 5 (DR5)-tumor necrosis factor-related apoptosis-inducing ligand (TRAIL) (DR5-TRAIL)-dependent mechanism, as well as C57BL/6J mice fed a high-fat diet protocol show activation of the inflammasome pathway and contribute to macrophages recruitment [23,36]. It is extensively well reported that the CCl_4 administration induces hepatocellular necrosis and apoptosis in the centrilobular zone, by interacting with the plasmatic membrane of hepatocytes, leading to the activation of hepatic macrophages, by enhancing both macrophage migration inhibitory factor (MIF) and monocyte chemoattractant protein-1 (MCP-1) levels [37,38]. So, we suggest that the hybrid protocol induces different complementary underlying

mechanisms that lead to the activation of KC, enhancing the number of hepatic CD68+ cells and contributing to the pro-inflammatory milieu.

In the context of NASH, the AT adipocytes underwent morphological and genic alterations that lead to the enhanced synthesis of pro-inflammatory molecules that promote metabolic disorders, as well as inflammatory cells recruitment molecules, such as MCP-1, contributing to the recruitment of adipose and NASH establishment [35,39,40]. Although obesity was not induced by the hybrid model, WD+CCl_4 BALB/c mice presented both adipocyte hypertrophy and enhanced number of $CD68_+$ cells in the AT, differently from the corresponding group of C57BL/6J mice, which featured increased number of $CD68^+$ cells infiltrate, only. Moreover, we assessed that only WD+CCl_4 BALB/c mice featured increased number of infiltrating MC, compared to other groups, suggesting that these cells might act coordinately with $CD68^+$ cells establishing the AT inflammation. Recent studies suggest that MC residents in the AT are a major cell subset population that contributes to type 2 diabetes (T2D) emerging/progression and AT inflammation, in a high-fat-induced obesity murine model [45]. Indeed, it was observed in patients that the enhanced number of MC correlates with markers of inflammation and AT fibrosis, suggesting that these cells act as drivers of metabolic disorders related to NAFLD/NASH [46]. Taken together, the evidence suggests that establishing a pro-inflammatory milieu in the AT occurs under adipocytes stress conditions, leading to the further infiltration and activation of ATM and MC, probably triggering the systemic low-grade inflammation that causes NASH.

The hepatocytes are responsible for the clearance of xenobiotic compounds, by metabolizing both organic and electrophilic molecules that exert an oxidative activity and, thus, implicating in NASH pathogenesis. These defense line activities, however, are associated with the activation of cytoprotective enzymes that are mostly encoded by the genes that contain antioxidant response elements (ARE) in their promoting regions, which promotes the transcriptional activation of under redox unbalanced conditions. The Nrf2 is a transcription factor that modulates the expression of ARE-containing genes. So, the Nrf2 expression has been targeted as a potential link between hepatic oxidative stress and NASH progression

[47]. Indeed, we observed that in both strains the hybrid protocol induced a striking decrease of the Nrf2 protein levels. It has been reported that Nrf2-null mice, submitted to a MCD diet model for 14 days, display pronounced steatosis and lobular inflammation and enhanced levels of hepatic CYP2E1, whereas total hepatic glutathione levels harshly fell (~70%). Thus, it is suggested that Nrf2 intensifies the susceptibility to NASH by inducing an oxidative stress state, caused by the simultaneous enhancement of CYP2E1 activity and GSH depletion [48]. Likewise, we assessed the effects of the hybrid protocol of NASH on the protein levels of NF-κB (p65) in both strains. However, only C57BL/6J mice featured increased levels of this transcription factor (~33% compared to the control group). As previously described, the SFA-induced NAFL leads to the endogenous DAMP signaling, triggering the activation of KC and TNF-α synthesis, which is a well-known activator of NF-κB in both hepatocytes and macrophages [51]. Moreover, the high intake of carbohydrates induces the activation and nuclear translocation of NF-κB, in a ChREPB-1-dependent mechanism, while its pharmacological inhibition alleviates the *de novo* lipogenesis [52]. It has been previously described that CCl_4-injured hepatocytes also activate NF-κB, leading to their apoptosis and hepatic inflammation [53]. The increased levels of NF-κB, compared to other groups, suggest that the hybrid protocol combines complementary mechanisms related to the activation of NF-κB activation by the hepatic cells subset, especially hepatocytes and KC, besides a strain-dependent response. Thus, we suggest that the Nrf2-NF-κB axis might be a pivotal molecular mechanism by which the hybrid protocol induces NASH, linking the compromised antioxidant defense of hepatocytes to the pro-inflammatory hepatic milieu where NASH emerges.

Seeking to assess the hepatic metabotype, a metabolomic profile determination was performed. Indeed, we observed a clustering trend regarding WD+CCl_4 and the corresponding control groups, according to mice strain, as well as a strain-dependent metabolomic profile, we compared C57BL/6J and BALB/c NASH-induced groups. In C57BL/6J, mice featured enhanced levels of valine and decreased levels of tyrosine, compared to the corresponding control group. Valine is a branched-chain essential amino acid (BCAA) that has been linked to energetic cell metabolism, by triggering the mitochondrial

catabolic pathways, during the tricarboxylic acid cycle (TCAC) activity and FAO activation [54]. Indeed, succinyl-CoA synthesis has been linked to the cellular bioavailability of valine and plays a pivotal activity in TCAC [55]. By these terms, the accumulation of valine suggests the compromising of the catabolic mechanisms that lead to adequate mitochondrial dynamics, leading to a lipotoxicity milieu that contributes to NASH emergence. Likewise, the tyrosine amino acid levels have been associated with NAFLD development, since a tyrosine-deficient diet induces a hepatic steatotic profile, by impairing the Nrf2 nuclear translocation and further activation, besides compromising lipid trafficking mechanisms [56]. Recently, the IMP has been linked to the energetic metabolism of hepatocytes, especially the adenosine monophosphate synthesis, and adequate energy metabolism of mitochondria. Indeed, the dietary supplementation with this molecule, an essential nucleotide, enhances the hepatic antioxidant activity, by attenuating the mitochondrial uncoupling, and reduces the plasmatic levels of alanine and aspartate aminotransferases (ALT and AST, respectively), an indication of damage to hepatocytes. Conversely, the hybrid protocol reduced the levels of IMP in BALB/c mice, compared to the corresponding control group, suggesting an unbalanced hepatic redox dynamics in the hepatic milieu that might contribute to NASH occurrence [57]. In addition, lactate is commonly known as a glycolytic metabolite involve in the bioenergetic metabolism and triggered under anaerobic and energy-demanding circumstances, as previously established by the Warburg effect [58]. However, recent findings suggest that the lactate might act as a signaling molecule that induces cell survival, by inducing the unfolded protein response and triggering the PI3K/AKT-Nrf2 pathway, which enhances the antioxidant cell line defense and alleviates the oxidative stress [59]. In NASH-induced BALB/c mice, we observed reduced hepatic levels of lactate compared to the control group, which is consistent with the previous findings of the reduced protein levels of Nrf2 and severe NAS grading.

We also observed a strain-dependent profile, when comparing C57BL/6J and BALB/c mice submitted to the hybrid protocol of NASH. Surprisingly, C57BL/6J mice featured decreased hepatic levels of tyrosine, compare to BALB/c mice, suggesting an underlying mechanism of the inhibition of the Nrf2

pathway and impaired lipid trafficking. On the other hand, BALB/c featured decreased levels of IMP, when compared to C57BL/6J mice, which might be a potential oxidative stress-related mechanism of NASH susceptibility. Thus, the valine accumulation and tyrosine decreasing levels in NASH-induced mice might be a potential signature of the mitochondrial FAO metabolism and Nrf2 impairment in C57BL/6J mice, whereas BALB/c mice feature decreased hepatic levels of IMP and lactate, leading to an alternative underlying mechanism of Nrf2-related oxidative stress that enables NASH progression.

Conclusions

Therefore, we attested that only mice strains at the E1 timepoint developed NASH since CCl_4 ceasing led to reduced NAS grade (reduced steatosis profile and inflammatory foci occurrence). Then, only mice at the E1 timepoint were further evaluated at molecular levels, in order to assess NASH-related features. Moreover, C57BL/6J mice are more sensitive to the hybrid protocol of NASH, compared to BALB/c mice, due to their susceptibility to developing an IR-associated NASH profile, with severe steatosis, lobular and diffuse inflammation, ballooning hepatocytes, and collagen deposition, remarking enhanced number of $CD68^+$, $Ki67^+$, and $casp3^+$ cells and NF-κB levels, whereas presented reduced levels of Nrf2 and an oxidative stress-related metabolomic signature, suggesting the compromising of the antioxidant cellular mechanisms and pro-inflammatory state. Taken together, we suggest that the CCl_4 protocol accelerates the SFA/sugar-induced lipotoxicity and sublethal grade inflammation, which leads to an adequate burden (pro-oxidant/inflammatory) for NASH development, enabling establishing a fast-inducing murine model of NASH that resembles both morphological and molecular aspects observed in patients.

References

1. Younossi, Z.M.; Koenig, A.B.; Abdelatif, D.; Fazel, Y.; Henry, L.; Wymer, M. Global epidemiology of nonalcoholic fatty liver disease—Meta-analytic assessment of prevalence, incidence, and

outcomes. *Hepatology* **2016**, *64*, 73–84, doi:10.1002/hep.28431.

2. Wree, A.; Broderick, L.; Canbay, A.; Hoffman, H.M.; Feldstein, A.E. From NAFLD to NASH to cirrhosis-new insights into disease mechanisms. *Nat. Rev. Gastroenterol. Hepatol.* **2013**, *10*, 627–636, doi:10.1038/nrgastro.2013.149.
3. Wong, R.J.; Aguilar, M.; Cheung, R.; Perumpail, R.B.; Harrison, S.A.; Younossi, Z.M.; Ahmed, A. Nonalcoholic Steatohepatitis Is the Second Leading Etiology of liver disease among adults awaiting liver transplantation in the United States. *Gastroenterology* **2015**, *148*, 547–555, doi:10.1053/j.gastro.2014.11.039.
4. Younossi, Z.M.; Koenig, A.B.; Abdelatif, D.; Fazel, Y.; Henry, L.; Wymer, M. Global epidemiology of nonalcoholic fatty liver disease—Meta-analytic assessment of prevalence, incidence, and outcomes. *Hepatology* **2016**, *64*, 73–84, doi:10.1002/hep.28431.
5. Dyson, J.; Jaques, B.; Chattopadyhay, D.; Lochan, R.; Graham, J.; Das, D.; Aslam, T.; Patanwala, I.; Gaggar, S.; Cole, M.; et al. Hepatocellular cancer: The impact of obesity, type 2 diabetes and a multidisciplinary team. *J. Hepatol.* **2014**, *60*, 110–117, doi:10.1016/j.jhep.2013.08.011.
6. Younossi, Z.M.; Blissett, D.; Blissett, R.; Henry, L.; Stepanova, M.; Younossi, Y.; Racila, A.; Hunt, S.; Beckerman, R. The economic and clinical burden of nonalcoholic fatty liver disease in the United States and Europe. *Hepatology* **2016**, *64*, 1577–1586, doi:10.1002/hep.28785.
7. Estes, C.; Anstee, Q.M.; Arias-Loste, M.T.; Bantel, H.; Bellentani, S.; Caballeria, J.; Colombo, M.; Craxi, A.; Crespo, J.; Day, C.P.; et al. Modeling NAFLD disease burden in China, France, Germany, Italy, Japan, Spain, United Kingdom, and United States for the period 2016–2030. *J. Hepatol.* **2018**, *69*, 896–904, doi:10.1016/j.jhep.2018.05.036.
8. Younossi, Z.M.; Loomba, R.; Rinella, M.E.; Bugianesi, E.; Marchesini, G.; Neuschwander-Tetri, B.A.; Serfaty, L.; Negro, F.; Caldwell, S.H.; Ratziu, V.; et al. Current and future therapeutic regimens for nonalcoholic fatty liver disease and nonalcoholic steatohepatitis. *Hepatology* **2018**,

68, 361–371, doi:10.1002/hep.29724.

9. Willebrords, J.; Pereira, I.V.A.; Maes, M.; Crespo Yanguas, S.; Colle, I.; Van Den Bossche, B.; Da Silva, T.C.; De Oliveira, C.P.M.S.; Andraus, W.; Vinken, M.; et al. Strategies, models and biomarkers in experimental non-alcoholic fatty liver disease research. *Prog. Lipid Res.* **2015**, *59*, 106–125, doi:10.1016/j.plipres.2015.05.002.
10. Asgharpour, A.; Cazanave, S.C.; Pacana, T.; Seneshaw, M.; Vincent, R.; Banini, B.A.; Kumar, D.P.; Daita, K.; Min, H.-K.; Mirshahi, F.; et al. A diet-induced animal model of non-alcoholic fatty liver disease and hepatocellular cancer. *J. Hepatol.* **2016**, *65*, 579–588, doi:10.1016/j.jhep.2016.05.005.
11. Tsuchida, T.; Lee, Y.A.; Fujiwara, N.; Ybanez, M.; Allen, B.; Martins, S.; Fiel, M.I.; Goossens, N.; Chou, H.; Hoshida, Y.; et al. A simple diet- and chemical-induced murine NASH model with rapid progression of steatohepatitis, fibrosis and liver cancer. *J. Hepatol.* **2018**, *69*, 385–395, doi:10.1016/j.jhep.2018.03.011.
12. Romualdo, G.R.; Prata, G.B.; da Silva, T.C.; Fernandes, A.A.H.; Moreno, F.S.; Cogliati, B.; Barbisan, L.F. Fibrosis-associated hepatocarcinogenesis revisited: Establishing standard medium-term chemically-induced male and female models. *PLoS One* **2018**, *13*, e0203879, doi:10.1371/journal.pone.0203879.
13. Weber, L.W.D.; Boll, M.; Stampfl, A. Hepatotoxicity and Mechanism of Action of Haloalkanes: Carbon Tetrachloride as a Toxicological Model. *Crit. Rev. Toxicol.* **2003**, *33*, 105–136, doi:10.1080/713611034.
14. National Research Council *Committee for the update of the guide for the care and use of laboratory animals. Guide for the care and use of laboratory animals*; 2011; ISBN 9780309154000.
15. Andrikopoulos, S.; Blair, A.R.; Deluca, N.; Fam, B.C.; Proietto, J. Evaluating the glucose tolerance test in mice. *Am. J. Physiol. - Endocrinol. Metab.* **2008**, *295*, 1323–1332,

doi:10.1152/ajpendo.90617.2008.

16. Liang, W.; Menke, A.L.; Driessen, A.; Koek, G.H.; Lindeman, J.H.; Stoop, R.; Havekes, L.M.; Kleemann., R.; Van Den Hoek, A.M. Establishment of a general NAFLD scoring system for rodent models and comparison to human liver pathology. *PLoS One* **2014**, *9*, 1–17, doi:10.1371/journal.pone.0115922.

17. Galarraga, M.; Campión, J.; Munõz-Barrutia, A.; Boqué, N.; Moreno, H.; Martínez, J.A.; Milagro, F.; Ortiz-de-Solórzano, C. Adiposoft: Automated software for the analysis of white adipose tissue cellularity in histological sections. *J. Lipid Res.* **2012**, *53*, 2791–2796, doi:10.1194/jlr.D023788.

18. Montgomery, M.K.; Hallahan, N.L.; Brown, S.H.; Liu, M.; Mitchell, T.W.; Cooney, G.J.; Turner, N. Mouse strain-dependent variation in obesity and glucose homeostasis in response to high-fat feeding. *Diabetologia* **2013**, *56*, 1129–1139, doi:10.1007/s00125-013-2846-8.

19. Kinoshita, M.; Uchida, T.; Sato, A.; Nakashima, M.; Nakashima, H.; Shono, S.; Habu, Y.; Miyazaki, H.; Hiroi, S.; Seki, S. Characterization of two F4/80-positive Kupffer cell subsets by their function and phenotype in mice. *J. Hepatol.* **2010**, *53*, 903–910, doi:10.1016/j.jhep.2010.04.037.

20. Marra, F.; Gastaldelli, A.; Svegliati Baroni, G.; Tell, G.; Tiribelli, C. Molecular basis and mechanisms of progression of non-alcoholic steatohepatitis. *Trends Mol. Med.* **2008**, *14*, 72–81, doi:10.1016/j.molmed.2007.12.003.

21. Li, Y.; Xu, S.; Mihaylova, M.M.; Zheng, B.; Hou, X.; Jiang, B.; Park, O.; Luo, Z.; Lefai, E.; Shyy, J.Y.J.; et al. AMPK phosphorylates and inhibits SREBP activity to attenuate hepatic steatosis and atherosclerosis in diet-induced insulin-resistant mice. *Cell Metab.* **2011**, *13*, 376–388, doi:10.1016/j.cmet.2011.03.009.

22. Friedman, S.L. Mechanisms of Hepatic Fibrogenesis. *Gastroenterology* **2008**, *134*, 1655–1669, doi:10.1053/j.gastro.2008.03.003.

23. Hirsova, P.; Ibrahim, S.H.; Krishnan, A.; Verma, V.K.; Bronk, S.F.; Werneburg, N.W.; Charlton,

M.R.; Shah, V.H.; Malhi, H.; Gores, G.J. Lipid-Induced Signaling Causes Release of Inflammatory Extracellular Vesicles from Hepatocytes. *Gastroenterology* **2016**, *150*, 956–967, doi:10.1053/j.gastro.2015.12.037.

24. Patterson, R.E.; Kalavalapalli, S.; Williams, C.M.; Nautiyal, M.; Mathew, J.T.; Martinez, J.; Reinhard, M.K.; Mcdougall, D.J.; Rocca, J.R.; Yost, R.A.; et al. Lipotoxicity in steatohepatitis occurs despite an increase in tricarboxylic acid cycle activity. *Am. J. Endocrinol Metab.* **2016**, *310*, 484–494, doi:10.1152/ajpendo.00492.2015.

25. Matsuzawa, N.; Takamura, T.; Kurita, S.; Misu, H.; Ota, T.; Ando, H.; Yokoyama, M.; Honda, M.; Zen, Y.; Nakanuma, Y.; et al. Lipid-Induced Oxidative Stress Causes Steatohepatitis in Mice Fed an Atherogenic Diet. *Hepatology* **2017**, doi:10.1002/hep.21874.

26. Uehara, T.; Ppogribny, I.P.; Rusyn, I. The DEN and CCl4-induced mouse model of fibrosis and inflammation-associated hepatocellular carcinoma. *Curr. Protoc. Pharmacol.* **2015**, *66*, 1–4, doi:10.1002/0471141755.ph1430s66.The.

27. Wobser, H.; Dorn, C.; Weiss, T.S.; Amann, T.; Bollheimer, C.; Büttner, R.; Schölmerich, J.; Hellerbrand, C. Lipid accumulation in hepatocytes induces fibrogenic activation of hepatic stellate cells. *Cell Res.* **2009**, *19*, 996–1005, doi:10.1038/cr.2009.73.

28. Wang, X.; Liu, J.Z.; Hu, J.X.; Wu, H.; Li, Y.L.; Chen, H.L.; Bai, H.; Hai, C.X. ROS-activated p38 MAPK/ERK-Akt cascade plays a central role in palmitic acid-stimulated hepatocyte proliferation. *Free Radic. Biol. Med.* **2011**, *51*, 539–551, doi:10.1016/j.freeradbiomed.2011.04.019.

29. Gonzalez, F.J. Role of cytochromes P450 in chemical toxicity and oxidative stress: Studies with CYP2E1. *Mutat. Res. - Fundam. Mol. Mech. Mutagen.* **2005**, *569*, 101–110, doi:10.1016/j.mrfmmm.2004.04.021.

30. Abdelmegeed, M.A.; Banerjee, A.; Jang, S.; Yoo, S.H.; Yun, J.W.; Gonzalez, F.J.; Keshavarzian, A.; Song, B.J. CYP2E1 potentiates binge alcohol-induced gut leakiness, steatohepatitis, and apoptosis. *Free Radic. Biol. Med.* **2013**, *65*, 1238–1245,

doi:10.1016/j.freeradbiomed.2013.09.009.

31. Satapati, S.; Browning, J.D.; Shawn, C.; Satapati, S.; Kucejova, B.; Duarte, J.A.G.; Fletcher, J.A.; Reynolds, L.; Sunny, N.E.; He, T.; et al. Mitochondrial metabolism mediates oxidative stress and inflammation in fatty liver. *J. Clin. Invest.* **2016**, *125*, 4447–4462, doi:10.1172/JCI82204.Introduction.

32. Wei, Y.; Wang, D.; Topczewski, F.; Pagliassotti, M.J.; Wang, D.; Topczewski, F.; Michael, J. Saturated fatty acids induce endoplasmic reticulum stress and apoptosis independently of ceramide in liver cells. *Am. J. Physiol. Metab.* **2006**, *291*, 275–281, doi:10.1152/ajpendo.00644.2005.

33. Wang, D.; Wei, Y.; Pagliassotti, M.J. Saturated fatty acids promote endoplasmic reticulum stress and liver injury in rats with hepatic steatosis. *Endocrinology* **2006**, *147*, 943–951, doi:10.1210/en.2005-0570.

34. Sunny, N.E.; Bril, F.; Cusi, K. Mitochondrial Adaptation in Nonalcoholic Fatty Liver Disease: Novel Mechanisms and Treatment Strategies. *Trends Endocrinol. Metab.* **2017**, *28*, 250–260, doi:10.1016/j.tem.2016.11.006.

35. Kazankov, K.; Jørgensen, S.M.D.; Thomsen, K.L.; Møller, H.J.; Vilstrup, H.; George, J.; Schuppan, D.; Grønbæk, H. The role of macrophages in nonalcoholic fatty liver disease and nonalcoholic steatohepatitis. *Nat. Rev. Gastroenterol. Hepatol.* **2019**, *16*, 145–159, doi:10.1038/s41575-018-0082-x.

36. Csak, T.; Ganz, M.; Pespisa, J.; Kodys, K.; Dolganiuc, A.; Szabo, G. Fatty acid and endotoxin activate inflammasomes in mouse hepatocytes that release danger signals to stimulate immune cells. *Hepatology* **2011**, *54*, 133–144, doi:10.1002/hep.24341.

37. Shi, J.; Aisaki, K.; Ikawa, Y.; Wake, K. Evidence of hepatocyte apoptosis in rat liver after the administration of carbon tetrachloride. *Am. J. Pathol.* **1998**, *153*, 515–525, doi:10.1016/S0002-9440(10)65594-0.

38. Xie, J.; Yang, L.; Tian, L.; Li, W.; Yang, L.; Li, L. Macrophage Migration Inhibitor Factor Upregulates MCP-1 Expression in an Autocrine Manner in Hepatocytes during Acute Mouse Liver Injury. *Sci. Rep.* **2016**, *6*, 1–12, doi:10.1038/srep27665.

39. Duval, C.; Thissen, U.; Keshtkar, S.; Accart, B.; Stienstra, R.; Boekschoten, M. V.; Roskams, T.; Kersten, S.; Müller, M. Adipose tissue dysfunction signals progression of hepatic steatosis towards nonalcoholic steatohepatitis in C57Bl/6 mice. *Diabetes* **2010**, *59*, 3181–3191, doi:10.2337/db10-0224.

40. Kanda, H.; Egashira, K.; Kasuga, M.; Kanda, H.; Tateya, S.; Tamori, Y.; Kotani, K.; Hiasa, K.; Kitazawa, R. MCP-1 contributes to macrophage infiltration into adipose tissue , insulin resistance , and hepatic steatosis in obesity Find the latest version : MCP-1 contributes to macrophage infiltration into adipose tissue , insulin resistance , and hepatic steatosi. *J. Clin. Invest.* **2006**, *116*, 1494–1505, doi:10.1172/JCI26498.1494.

41. Plessis, J.; Pelt, J. Van; Korf, H.; Mathieu, C.; Schueren, B. Van Der; Lannoo, M.; Oyen, T.; Topal, B.; Fetter, G.; Nayler, S.; et al. Severity of Nonalcoholic Fatty Liver Disease. *Gastroenterology* **2015**, *149*, 635-648.e14, doi:10.1053/j.gastro.2015.05.044.

42. Stanton, M.C.; Chen, S.; Jackson, J. V; Rojas-triana, A.; Kinsley, D.; Cui, L.; Fine, J.S.; Greenfeder, S.; Bober, L.A.; Jenh, C. Inflammatory Signals shift from adipose to liver during high fat feeding and influence the development of steatohepatitis in mice. *J. Inflamm.* **2011**, 1–14.

43. Liu, Y.; Lu, X.; Li, X.; Du, P.; Qin, G. High-fat diet triggers obesity-related early infiltration of macrophages into adipose tissue and transient reduction of blood monocyte count. *Mol. Immunol.* **2020**, *117*, 139–146, doi:10.1016/j.molimm.2019.11.002.

44. Weisberg, S.P.; Hunter, D.; Huber, R.; Lemieux, J.; Slaymaker, S.; Vaddi, K.; Charo, I.; Leibel, R.L.; Jr, A.W.F. CCR2 modulates inflammatory and metabolic effects of high-fat feeding. **2006**, *116*, doi:10.1172/JCI24335.or.

45. Kumar, D.; Pandya, S.K.; Varshney, S.; Shankar, K.; Rajan, S.; Srivastava, A.; Gupta, A.; Gupta,

S.; Vishwakarma, A.L.; Misra, A.; et al. Temporal immunometabolic profiling of adipose tissue in HFD-induced obesity: manifestations of mast cells in fibrosis and senescence. *Int. J. Obes.* **2019**, *43*, 1281–1294, doi:10.1038/s41366-018-0228-5.

46. Gurung, P.; Moussa, K.; Adams-huet, B.; Devaraj, S.; Jialal, I. Increased mast cell abundance in adipose tissue of metabolic syndrome : relevance to the proinflammatory state and increased adipose tissue fibrosis. *Am. J. Physiol. - Endocrinol. Metab.* **2019**, *316*, 504–509, doi:10.1152/ajpendo.00462.2018.

47. Chambel, S.S.; Santos-Gonçalves, A.; Duarte, T.L. The Dual Role of Nrf2 in Nonalcoholic Fatty Liver Disease: Regulation of Antioxidant Defenses and Hepatic Lipid Metabolism. *Biomed Res. Int.* **2015**, *2015*, 1–10, doi:10.1155/2015/597134.

48. Chowdhry, S.; Nazmy, M.H.; Meakin, P.J.; Dinkova-Kostova, A.T.; Walsh, S. V.; Tsujita, T.; Dillon, J.F.; Ashford, M.L.J.; Hayes, J.D. Loss of Nrf2 markedly exacerbates nonalcoholic steatohepatitis. *Free Radic. Biol. Med.* **2010**, *48*, 357–371, doi:10.1016/j.freeradbiomed.2009.11.007.

49. Meakin, P.J.; Chowdhry, S.; Sharma, R.S.; Ashford, F.B.; Walsh, S. V.; McCrimmon, R.J.; Dinkova-Kostova, A.T.; Dillon, J.F.; Hayes, J.D.; Ashford, M.L.J. Susceptibility of Nrf2-Null Mice to Steatohepatitis and Cirrhosis upon Consumption of a High-Fat Diet Is Associated with Oxidative Stress, Perturbation of the Unfolded Protein Response, and Disturbance in the Expression of Metabolic Enzymes but Not with I. *Mol. Cell. Biol.* **2014**, *34*, 3305–3320, doi:10.1128/mcb.00677-14.

50. Sharma, R.S.; Harrison, D.J.; Kisielewski, D.; Cassidy, D.M.; McNeilly, A.D.; Gallagher, J.R.; Walsh, S. V.; Honda, T.; McCrimmon, R.J.; Dinkova-Kostova, A.T.; et al. Experimental Nonalcoholic Steatohepatitis and Liver Fibrosis Are Ameliorated by Pharmacologic Activation of Nrf2 (NF-E2 p45-Related Factor 2). *Cmgh* **2018**, *5*, 367–398, doi:10.1016/j.jcmgh.2017.11.016.

51. Diehl, K.L.; Vorac, J.; Hofmann, K.; Meiser, P.; Unterweger, I.; Kuerschner, L.; Weighardt, H.;

Förster, I.; Thiele, C. Kupffer Cells Sense Free Fatty Acids and Regulate Hepatic Lipid Metabolism in High-Fat Diet and Inflammation. *Cells* **2020**, *9*, doi:10.3390/cells9102258.

52. Vineeth Daniel, P.; Dogra, S.; Rawat, P.; Choubey, A.; Khan, A.S.; Rajak, S.; Kamthan, M.; Mondal, P. NF-κB p65 regulates hepatic lipogenesis by promoting nuclear entry of ChREBP in response to a high carbohydrate diet. *J. Biol. Chem.* **2021**, *296*, 100714, doi:10.1016/j.jbc.2021.100714.

53. Shu, M.; Huang, D.D.; Hung, Z.A.; Hu, X.R.; Zhang, S. Inhibition of MAPK and NF-κB signaling pathways alleviate carbon tetrachloride (CCl4)-induced liver fibrosis in Toll-like receptor 5 (TLR5) deficiency mice. *Biochem. Biophys. Res. Commun.* **2016**, *471*, 233–239, doi:10.1016/j.bbrc.2016.01.119.

54. Sunny, N.E.; Kalavalapalli, S.; Bril, F.; Garrett, T.J.; Nautiyal, M.; Mathew, J.T.; Williams, C.M.; Cusi, K. Cross-talk between branched-chain amino acids and hepatic mitochondria is compromised in nonalcoholic fatty liver disease. *Am. J. Physiol. Metab.* **2015**, *309*, E311–E319, doi:10.1152/ajpendo.00161.2015.

55. Gorissen, S.H.M.; Phillips, S.M. Branched-Chain Amino Acids (Leucine, Isoleucine, and Valine) and Skeletal Muscle. In *Nutrition and Skeletal Muscle*; Elsevier, 2019; pp. 283–298 ISBN 9780128104224.

56. Sano, A.; Kakazu, E.; Hamada, S.; Inoue, J.; Ninomiya, M.; Iwata, T.; Tsuruoka, M.; Sato, K.; Masamune, A. Steatotic Hepatocytes Release Mature VLDL Through Methionine and Tyrosine Metabolism in a Keap1-Nrf2–Dependent Manner. *Hepatology* **2021**, *74*, 1271–1286, doi:10.1002/hep.31808.

57. Bonagurio, L.P.; Murakami, A.E.; Moreira, C.A.; Comar, J.F.; Pozza, P.C. Dietary supplementation with inosine-5'-monophosphate improves the functional, energetic, and antioxidant status of liver and muscle growth in pigs. *Sci. Rep.* **2022**, *12*, 350, doi:10.1038/s41598-021-04023-y.

58. Vaupel, P.; Multhoff, G. Revisiting the Warburg effect: historical dogma versus current understanding. *J. Physiol.* **2021**, *599*, 1745–1757, doi:10.1113/JP278810.

59. Tauffenberger, A.; Fiumelli, H.; Almustafa, S.; Magistretti, P.J. Lactate and pyruvate promote oxidative stress resistance through hormetic ROS signaling. *Cell Death Dis.* **2019**, *10*, doi:10.1038/s41419-019-1877-6.

Chapter 3

Effects of indole-3-carbinol and/or chlorogenic acid on a murine model of NASH: a new preclinical strategy?

Abstract

Nonalcoholic fatty liver disease (NAFLD) is a wide spectrum chronic liver disease, that affects around 25% of the worldwide population, whereas nonalcoholic steatohepatitis (NASH), affects almost 5%. Recent reports suggest that the high intake of fat/sugars might be a potential driver of NAFLD. Moreover, NAFLD-related annual economic cost was projected to reach $103 and €35 billion, for the USA and Europe, respectively. Although there are several efforts, still there is no approved therapy for NAFLD patients. Otherwise, *Brassicaceae* family vegetables comprise a pharmacopeia of bioactive compounds, due to the antioxidant, anti-inflammatory, and anti-lipogenic properties of isothiocyanates and polyphenols, especially indole-3-carbinol (I3C) and chlorogenic acid (CGA). Thus, we sought to assess if I3C and/or CGA exert a beneficial effect on a murine NASH model. Mice (C57BL/6J) were fed a western diet protocol [high-fat chow and a high-sugar solution (HSS) for drinking], besides intraperitoneal injections of weekly-increases doses of a 10% oil-diluted solution of carbon tetrachloride (CCl_4, 0.25-1.50 μL/g of body weight), for 8 weeks. I3C+CGA-treated mice showed a reduction in relative liver weight ($p<0.0001$), microvesicular steatosis ($p<0.0001$), α-smooth muscle actin (α-SMA) levels ($p<0.0001$), and hepatic CD68+ cells ($p<0.0001$). The combination I3C+CGA also slightly decreased the hepatic lipid ($p=0.0011$) and collagen fibers content ($p<0.0001$), and alleviated the NAFLD activity score (NAS) grading ($p=0.0005$). Thus, we suggest that I3C and CGA association alleviate NASH severity, by attenuating the impacts of saturated fatty acid and simple carbohydrate overload, which has been related to the redox-lipid dynamics, as well as reducing the lipid peroxidation activity of the CCl_3 radicals, derivative from CCl_4 metabolization, and hence, alleviating the hepatic pro-inflammatory microenvironment state.

Introduction

Nonalcoholic fatty liver disease (NAFLD) is expected to become the most common cause of chronic liver disease, affecting almost 25% of the global population. In addition, nonalcoholic steatohepatitis (NASH), the most advanced stage of NAFLD, affects 5% [1]. In parallel, it is also observed that changes in lifestyle and dietary habits have led to a striking increase in the incidence and prevalence of the "civilization diseases", like obesity and type 2 *diabetes mellitus* (T2D), since the end of the XXth century [2,3]. Indeed, both obesity and T2D have been appointed as risk factors of NAFLD/NASH, and NAFLD-related deaths should double in the period 2016-2030 [1,4–6]. Thus, there is an urgent need to develop potential new strategies for early diagnosis, prevention, therapy, and effective therapy [6,7]. Otherwise, still imprecise the molecular mechanisms related to the corresponding disease emergence and progression, along with no effective therapy approved by the health and governmental agencies for NAFLD patients [7]. Recently, *in vivo* experimental models have been designed, seeking to establish a reliable model that revisits morphological, metabolical, and molecular traits of the corresponding disease [8]. Asgharpour *et al*. [9] reported that mice fed a western diet [high-fat chow with a high-sugar solution (HSS) for drinking] feature hepatic steatosis (HS), insulin resistance (IR), and lobular inflammation, although a long period protocol (8-52 weeks) is necessary for developing NASH traits. Similarly, it has been established a fast-induced protocol of NASH, by associating the WD protocol with weekly doses of carbon tetrachloride (CCl_4), acting as an accelerator in the progression of NAFLD and mimicking morphological and transcriptomic aspects of the corresponding disease in humans [10].

On the other hand, the bioactive compounds of food feature as a potential strategy against metabolic diseases, due to the pharmacopeia of antioxidant and anti-inflammatory molecules [11]. In agreement, it has been reported that adherence to the Mediterranean diet, which is mainly composed of vegetables, fruits, polyunsaturated fatty acids (PUFA), and phenolic compounds, alleviates NAFLD severity, by modulating the HS and IR profile of patients, whereas low adherence has been related to 5-fold higher risk of developing NAFLD [11–13]. However, only ~9% of USA adults meet the daily intake of

vegetable recommendations (150-450g of vegetable/day), according to the Center for Disease Control [14]. The *Brassicaceae* family comprises a wide group of vegetables (~350 genera and 3500 species), besides featuring among the most harvested and produced globally (broccoli, cabbages, cauliflower, and others) [15]. Estimates show that the daily intake of Brassica vegetables meets ~20g/day [15]. However, food frequency questionaries indicate that the daily intake of Brassicaceae vegetables by an adult was about 84g/day [16].

The bioactive effects of Brassica vegetables have been attributed to both glucobrassicin-derivative molecules, the isothiocyanates (ITC), as indole-3-carbinol (I3C, PubChem CID 3712), and the polyphenols molecules, like chlorogenic acid (CGA, PubChem CID 1794427) [17–19]. I3C is a high abundance molecule and its synthesis occurs by the activity of the myrosinase (vegetable cell) or myrosinase-like (bacteria) enzymes, by converting ITC into I3C under neutral pH conditions, whereas CGA is the most abundant hydroxycinnamic acid in Brassica vegetables [17,19]. The recent findings regarding the bioactive propertieos of I3C and CGA suggest that these molecules might be a potential preclinical strategy against NAFLD and related metabolic disorders, by modulating the pivotal gut-liver-adipose axis, due to their anti-lipogenic, antioxidant, and anti-inflammatory effects, as reviewed by our research group [20–24]. Nonetheless, combined administration of these bioactive compounds is not fully explored in literature.Thus, we sought to assess the effects of I3C and/or CGA treatment on a hybrid model (diet- and chemically-induced) model of NASH.

Materials and methods

2. Experimental design and treatments

Eight-week-old male C57BL/6J mice were randomly distributed into 5 experimental groups (N = 12; control; NASH; I3C; CGA; I3C+CGA) and submitted to the hybrid NASH protocol established by our group [25], in which mice were fed a western diet style [WD, chow enriched with fat/sucrose (200g/Kg or ~37.5

and ~17% of total calories; Pragsoluções Biociências, Brazil) and a HSS, for drinking (55/45% weight/weight (w/w) proportion of D-fructose/D-glucose or 23.1 and 18.9g/L diluted in drinking water, respectively; Dinâmica, Brazil), for 8 weeks (Figure 1). In addition, mice received weekly-increased intraperitoneal injections of a 10% oil-diluted solution of CCl_4 [0.25-1.50µL/g of body weight (b.wt.), 3x/week] protocol, for 8 weeks[26]. Concomitantly, mice received the intragastric administrations of an oil-diluted solution of I3C (5mg/Kg b.w.)or water-diluted solution of CGA (125mg/Kg b.w.) or both bioactive compounds of *Brassicaceae* family or the respective vehicles 5x/week, during 8 weeks. The control group received a basal diet, composed by a basal chow and filtered water for drinking. Mice were euthanized by exsanguination under ketamine/xylazine anesthesia, and the blood was collected in heparinized syringes from cardiac puncture, centrifuge (1500xg, 15 min.), and serum samples were collected and stored in -80ºC for further analysis. At the necropsy, the liver, adipose tissue (AI) were removed, weighted, and then liver samples from the left lobe, epididymal adipose tissue, and small intestine samples were collected and fixed in 10% formalin or snap-frozen into liquid nitrogen for further analysis. Additional liver samples from left and medial lobes and adipose tissue (AT) were collected and stored at -80ºC for biochemical and molecular analysis. Additionally, colonic feces were collected and stored at -80ºC for further 16S bacterial DNA sequencing.

The animals were obtained from the School of Veterinary Medicine and Animal Science of the University of São Paulo (FMVZ, USP, São Paulo-SP, Brazil) and kept in Botucatu Medical School of the São Paulo State University (FMB, UNESP, São Paulo – SP, Brazil) in a room with continuous ventilation, relative humidity (45-65%), controlled temperature (20-24ºC) and light/dark cycle 12:12 hours, with *ad libitum* offering of chow and water. Body weight and food/water consumption were recorded once a week during the experimental period. This experiment was carried out under protocols approved by Botucatu Medical School/UNESP Ethics Committee on Use of Animals (CEUA, Protocol number 1343/2020), and animals received human care according to the “Guide for the Care and Use of Laboratory Animals” [27].

3. I3C and CGA: dose determination

The doses were determined according to the Human Equivalent Dose (HED), as previously established, and based on estimates of global consumption of I3C and CGA (22.5 and 600.0 mg/day, respectively), following the equations (I-IV) [15,28,29]. The final doses of I3C and CGA were determined as ~4.5 and 125.0 mg/day, respectively.

HED

(I) Animal dose $(\frac{mg}{Kg}\, b.wt.)$ = Human dose $(\frac{mg}{Kg}\, b.wt.)$ x Km human/Km animal

(II) Animal dose $(\frac{mg}{Kg}\, b.wt.)$ = Human dose $(\frac{mg}{Kg}\, b.wt.)$ x 37/3

(III) Animal dose of I3C $(\frac{mg}{Kg}\, b.wt.)$ = 0.375 $(\frac{mg}{Kg}\, b.wt.)$ x 37/3 = ~4.5 $(\frac{mg}{Kg}\, b.wt.)$

(IV) Animal dose of CGA $(\frac{mg}{Kg}\, b.wt.)$ = 10 $(\frac{mg}{Kg}\, b.wt.)$ x 37/3 = ~125.5 $(\frac{mg}{Kg}\, b.wt.)$

3. Glucose tolerance test

Four days before the euthanasia, mice were fasted for 12 hours and submitted to a glucose tolerance test (GTT). For that, mice have been weighted and blood samples collected from the caudal vein, in order to measure the glucose level in an Accu-Chek glucometer (Roche, Germany). Further, animals received an i.p. injection of a water-diluted D-glucose solution (2g/Kg b.w.) (Dinâmica, Brazil). Glucose levels were measured following 30, 60, 90, and 120 min. after the injection [30].

4. Histological analysis

The left liver lobe, small intestine, and the epididymal adipose tissue (EAT) samples fixed in 10% formalin were embedded in paraffin. Then, 5 µm thick sections were obtained and disposed on regular or silanized glass slides, and further, liver sections were stained with Hematoxylin & Eosin (H&E) or Sirius Red, and immunohistochemistry reactions, while EAT sections were stained with Toluidine Blue (pH= 4,0). Also, 10 µm thick liver sections were obtained from snap-frozen (-80ºC) samples embedded in Optimal Cutting Temperature (Tissue-Trek, USA) for Oil Red staining (Sigma Aldrich, USA).

4.1 Evaluation of Non-alcoholic Fatty Liver Diseases Activity Score and Fibrosis

The liver sections stained with H&E were used for evaluating the NAFLD Activity Score (NAS), according to the criteria previously established [31], while sections stained with Oil Red were used to evaluate lipid deposits. The NAS analysis was performed according to Liang *et al*. [31] Photomicrographs of 5 randomly selected fields/animal liver sections stained with Oil Red were acquired for morphometric analysis to evaluate the lipid deposit (%). Similarly, photomicrographs of 10 randomly selected fields/animals were acquired to perform the morphometric analysis to evaluate the total area filled with collagen fibers (%) in liver sections stained with Sirius Red.

4.2 Morphometric analysis of adipocytes and mast cells counting

Five-micron thickness EAT sections, stained with H&E and toluidine blue (Sigma Aldrich, USA), were used for evaluating the number/mm² of adipocytes and its occupied area (%), and mastocytes infiltration (number of mastocytes/mm²), respectively, as established previously [32]. For that, photomicrographs of 10 randomly selected fields were acquired (200x magnification, software CellSense, Olympus Corporation, Japan) and analyzed by the software Image J (NIH, USA). For adipocytes analysis, the extension Adiposoft, from Image J (NIH, USA) was used.

4.3 Immunohistochemistry

Semiquantitative analysis of immunoreactivities for Ki67 (*i.e.,* a marker for cellular proliferation), CD68 (*i.e.,* a marker of macrophages), and α-smooth muscle actin (α-SMA) (*i.e.,* a marker of active hepatic stellate cells, HSC) were performed in liver sections. For that, deparaffinated 5-micron sections in silane-covered slides were submitted to antigen retrieval in 0.01M citrate buffer (pH 6.0, 120ºC, 5 min) in a Pascal Pressure Chamber (Dako Cytomation, Denmark). Then, a blockade of endogenous peroxidase and nonspecific bindings with 10% H_2O_2 in phosphate-buffered saline (PBS) (15 min.), followed by treatment with skim milk (60 min.) and overnight incubation in a humidified chamber (4ºC) with Ki67 (MA5-14520, 1:50 dilution, ThermoFisher, USA), CD68 (ab125212, 1:400 dilution, Abcam, UK), and α-SMA (ab124964, 1:500 dilution, Abcam, UK) antibodies diluted in 1% bovine serum albumin solution were performed. After three wash-steps with PBS (5 min. each), slides were incubated with a single step horseradish peroxidase (HRP)-polymer (EasyPath - Erviegas, Brazil) (20 min). Reactions were

visualized with 3´3-diaminobenzidine (DAB) chromogen (Sigma–Aldrich, USA) and counterstained with Harris hematoxylin.

Photomicrographs of 10 randomly-selected fields/animal (200x or 400x magnification, software CellSense, Olympus Corporation, Japan) from liver sections immunostained for α-SMA were acquired and % positive area marker was performed with software Leica Qwin (Leica Biosystems, Germany), by calculating the total area filled by α-SMA (%). Similarly, CD68 and Ki67 analyses were performed by acquiring photomicrographs of 10 randomly selected fields/animal (200x or 400x magnification, software CellSense, Olympus Corporation, Japan). Then, the mean number of CD68 positive macrophages and Ki67 positive hepatocytes were expressed by liver area analyzed (mm^2) using the software ImageJ (NIH, USA).

5. Statistical analysis

The GTT data were used to draw a glycemic curve and the area under the curve (AUC), which was measured and analyzed by two-way ANOVA, while the score data were evaluated by the non-parametrical Kruskal-Wallis test and a *post hoc* Tukey's test. The other collected data were analyzed by one-way ANOVA or Kruskal-Wallis, followed by a *post hoc* Tukey's test. Differences were considered significant when $p<0.05$. Data were presented as mean ± standard deviation (S.D.) or median and 25% and 75% interquartile (box plot). All data were analyzed with the software GraphPad Prism 6.01 (GraphPad, USA).

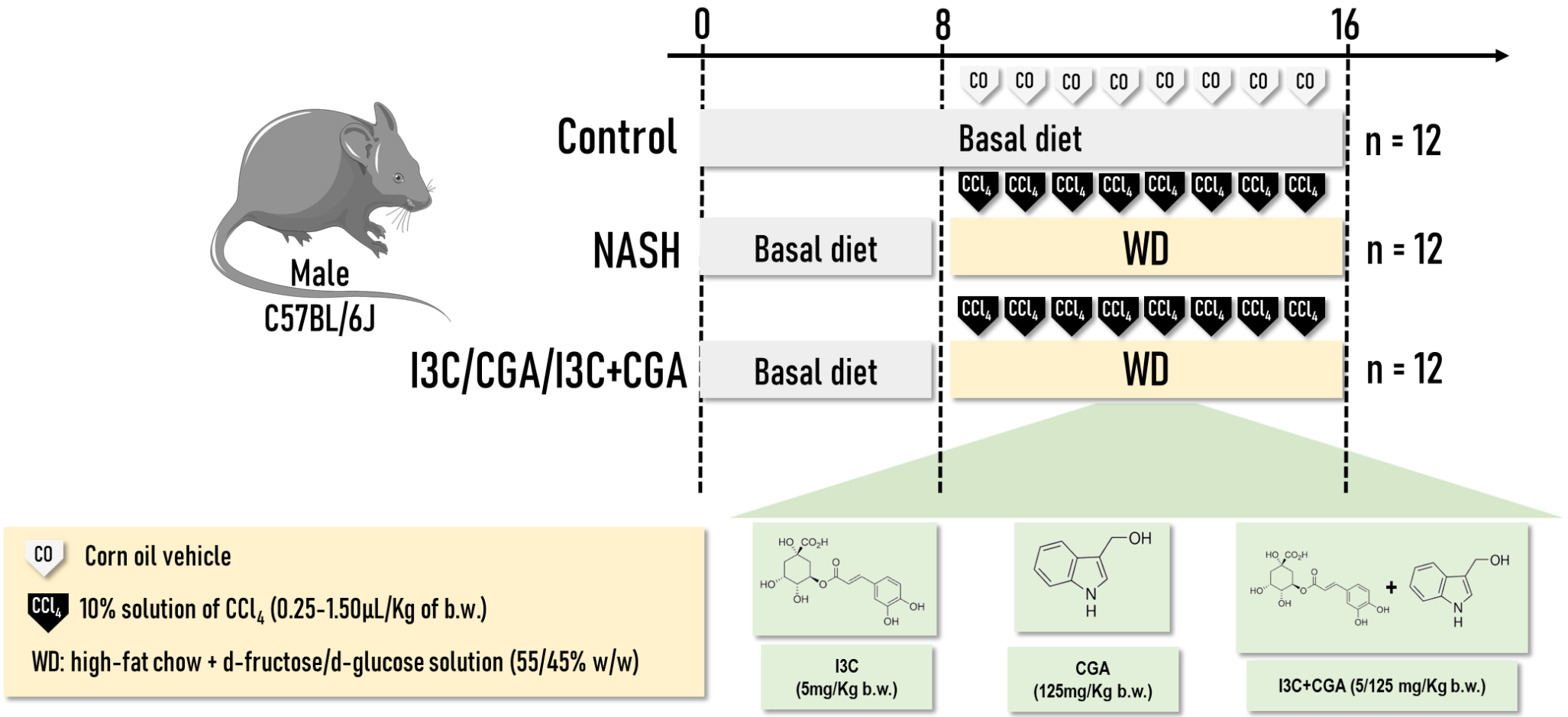

Figure 1. **Experimental design.** Effects of indole-3-carbinol (I3C) and/or chlorogenic acid (CGA) on the hybrid-induced model of fibrosis-associated non-alcoholic steatohepatitis (NASH). Control [standard chow and 3x weekly intraperitoneal (i.p.) injections of corn oil vehicle]; NASH [chow enriched with fat (20%) and sucrose (20%) and carbon tetrachloride protocol (3x weekly i.p. injections of 10% corn oil solution of CCl_4, with weekly-increased doses of 0.25-1.50µL/g of body weight (b.w.)]; I3C [hybrid protocol of NASH with addition of intragastric injections of indol-3-carbinol (I3C, 5x weekly, 5mg/Kg b.w.)]; CGA [hybrid protocol of NASH with addition of intragastric injections of chlorogenic acid (CGA, 5x weekly, 125mg/Kg b.w.)]; I3C+CGA [hybrid protocol of NASH with addition of intragastric injections of both I3C and CGA. N = 6 (control) or 8-9 (I3C, CGA, and I3C+CGA). CO: corn oil; CCl_4: carbon tetrachloride; WD: western diet. Representative images were acquired from Servier Medical Art (smart.servier.com).

Results

6. General findings

Mice were submitted to a GTT, but no effect of I3C and/or CGA was observed (Figure 2). As expected, we observed that the liver of all mice submitted to the hybrid NASH protocol presented a yellowish color and a rough surface aspect, due to the high levels of fat/sugar consumption and the hepatotoxin CCl_4 administrations, while a smooth surface aspect was observed in the macroscopic analysis of the control group, suggesting an hepatic lipid and collagen deposition occurs in the liver of mice submitted to the hybrid protocol of NASH (Figure 3). After 8 weeks of the hybrid protocol, there were no differences related to the body weight evolution and final body weight of mice among groups (Table 1) (Figure 2). Moreover, all groups featured similar levels of chow consumption, whereas WD-receiving groups consumed higher levels of HSS (g/mouse/day) than the control group ($p<0.0001$). Additionally, I3C, CGA, and I3C+CGA-treated groups featured decreased absolute liver weight ($p=0.0078$) (Table 1), compared to the NASH group. Further, we observed that all treated groups featured reduced relative liver weight ($p<0.0001$) (Table 1), compared to the NASH group. Finally, there were no differences regarding the total AT weight (epididymal, retroperitoneal, and intestinal) and relative AT weight among groups (Figure 2).

7. The combination I3C+CGA reduces NAS parameters

Regarding the lipid content profile, it was observed that the hybrid protocol of NASH induced microvesicular steatosis, rather than a macrovesicular profile (Table 2) (Figure 4). In addition, both CGA and I3C+CGA mice groups showed a reduced score of microvesicular steatosis ($p<0.0001$). Mice also featured frequent occurrence of inflammatory foci and, hence, locular inflammation, but the were no differences among NASH and I3C- and/or CGA-treated groups($p=0.0005$) (Table 2) (Figure 4).

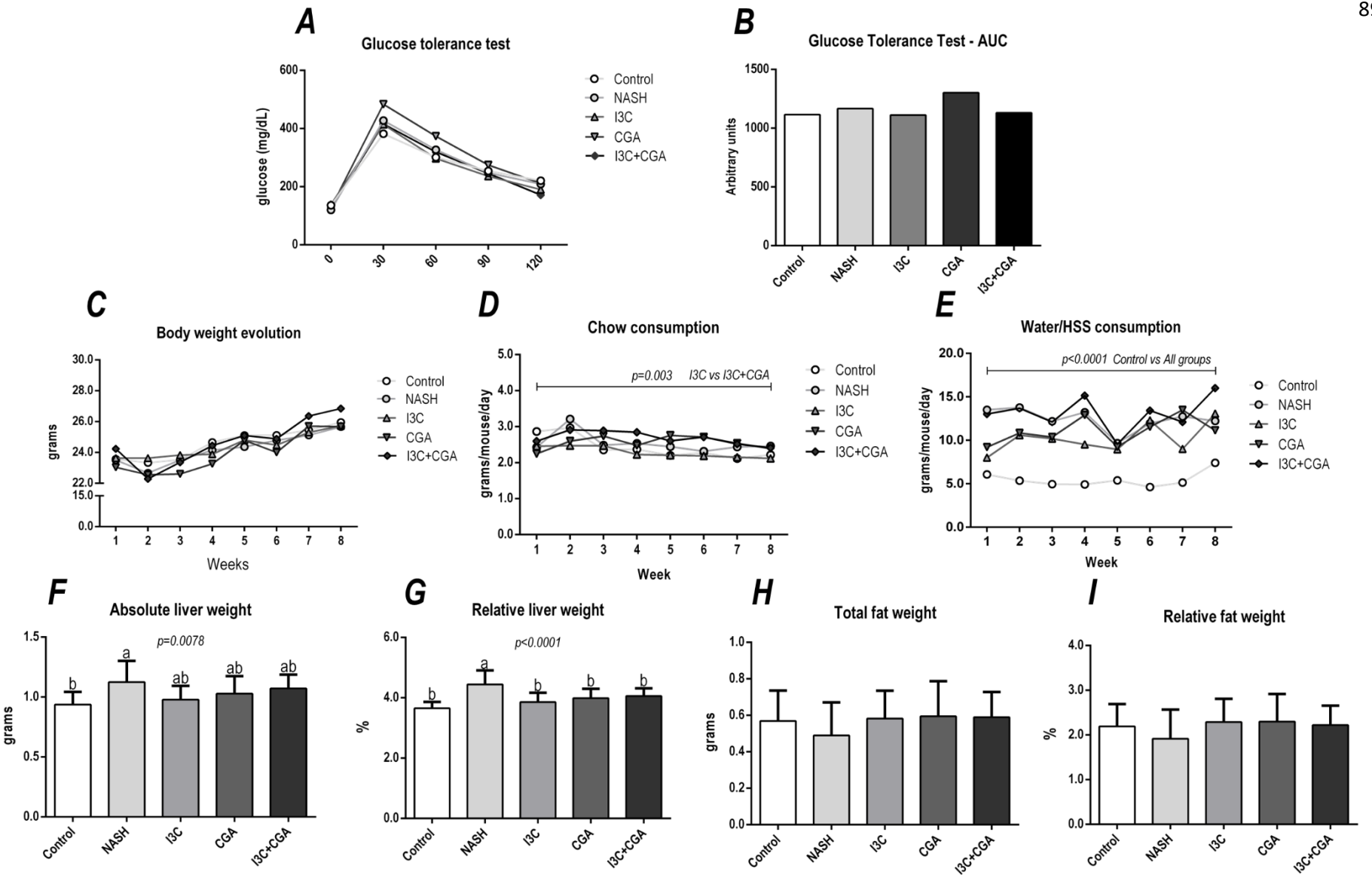

Figure 2. Effects of indole-3-carbinol and/or chlorogenic acid over the glucose tolerance test (GTT), body weight evolution, chow/HSS consumption, and absolute/total or relative liver and adipose tissue (AT) weight in a hybrid model of NASH in C57BL/6J mice. **(A and B)** The blood glucose levels were measured in different timepoints (0, 30, 60, 90, and 120 min.) by a glucometer and the area under the curve was measured and plotted. **(C, D, and E)** Animals were weighted and their chow and HSS consumption was measured 1x/week, during 8 weeks. **(F, G, H, and I)** After the euthanasia, the liver and the AT were weighted and compared to the body weight, for the relative weights. Control [standard chow and 3x weekly intraperitoneal (i.p.) injections of corn oil vehicle]; NASH [chow enriched with fat (20%) and sucrose (20%) and carbon tetrachloride protocol (3x weekly i.p. injections of 10% corn oil solution of CCl_4, with weekly-increased doses of 0.25-1.50μL/g of body weight (b.w.)]; I3C [hybrid protocol of NASH with addition of intragastric injections of indol-3-carbinol (I3C, 5x weekly, 5mg/Kg b.w.)]; CGA [hybrid protocol of NASH with addition of intragastric injections of chlorogenic acid (CGA, 5x weekly, 125mg/Kg b.w.)]; I3C+CGA [hybrid protocol of NASH with addition of intragastric injections of both I3C and CGA. N = 6 (control) or 8-9 (I3C, CGA, and I3C+CGA). The data are expressed in mean±standard deviation, and were analyzed by One-Way ANOVA, and Tukey pos-hoc test.

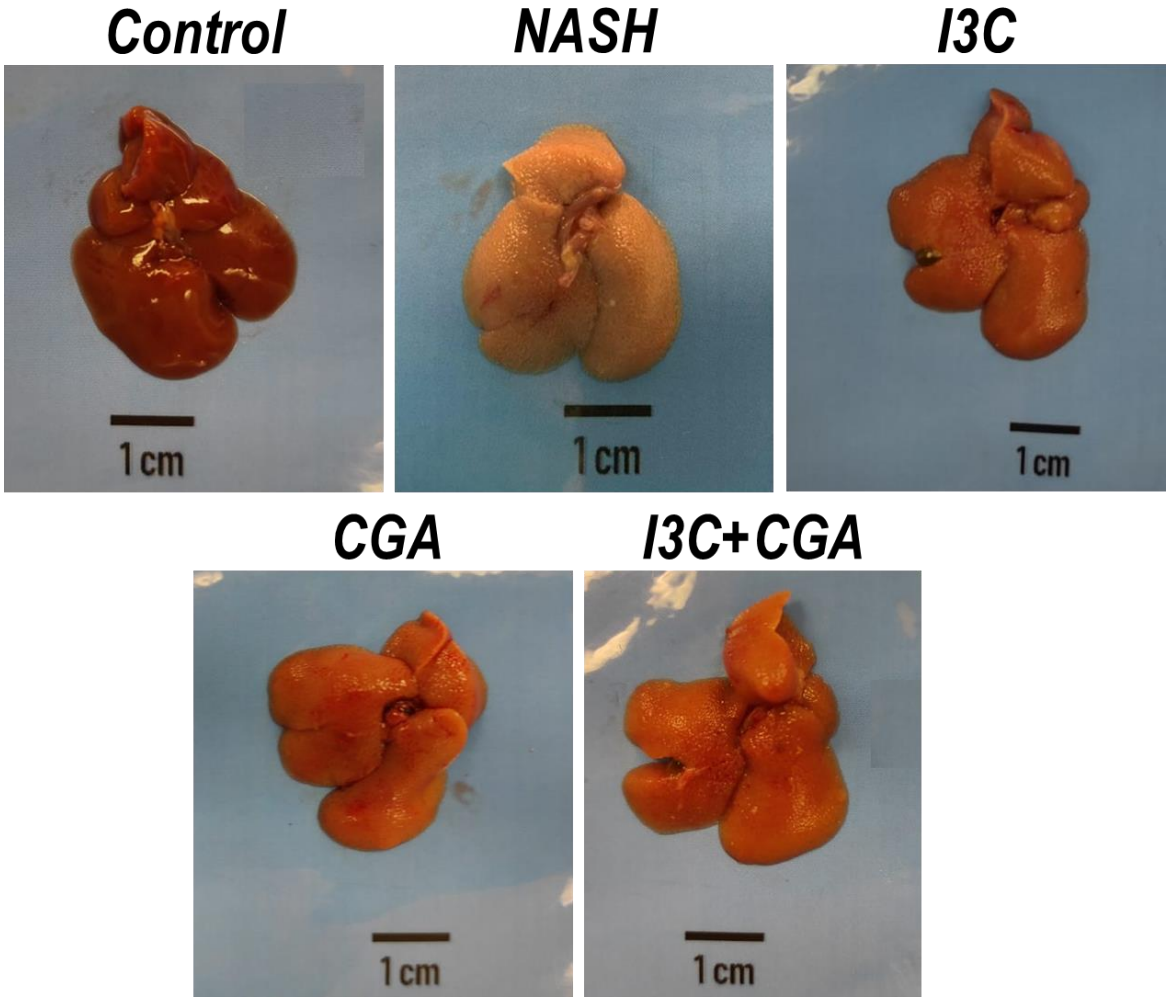

Figure 3. Effects of indole-3-carbinol (I3C) and/or chlorogenic acid (CGA) on the hybrid model of NASH. Macroscopic overview. Control [standard chow and 3x weekly intraperitoneal (i.p.) injections of corn oil vehicle]; NASH [chow enriched with fat (20%) and sucrose (20%) and carbon tetrachloride protocol (3x weekly i.p. injections of 10% corn oil solution of CCl_4, with weekly-increased doses of 0.25-1.50µL/g of body weight (b.w.)]; I3C [hybrid protocol of NASH with addition of intragastric injections of indol-3-carbinol (I3C, 5x weekly, 5mg/Kg b.w.)]; CGA [hybrid protocol of NASH with addition of intragastric injections of chlorogenic acid (CGA, 5x weekly, 125mg/Kg b.w.)]; I3C+CGA [hybrid protocol of NASH with addition of intragastric injections of both I3C and CGA. N = 6 (control) or 8-9 (I3C, CGA, and I3C+CGA).

Table 1. Effects of I3C and/or CGA on body, liver, and fat weight during the NASH establishment.

Parameters	Groups				
	Control	**NASH**	**I3C**	**ACG**	**I3C+ACG**
Final body weight (g)	25.6 ± 2.2	25.2 ± 2.3	25.3 ± 1.6	25.7 ± 2.3	26.4 ± 1.7
Absolute liver weight (g)	0.94 ± 0.1^{b}	1.12 ± 2.3^{a}	0.98 ± 0.1^{ab}	1.03 ± 0.1^{ab}	1.07 ± 0.1^{ab}
Relative liver weight (%)	3.65 ± 0.2^{b}	4.52 ± 0.5^{a}	3.99 ± 0.3^{b}	4.06 ±0.3^{b}	4.16 ± 0.2^{b}
Total fat weight (g)*	0.57 ± 0.2	0.49 ± 0.2	0.58 ± 0.2	0.59 ± 0.2	0.59 ± 0.1
Relative total fat weight (%)	2.19 ± 0.5	1.92 ± 0.7	2.29 ± 0.5	2.30 ± 0.6	2.22 ± 0.4
Absolute epidydimal fat weight (g)	0.27 ± 0.1	0.26 ± 0.1	0.30 ± 0.1	0.29 ± 0.1	0.33 ± 0.1
Absolute retroperitoneal fat weight (g)	0.12 ± 0.0	0.13 ± 0.1	0.15 ± 0.1	0.14 ± 0.1	0.14 ± 0.1
Absolute intestinal fat weight (g)	0.18 ± 0.1	0.10 ± 0.1	0.13 ± 0.1	0.17 ± 0.1	0.13 ± 0.1

Data are mean ± S.D. N = 12-13 mice/group. *Sum of absolute epidydimal, retroperitoneal, and intestinal fat weights. Control [standard chow and 3x weekly intraperitoneal (i.p.) injections of corn oil vehicle]; NASH [chow enriched with fat (20%) and sucrose (20%) and carbon tetrachloride protocol (3x weekly i.p. injections of 10% corn oil solution of CCl_4, with weekly-increased doses of 0.25-1.50µL/g of body weight (b.w.)]; I3C [hybrid protocol of NASH with addition of intragastric injections of indol-3-carbinol (I3C, 5x weekly, 5mg/Kg b.w.)]; CGA [hybrid protocol of NASH with addition of intragastric injections of chlorogenic acid (CGA, 5x weekly, 125mg/Kg b.w.)]; I3C+CGA [hybrid protocol of NASH with addition of intragastric injections of both I3C and CGA. N = 6 (control) or 8-9 (I3C, CGA, and I3C+CGA). Different letters correspond to statistical differences among groups by ANOVA and *post hoc* Tukey test ($p<0.05$).

Table 2 – Effects of I3C and/or CGA on nonalcoholic fatty liver disease activity score (NAS) and hepatocellular ballooning.

NAS Parameters	*Control*	*NASH*	*I3C*	*CGA*	*I3C+CGA*
Macrovesicular steatosis (0-3)	0 (0;0)	0 (0;0)	0 (0;0)	0 (0;0)	0 (0;0)
Microvesicular steatosis (0-3)	0 (0;0)^{b}	3.0 (2.3;3.0)^{ab}	1.5 (1.0;2.0)^{ab}	0.0 (0.0;1.8)^{b}	1.0 (0.0;2.0)^{b}
Hepatocellular hypertrophy (0-3)	0 (0;0)^{b}	2.0 (0.0;3.0)^{a}	0.0 (0.0;0.0)^{b}	0.0 (0.0;0.0)^{b}	0.0 (0.0;0.8)^{ab}
Inflammatory foci (0-3)	0 (0;0)^{b}	2.8 (1.6;3.0)^{a}	2.3 (2.0;3.0)^{a}	1.8 (1.5;2.8)^{a}	1.8 (1.1;2.0)^{ab}
Hepatocellular ballooning*	0±0	0.2±0.2	0.2±0.2	0.4±0.5	0.3±0.2
NAFLD activity score (0-12)	0 (0;0)^{b}	7.5 (5.3;8.3)^{a}	4.0 (3.1;4.4)^{a}	2.8 (1.6;3.4)^{b}	3.0 (2.1;4.5)^{ab}

Table 2. Effects of indole-3-carbinol (I3C) and/or chlorogenic acid (CGA) on the nonalcoholic fatty liver disease activity score (NAS, sum of macrovesciular and microvesicular steatosis, hepatocellular hypertrophy, and inflammatory foci scores) and hepatocellular ballooning. Parameters were analyzed by Kruskall-Wallis and post-hoc Dunn's test, or One-Way ANOVA and post-hoc Tukey's test, and data were expressed as median and first and third quartile, or mean ± standard deviation (S.D) (*). The hepatocellular ballooning analysis was performed evaluating the number of hepatocellular ballooning/field. Different letters correspond to statistical differences among the groups ($p<0.05$). Control [standard chow and 3x weekly intraperitoneal (i.p.) injections of corn oil vehicle]; NASH [chow enriched with fat (20%) and sucrose (20%) and carbon tetrachloride protocol (3x weekly i.p. injections of 10% corn oil solution of CCl_4, with weekly-increased doses of 0.25-1.50µL/g of body weight (b.w.)]; I3C [hybrid protocol of NASH with addition of intragastric injections of I3C (5x weekly, 5mg/Kg b.w.)]; CGA [hybrid protocol of NASH with addition of intragastric injections of CGA (5x weekly, 125mg/Kg b.w.)]; I3C+CGA [hybrid protocol of NASH with addition of intragastric injections of both I3C and CGA. N = 6 (control) or 8-9 (I3C, CGA, and I3C+CGA).

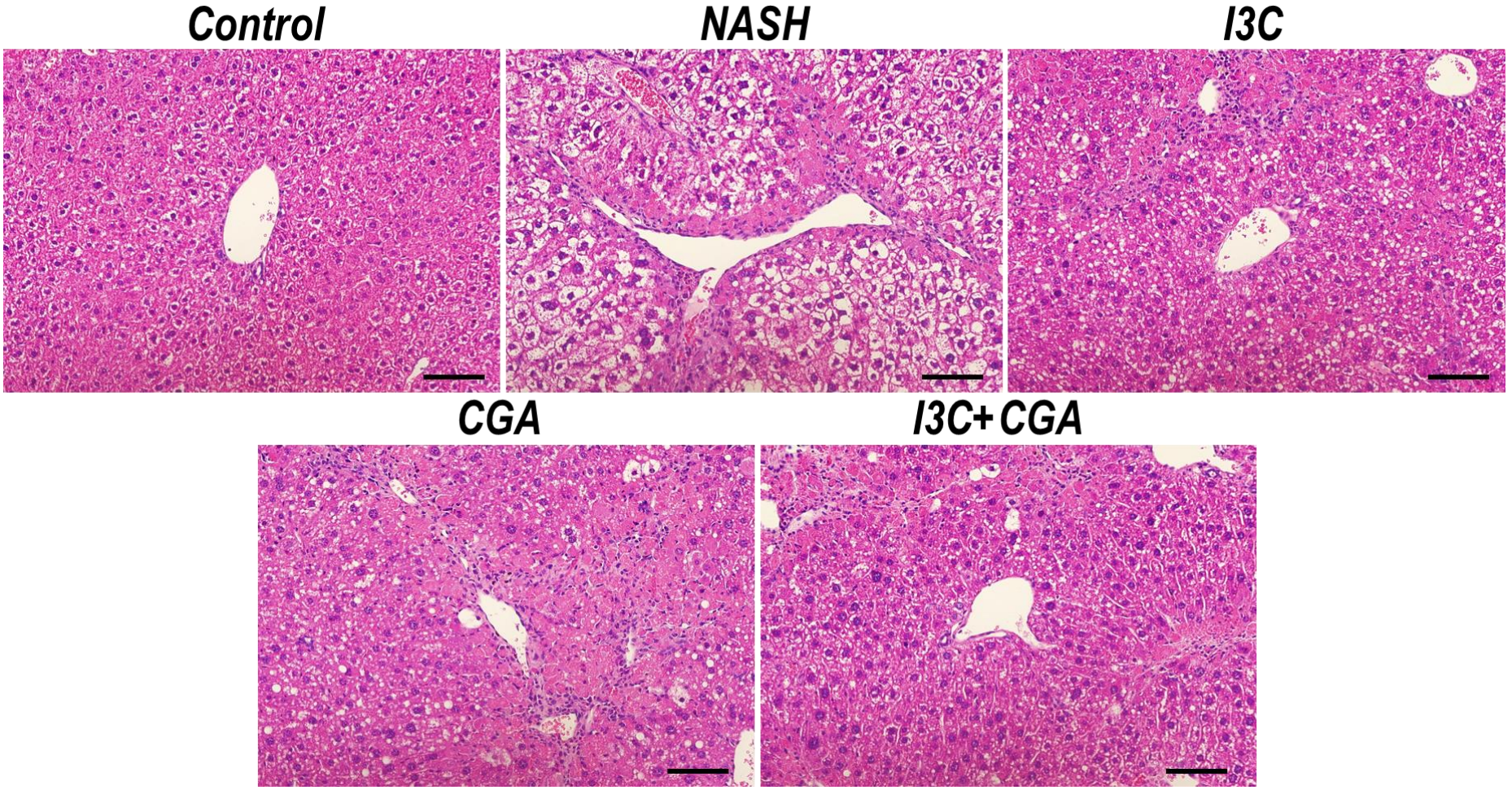

Figure 4. Effects of índole-3-carbinol (I3C) and/or chlorogenic acid (CGA) on nonalcoholic fatty liver disease activity score (NAS). Representative photomicrographs (20x objective, scale bar=50µm) of sections stained with hematoxilin and eosin (H&E). Control [standard chow and 3x weekly intraperitoneal (i.p.) injections of corn oil vehicle]; NASH [chow enriched with fat (20%) and sucrose (20%) and carbon tetrachloride protocol (3x weekly i.p. injections of 10% corn oil solution of CCl_4, with weekly-increased doses of 0.25-1.50µL/g of body weight (b.w.)]; I3C [hybrid protocol of NASH with addition of intragastric injections of I3C (5x weekly, 5mg/Kg b.w.)]; CGA [hybrid protocol of NASH with addition of intragastric injections of CGA (5x weekly, 125mg/Kg b.w.)]; I3C+CGA [hybrid protocol of NASH with addition of intragastric injections of both I3C and CGA. N = 6 (control) or 8-9 (I3C, CGA, and I3C+CGA).

Of note, only I3C+CGA-treated mice featured a slightly reduction of the number of inflammatory foci grade, in comparison to the other groups (p=0.0005) (Table 2) (Figure 4). Moreover, the NASH group featured enhanced levels of hepatocytes hypertrophy, differently from all I3C- and/or CGA-treated groups, which displayed a reduced score of the hypertrophy of hepatocytes (p=0.0005) (Table 2), suggesting that I3C and/or CGA treatment alleviates the hepatocytes-related stress that causes hepatocellular hypertrophy (Figure 3). Finally, when assessing the final NAS grade, both CGA and I3C+CGA-treated groups presented a decreased score compared to the NASH group (p<0.0001) (Table 2), suggesting that CGA, more than I3C, alleviates the NASH-related parameters.

8. The combination I3C+CGA reduces the hepatic lipid and collagen content

In agreement with the microvesicular steatosis score in the NAS analysis, the NASH group featured enhanced levels of lipid content in oil-red staining and collagen in sirius red-staining in comparison to the control group (p=0.0011 and p<0.0001) (Figure 5 and 6). All treated groups featured decreased levels of hepatic lipid content (Figure 5), although only the CGA-treated group featured a significant difference (p=0.0011). Moreover, we assessed the levels of HSC activation by immunoreactivity for α-SMA. Indeed, the combination of only I3C+CGA decreased the HSC activation (p<0.0001), and the collagen content (~25%), although no statistical difference was observed in sirius red analysis (Figure 6), compared to the NASH group. Thus, we suggest that the combination I3C+CGA attenuates NASH severity, by reducing the hepatic lipid and collagen content (~25%), further confirmed by the reduced levels of HSC activation, probably by modulating the pro-inflammatory/lipogenic hepatic microenvironment, in which NASH is susceptible to emerge.

9. The combination I3C+CGA reduces the number of CD68+ cells, but not Ki67+ hepatocytes

We also assessed the number of Ki67-positive hepatocytes and CD68-positive in the liver sections. Regarding the number of $Ki67^+$ hepatocytes, we observed that mice submitted to the hybrid protocol of NASH displayed an enhanced number of $Ki67^+$ (p=0.0005), while no effect of the I3C and/or CGA was observed (Figure 7). On the other hand, we observed that only the I3C+CGA-treated group showed a

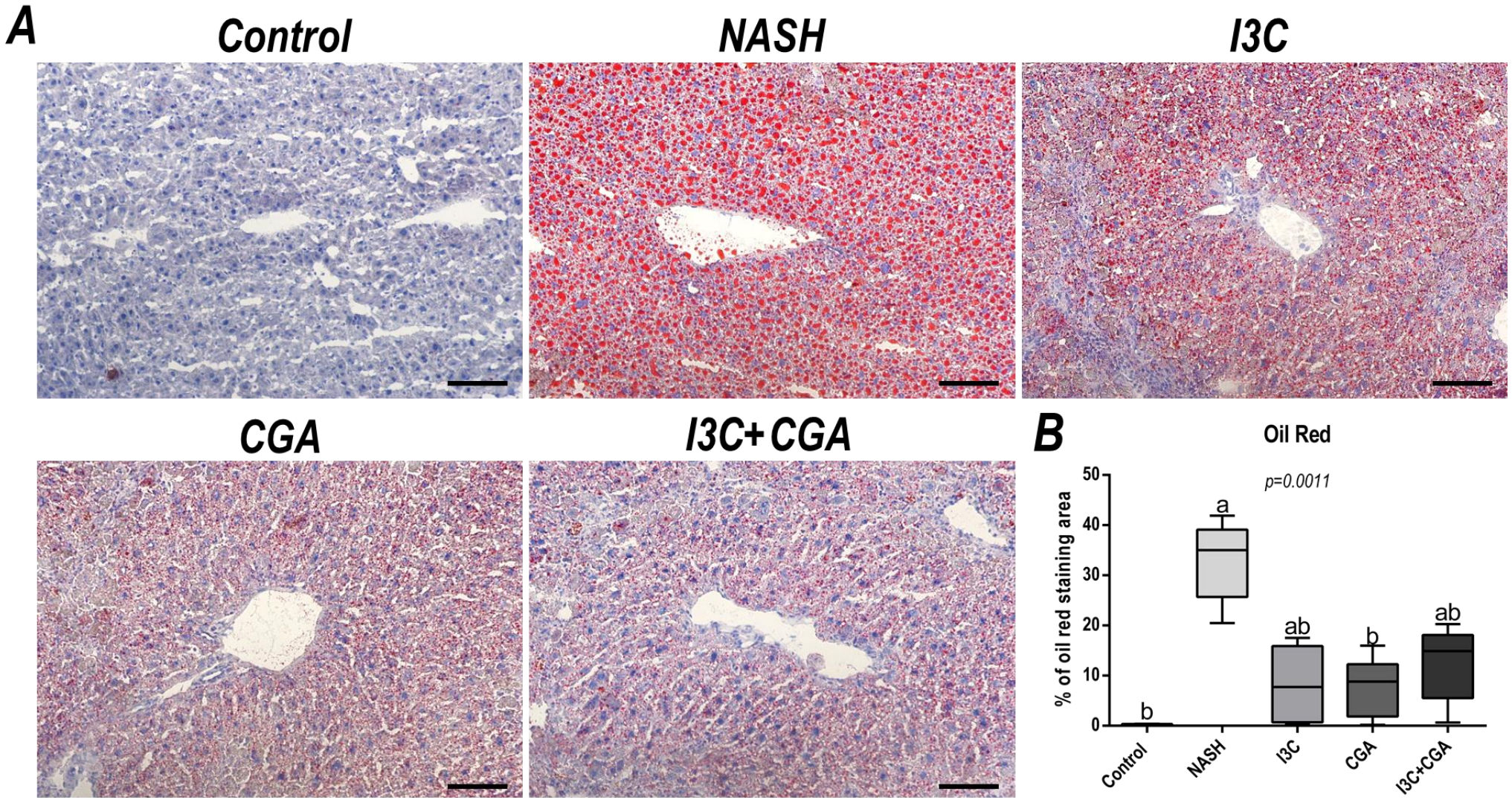

Figure 5. Effects of indole-3-carbinol and/or chlorogenic acid on the hepatic oil-red content. **(A)** Representative photomicrographs (20x objective, scale bar=50µm) of oil-red stained sections. **(B)** Semiquantitative analysis of oil-red content (% of oil-red area). The data are expressed in median±quartiles, and were analyzed by One-Way ANOVA, and Tukey pos-hoc test. Control [standard chow and 3x weekly intraperitoneal (i.p.) injections of corn oil vehicle]; NASH [chow enriched with fat (20%) and sucrose (20%) and carbon tetrachloride protocol (3x weekly i.p. injections of 10% corn oil solution of CCl_4, with weekly-increased doses of 0.25-1.50µL/g of body weight (b.w.)]; I3C [hybrid protocol of NASH with addition of intragastric injections of I3C (5x weekly, 5mg/Kg b.w.)]; CGA [hybrid protocol of NASH with addition of intragastric injections of CGA (5x weekly, 125mg/Kg b.w.)]; I3C+CGA [hybrid protocol of NASH with addition of intragastric injections of both I3C and CGA. N = 6 (control) or 8-9 (I3C, CGA, and I3C+CGA).

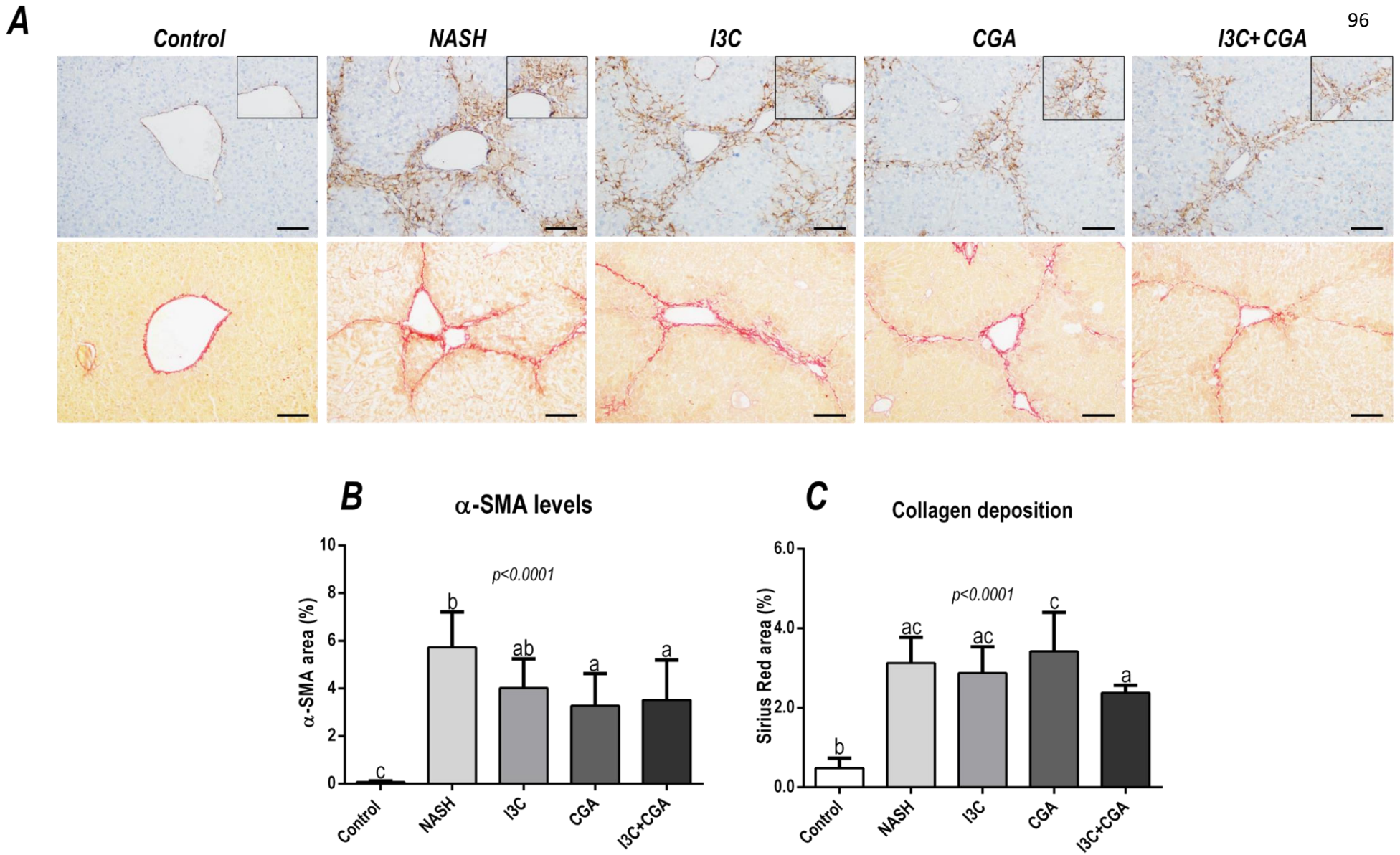

Figure 6. Effects of indole-3-carbinol and/or chlorogenic acid over hybrid model of NASH in C57BL/6J mice. **(A)** Representative photomicrographs (20x objective, scale bar=50μm) of C57BL/6J of sections immunoreacted for α-smooth muscle actin (α-SMA) or stained with sirius red. **(B)** Semiquantitative analysis of α-SMA expression (% of α-SMA area) and **(C)** collagen deposition (% of sirius red area) in hepatic sections of C57BL/6J mice. The data are expressed in mean±standard deviation, and were analyzed by One-Way ANOVA, and Tukey pos-hoc test. Control [standard chow and 3x weekly intraperitoneal (i.p.) injections of corn oil vehicle]; NASH [chow enriched with fat (20%) and sucrose (20%) and carbon tetrachloride protocol (3x weekly i.p. injections of 10% corn oil solution of CCl_4, with weekly-increased doses of 0.25-1.50μL/g of body weight (b.w.)]; I3C [hybrid protocol of NASH with addition of intragastric injections of I3C (5x weekly, 5mg/Kg b.w.)]; CGA [hybrid protocol of NASH with addition of intragastric injections of CGA (5x weekly, 125mg/Kg b.w.)]; I3C+CGA [hybrid protocol of NASH with addition of intragastric injections of both I3C and CGA. N = 6 (control) or 8-9 (I3C, CGA, and I3C+CGA).

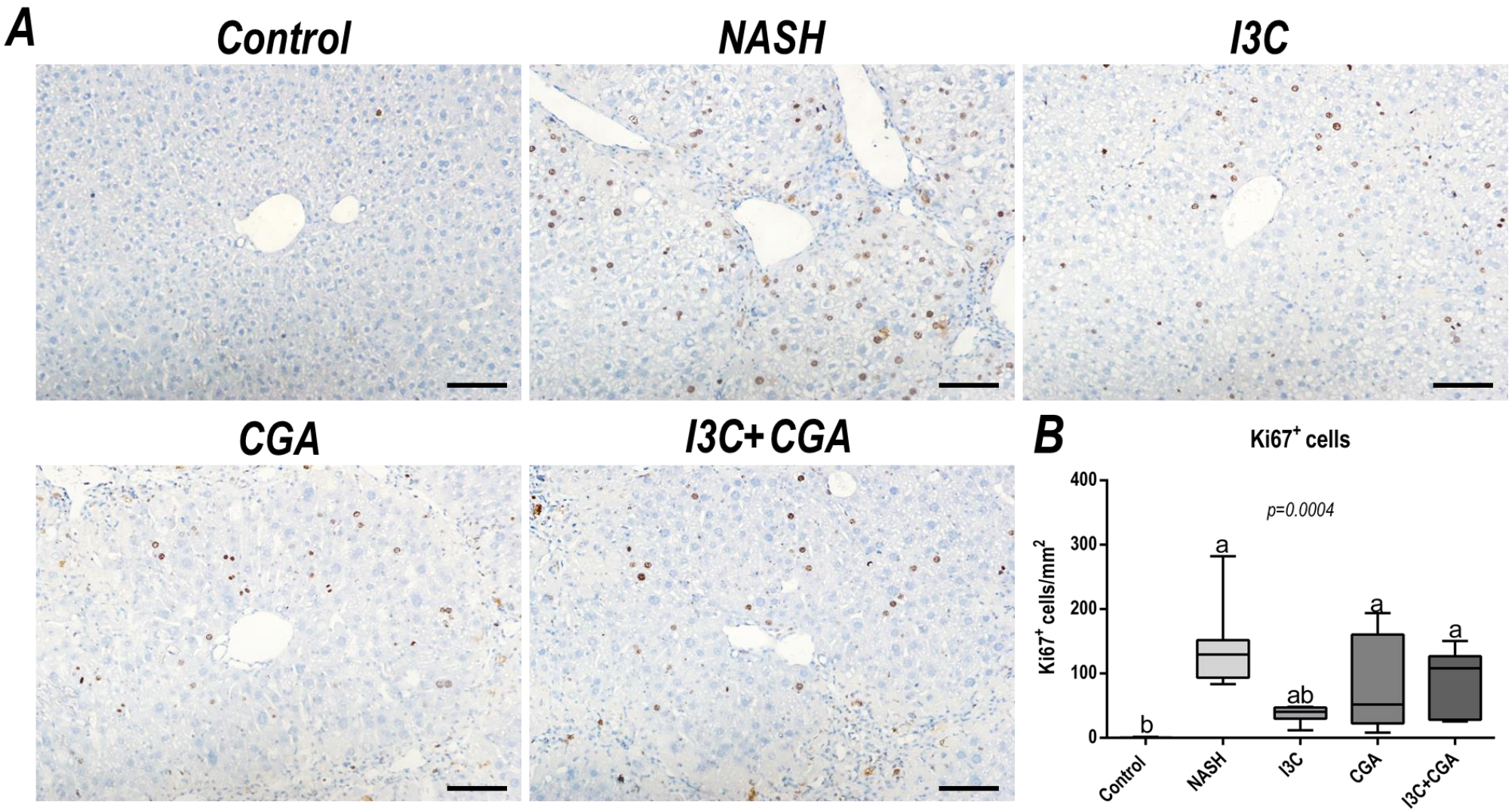

Figure 7. Effects of indole-3-carbinol and/or chlorogenic acid on the Ki67⁺ hepatocytes. **(A)** Representative photomicrographs (20x objective, scale bar=50µm) of immunoreacted sections. **(B)** Quantitative analysis of the number of Ki67⁺ cells. The data are expressed in median±quartiles, and were analyzed by Krskall-Wallis test. Control [standard chow and 3x weekly intraperitoneal (i.p.) injections of corn oil vehicle]; NASH [chow enriched with fat (20%) and sucrose (20%) and carbon tetrachloride protocol (3x weekly i.p. injections of 10% corn oil solution of CCl_4, with weekly-increased doses of 0.25-1.50µL/g of body weight (b.w.)]; I3C [hybrid protocol of NASH with addition of intragastric administrations of I3C (5x weekly, 5mg/Kg b.w.)]; CGA [hybrid protocol of NASH with addition of intragastric injections of CGA (5x weekly, 125mg/Kg b.w.)]; I3C+CGA [hybrid protocol of NASH with addition of intragastric injections of both I3C and CGA. N = 6 (control) or 8-9 (I3C, CGA, and I3C+CGA).

reduced number of hepatic $CD68^+$ cells ($p<0.0001$) (Figure 8), compared to the NASH group, suggesting that the beneficial effects of the combination of the bioactive compounds of *Brassicaceae* family vegetables might be linked to the modulation of the dynamics of the CD68-positive macrophages.

Discussion

The I3C is a glucosinolate (GLS)-derived molecule widely present in the *Brassicaceae* family, which contains cruciferous vegetables, like cabbage, broccoli, kale, and cauliflowers, as examples. The GLS, however, are synthesized during vegetable chewing, by inducing the activity of the myrosinase, an effector enzyme that hydrolyzes the GLS, removing the β-D-thioglucose group from its chemical structure. Hence, the synthesized molecules, like indoles, are unstable, exerting bioactive functions [17]. On the other hand, the CGA is a well-known bioactive molecule, found in many vegetables and beans, like cruciferous vegetables and coffee. The CGA is the most common form of the caffeoylquinic acid (CQA) isomers and both the small and large intestines feature as the main site for its absorption in the organism [34]. Recently, several studies show that both I3C and CGA are bioactive molecules that might have beneficial effects on NAFLD/NASH, due to their activities as an antioxidant molecule or by modulating the lipid metabolism and the inflammatory response [35–39]. However, it was never described whether the I3C and CGA combination, more than isolated, modulates the NASH development/progression. Thus, we evaluated the beneficial effects of the combination I3C+CGA in a murine NASH model.

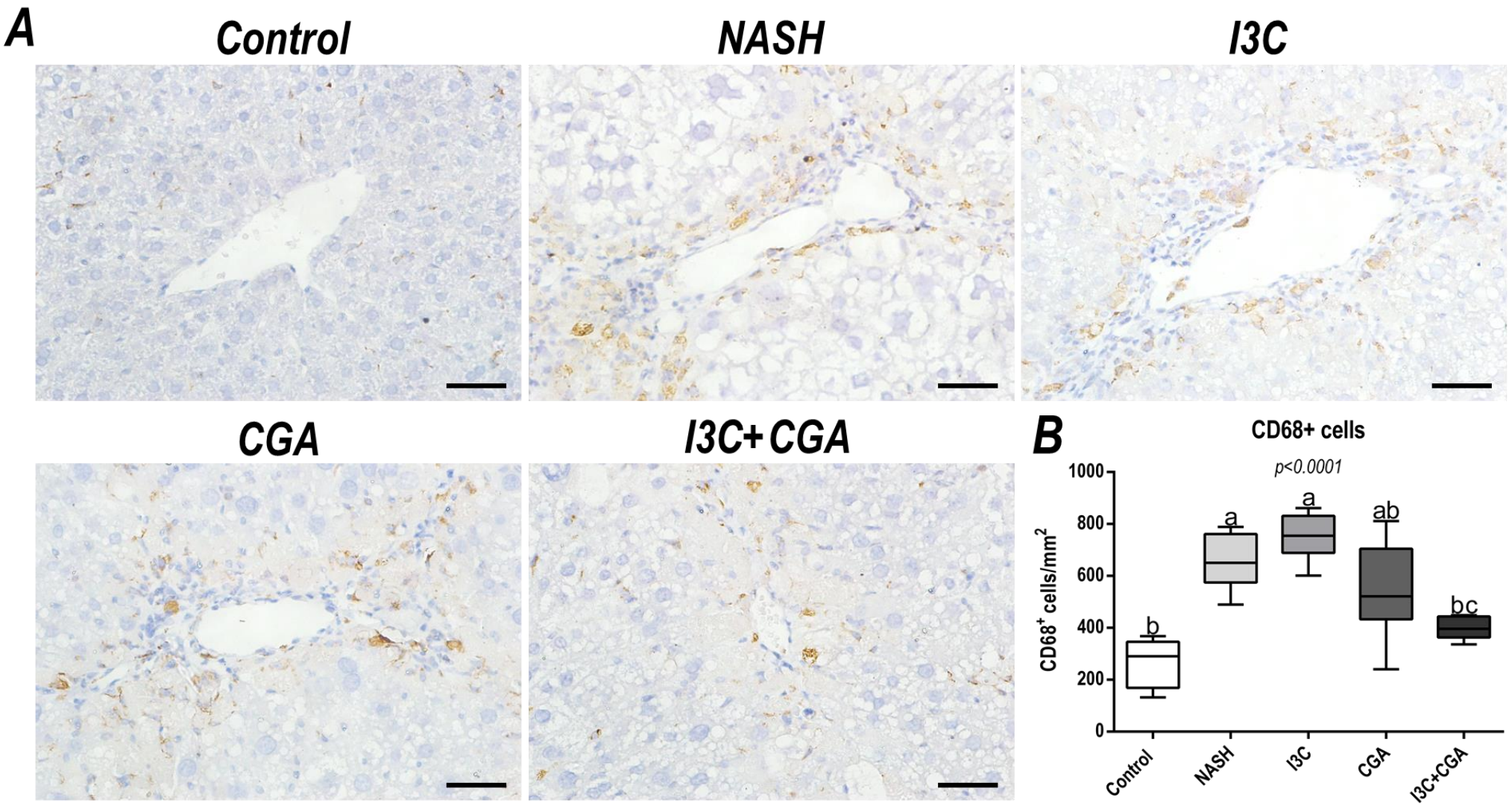

Figure 8. Effects of indole-3-carbinol and/or chlorogenic acid on the CD68⁺ cells. **(A)** Representative photomicrographs (20x objective, scale bar=50µm) of immunoreacted sections. **(B)** Quantitative analysis of the number of CD68⁺ cells. The data are expressed in median±quartiles, and were analyzed by Kruskall-Wallis test. Control [standard chow and 3x weekly intraperitoneal (i.p.) injections of corn oil vehicle]; NASH [chow enriched with fat (20%) and sucrose (20%) and carbon tetrachloride protocol (3x weekly i.p. injections of 10% corn oil solution of CCl_4, with weekly-increased doses of 0.25-1.50µL/g of body weight (b.w.)]; I3C [hybrid protocol of NASH with addition of intragastric administrations of I3C (5x weekly, 5mg/Kg b.w.)]; CGA [hybrid protocol of NASH with addition of intragastric injections of CGA (5x weekly, 125mg/Kg b.w.)]; I3C+CGA [hybrid protocol of NASH with addition of intragastric injections of both I3C and CGA. N = 6 (control) or 8-9 (I3C, CGA, and I3C+CGA).

Although there were no differences regarding the final body weight, the glucose tolerance profile, and AT relative fat pad weight, we observed that the combination I3C+CGA alleviates NASH-related morphologic (microvesicular steatosis, hepatocellular hypertrophy, and inflammatory foci occurrence) and, hence, the final NAS grading. It has been previously reported that under conditions of fatty acid (FA)-related oxidative stress, the hepatocytes are submitted to sublethal grade stress that contributes to morphologic alterations, especially the enlargement of the cytoplasm/nucleus ratio, characterizing the hypertrophy of hepatocytes [40]. Additionally, the CCl_4 is a well-known hepatotoxin that converted into CCl_3* and acts causing the lipid peroxidation of hepatocytes and, hence, leading to an hepatic pro-inflammatory microenvironment [26,42]. Otherwise, both compounds I3C and CGA have been previously described as potential antioxidant molecules, due to their protective effect under conditions of oxidative stress [35,43]. Indeed, in a CCl_4-induced acute liver injury, the pre-treatment with I3C (50.0 or 100.0 mg/Kg) reduced markers of hepatocytes injury alanine aminotransferase (ALT) and aspartate aminotransferase (AST), suggesting that I3C inhibits the CCl_4-associated injury of hepatocytes [44]. Moreover, I3C modulates the HepG2 (hepatocytes-like cells) antioxidant cell line defense, by enhancing the levels of the nuclear factor erythroid-2-related factor 2 (Nrf2) and Nrf2-related antioxidant enzymes, like superoxide dismutase (SOD), catalase (CAT), and glutathione peroxidase (GPx), suggesting an underlying mechanism that inhibits the CCl_3* activity as a lipid peroxidation-inducer, hepatocellular death, and further infiltration of inflammatory cells [45]. Likewise, the CGA is a polyphenol molecule that features a dual-role as a modulator of NASH parameters, by interfering in the lipid-redox dynamics [34]. The CGA administrations (60 mg/Kg of b.wt.) reduce the CCl_4-induced oxidative stress, by attenuating the CYP2E1 activity and increasing the protein levels of Nrf2 and its encoding antioxidant enzymes (SOD and CAT), similarly to I3C, as well as decreasing the malondialdehyde (MDA) levels, a marker of oxidative stress [43]. Taken together, we suggest that the combination I3C+CGA might modulate the oxidant/pro-inflammatory axis and, hence, the NASH-related

parameters, alleviating the hepatocellular hypertrophy, inflammatory foci occurrence, and steatosis profile.

In agreement with the NAS analysis, we observed that the combination I3C+CGA attenuates the hepatic lipid and collagen content (~25%), compared to the NASH group. Besides, the I3C+CGA-treated mice featured reduced levels of HSC activation, assessed by the immunoreactivity for α-SMA, suggesting that the bioactive compounds of the *Brassicaceae* attenuate the fibrotic hepatic milieu by reducing the HSC activation. Both I3C and CGA have been previously linked to lipid metabolism modulation, by enhancing the FA oxidation (FAO) activity and attenuating the lipogenesis-related mechanisms [37,38]. Indeed, mice fed an I3C-supplemented HFD displayed alleviated steatosis and inflammatory profile, by decreasing the mRNA levels of sterol regulator element-binding protein-1c (SREBP-1c), a transcription factor that modulates the expression of lipogenesis-related enzymes [37]. Similarly, CGA has been described as a modulator of FAO, by triggering the β-oxidation mechanism, and peroxisome proliferator-activated receptor γ (PPARγ), a master driver of the activation of lipogenesis-related genes, like FA synthases (FAS) and acetyl-CoA carboxylase (ACC). Additionally, there is also evidence that CGA also modulates *de novo* lipogenesis, by strikingly reducing FAS and SREBP-1c mRNA levels [38,46]. Thus, since both I3C and CGA modulate the cross-play between redox dynamics and lipid metabolism, by reducing oxidative stress and the *de novo* lipogenesis pathways, whereas enhancing the FAO, we suggest that the combination I3C+CGA might act on complementary underlying mechanisms that alleviates the NASH-related parameters, NAS grading, and the hepatic lipid and collagen content.

Several studies reported that both I3C and CGA are bioactive molecules that exert antioxidant activities scavenging free radicals and ROS [35,47]. In an acetaldehyde-induced murine model, the I3C treatment reduced the hepatic collagen deposition, by attenuating K63-ubiquitinated receptor-interacting protein 1 (RIP1), which signals for nuclear factor *kappa* B (NF-κB/p65) [48,49]. Additionally, in a fibrosis-induced murine model by CCl_4 administration, the CGA treatment reduced

the mRNA levels of α-SMA, collagen I and III, and tissue inhibitor metalloproteinase-1 (TIPM-1). Moreover, the CGA inhibited the oxidative stress levels, indicated by malondialdehyde levels (indicative of lipid peroxidation levels), by inducing the Nrf2 and reducing the CYP2E1 protein levels [43]. Thus, we suggest that the combination I3C+CGA might act by two different mechanisms: directly, scavenging ROS and free radicals, or indirectly, by modulating the pro-oxidant/inflammatory microenvironment, hence, attenuating NASH development and hepatic fibrosis progression.

The infiltrating and resident macrophages, the Kupffer cells (KC), has been appointed as pivotal cells that act coordinately inducing the pro-inflammatory/oxidant hepatic milieu, and it has been related to late-stage NASH, expressing high levels of CD68, a marker of monocyte-derivative cells that exert phagocytic activity [50,51]. It has been previously reported that both I3C, diindolylmethane (DIM), the major I3C-derivative molecule, and CGA inhibited RAW264.7 cells activation and pro-inflammatory cytokines synthesis [52,53]. Accordingly, we observed that only the combination I3C+CGA was able to reduce the number of hepatic $CD68^+$ cells, compared to the NASH group. Indeed, both I3C and CGA display a potential attenuating effect on the pro-inflammatory of LPS-induced RAW264.7 cells, by inhibiting iNOS and NF-κB-COX-2 pathways and suppressing the levels of inflammatory-drivers cytokines IL-1β and IL-6. Additionally, CGA is known to reduce the hepatic mRNA levels of *Cd68* and Ccr2, suggesting that CGA also modulates the recruitment of macrophages, further alleviating NASH [38]. Thus, we suggest that the combination I3C and CGA, rather than I3C or CGA individually, might act on complementary and pivotal molecular mechanisms drivers of NASH, by reducing the infiltration/activation of macrophages, as well as oxidative stress and pro-inflammatory pathways related to $CD68^+$ cells activation and, hence, alleviating NASH severity [52,54].

Conclusions

We observed that the combination I3C+CGA was able to reduce the severity of NASH, by alleviating both the hepatic lipid and collagen content, as well as reducing the activation of HSC, and infiltration of $CD68^+$ cells, drivers pro-inflammatory microenvironment in which NASH is susceptible to emerge. Finally, we suggest that I3C and CGA association act on the lipid-redox-inflammation axis, attenuating some of the hallmarks of NAFLD, and prospecting as a reliable chemopreventive approach.

References

1. Younossi, Z.M.; Koenig, A.B.; Abdelatif, D.; Fazel, Y.; Henry, L.; Wymer, M. Global epidemiology of nonalcoholic fatty liver disease—Meta-analytic assessment of prevalence, incidence, and outcomes. *Hepatology* **2016**, *64*, 73–84, doi:10.1002/hep.28431.
2. Zhou, B.; Lu, Y.; Hajifathalian, K.; Bentham, J.; Di Cesare, M.; Danaei, G.; Bixby, H.; Cowan, M.; Ali, M.; Taddei, C.; et al. Worldwide trends in diabetes since 1980: a pooled analysis of 751 population-based studies with 4·4 million participants. *Lancet* **2016**, *387*, 1513–1530, doi:10.1016/S0140-6736(16)00618-8.
3. Abarca-Gómez, L.; Abdeen, Z.A.; Hamid, Z.A.; Abu-Rmeileh, N.M.; Acosta-Cazares, B.; Acuin, C.; Adams, R.J.; Aekplakorn, W.; Afsana, K.; Aguilar-Salinas, C.A.; et al. Worldwide trends in body-mass index, underweight, overweight, and obesity from 1975 to 2016: a pooled analysis of 2416 population-based measurement studies in 128·9 million children, adolescents, and adults. *Lancet* **2017**, *390*, 2627–2642, doi:10.1016/S0140-6736(17)32129-3.
4. Li, L.; Liu, D.-W.; Yan, H.-Y.; Wang, Z.-Y.; Zhao, S.-H.; Wang, B. Obesity is an independent risk factor for non-alcoholic fatty liver disease: evidence from a meta-analysis of 21 cohort studies. *Obes. Rev.* **2016**, *17*, 510–519, doi:10.1111/obr.12407.
5. Duseja, A.; Chalasani, N. Epidemiology and risk factors of nonalcoholic fatty liver disease (NAFLD). *Hepatol. Int.* **2013**, *7*, 755–764, doi:10.1007/s12072-013-9480-x.

6. Estes, C.; Anstee, Q.M.; Arias-Loste, M.T.; Bantel, H.; Bellentani, S.; Caballeria, J.; Colombo, M.; Craxi, A.; Crespo, J.; Day, C.P.; et al. Modeling NAFLD disease burden in China, France, Germany, Italy, Japan, Spain, United Kingdom, and United States for the period 2016–2030. *J. Hepatol.* **2018**, *69*, 896–904, doi:10.1016/j.jhep.2018.05.036.

7. Younossi, Z.M.; Loomba, R.; Rinella, M.E.; Bugianesi, E.; Marchesini, G.; Neuschwander-Tetri, B.A.; Serfaty, L.; Negro, F.; Caldwell, S.H.; Ratziu, V.; et al. Current and future therapeutic regimens for nonalcoholic fatty liver disease and nonalcoholic steatohepatitis. *Hepatology* **2018**, *68*, 361–371, doi:10.1002/hep.29724.

8. Willebrords, J.; Veloso, I.; Pereira, A.; Maes, M.; Crespo, S.; Colle, I.; Bossche, B. Van Den; Cristina, T.; Silva, D.; Pinto, C.; et al. Strategies , models and biomarkers in experimental non-alcoholic fatty liver disease research. *Prog. Lipid Res.* **2015**, *59*, 106–125, doi:10.1016/j.plipres.2015.05.002.

9. Asgharpour, A.; Cazanave, S.C.; Pacana, T.; Seneshaw, M.; Vincent, R.; Banini, B.A.; Kumar, D.P.; Daita, K.; Min, H.; Mirshahi, F.; et al. A diet-induced animal model of non-alcoholic fatty liver disease and hepatocellular cancer. *J. Hepatol.* **2016**, *65*, 579–588, doi:10.1016/j.jhep.2016.05.005.

10. Tsuchida, T.; Lee, Y.A.; Fujiwara, N.; Ybanez, M.; Allen, B.; Martins, S.; Fiel, M.I.; Goossens, N.; Chou, H.; Hoshida, Y.; et al. A simple diet- and chemical-induced murine NASH model with rapid progression of steatohepatitis, fibrosis and liver cancer. *J. Hepatol.* **2018**, *69*, 385–395, doi:10.1016/j.jhep.2018.03.011.

11. Saura-Calixto, F.; Goñi, I. Definition of the Mediterranean Diet Based on Bioactive Compounds. *Crit. Rev. Food Sci. Nutr.* **2009**, *49*, 145–152, doi:10.1080/10408390701764732.

12. Kontogianni, M.D.; Tileli, N.; Margariti, A.; Georgoulis, M.; Deutsch, M.; Tiniakos, D.; Fragopoulou, E.; Zafiropoulou, R.; Manios, Y.; Papatheodoridis, G. Adherence to the Mediterranean diet is associated with the severity of non-alcoholic fatty liver disease. *Clin. Nutr.* **2014**, *33*, 678–683, doi:10.1016/j.clnu.2013.08.014.

13. Della Corte, C.; Mosca, A.; Vania, A.; Alterio, A.; Iasevoli, S.; Nobili, V. Good adherence to the Mediterranean diet reduces the risk for NASH and diabetes in pediatric patients with obesity: The

results of an Italian Study. *Nutrition* **2017**, *39–40*, 8–14, doi:10.1016/j.nut.2017.02.008.

14. Centers for Disease Control *2018 State Indicator Report On Fruits And Vegetables*; 2018;
15. Internatonal Agency For Research On Cancer *IARC Handbook of Cancer Prevention: Cruciferous Vegetables, Isothiocyanates and Indoles*; International Agency for Research on Cancer: Lyon, France, 2004; ISBN 9283230094.
16. Thomson, C.A.; Newton, T.R.; Graver, E.J.; Jackson, K.A.; Reid, P.M.; Hartz, V.L.; Cussler, E.C.; Hakim, I.A. Cruciferous Vegetable Intake Questionnaire Improves Cruciferous Vegetable Intake Estimates. *J. Am. Diet. Assoc.* **2007**, *107*, 631–643, doi:10.1016/j.jada.2007.01.016.
17. Esteve, M. Mechanisms Underlying Biological Effects of Cruciferous Glucosinolate-Derived Isothiocyanates/Indoles: A Focus on Metabolic Syndrome. *Front. Nutr.* **2020**, *7*, 1–22, doi:10.3389/fnut.2020.00111.
18. Fahey, J.W.; Zalcmann, A.T.; Talalay, P. The chemical diversity and distribution of glucosinolates and isothiocyanates among plants. *Phytochemistry* **2001**, *56*.
19. Cartea, M.E.; Francisco, M.; Soengas, P.; Velasco, P. Phenolic Compounds in Brassica Vegetables. *Molecules* **2010**, *16*, 251–280, doi:10.3390/molecules16010251.
20. Chang, H.-P.; Wang, M.-L.; Chan, M.-H.; Chiu, Y.-S.; Chen, Y.-H. Antiobesity activities of indole-3-carbinol in high-fat-diet–induced obese mice. *Nutrition* **2011**, *27*, 463–470, doi:10.1016/j.nut.2010.09.006.
21. Jayakumar, P.; Pugalendi, K.V.; Sankaran, M. Attenuation of hyperglycemia-mediated oxidative stress by indole-3-carbinol and its metabolite 3, 3'- diindolylmethane in C57BL/6J mice. *J. Physiol. Biochem.* **2014**, *70*, 525–534, doi:10.1007/s13105-014-0332-5.
22. Cho, A.; Jeon, S.; Kim, M.; Yeo, J.; Seo, K.; Choi, M.; Lee, M. Chlorogenic acid exhibits anti-obesity property and improves lipid metabolism in high-fat diet-induced-obese mice. *Food Chem. Toxicol.* **2010**, *48*, 937–943, doi:10.1016/j.fct.2010.01.003.
23. Wang, Z.; Lam, K.L.; Hu, J.; Ge, S.; Zhou, A.; Zheng, B.; Zeng, S.; Lin, S. Chlorogenic acid alleviates obesity and modulates gut microbiota in high-fat-fed mice. *Food Sci. Nutr.* **2019**, *7*, 579–588, doi:10.1002/fsn3.868.
24. Bacil, G.; Cogliati, B.; Cardoso, D.R.; Barbisan, L.F.; Romualdo, G.R. Are isothiocyanates and

polyphenols emerging preventive/therapeutic strategies for NAFLD? The landscape of recent preclinical findings. **2021**.

25. Bacil, G.; Romualdo, G.R.; Fernandes, A.A.H.; Cardoso, D.R.; Cogliati, B.; Barbisan, L.F. Establishment of a fibrosis-associated model of NASH: outcomes in different mice strains. **2021**.
26. Romualdo, G.R.; Prata, G.B.; da Silva, T.C.; Fernandes, A.A.H.; Moreno, F.S.; Cogliati, B.; Barbisan, L.F. Fibrosis-associated hepatocarcinogenesis revisited: Establishing standard medium-term chemically-induced male and female models. *PLoS One* **2018**, *13*, e0203879, doi:10.1371/journal.pone.0203879.
27. National Research Council *Committee for the update of the guide for the care and use of laboratory animals. Guide for the care and use of laboratory animals*; 2011; ISBN 9780309154000.
28. Reagan-Shaw, S.; Nihal, M.; Ahmad, N. Dose translation from animal to human studies revisited. *FASEB J.* **2007**, *22*, 659–661, doi:10.1096/fj.07-9574LSF.
29. Corrêa, V.G.; Tureck, C.; Locateli, G.; Peralta, R.M.; Koehnlein, E.A. Estimate of consumption of phenolic compounds by Brazilian population Estimativa do consumo de compostos fenólicos pela população brasileira. *Rev. Nutr.* **2015**, *28*, 185–196.
30. Andrikopoulos, S.; Blair, A.R.; Deluca, N.; Fam, B.C.; Proietto, J. Evaluating the glucose tolerance test in mice. *Am. J. Physiol. - Endocrinol. Metab.* **2008**, *295*, 1323–1332, doi:10.1152/ajpendo.90617.2008.
31. Liang, W.; Menke, A.L.; Driessen, A.; Koek, G.H.; Lindeman, J.H.; Stoop, R.; Havekes, L.M.; Kleemann., R.; Van Den Hoek, A.M. Establishment of a general NAFLD scoring system for rodent models and comparison to human liver pathology. *PLoS One* **2014**, *9*, 1–17, doi:10.1371/journal.pone.0115922.
32. Galarraga, M.; Campión, J.; Munõz-Barrutia, A.; Boqué, N.; Moreno, H.; Martínez, J.A.; Milagro, F.; Ortiz-de-Solórzano, C. Adiposoft: Automated software for the analysis of white adipose tissue cellularity in histological sections. *J. Lipid Res.* **2012**, *53*, 2791–2796, doi:10.1194/jlr.D023788.
33. Marra, F.; Gastaldelli, A.; Svegliati Baroni, G.; Tell, G.; Tiribelli, C. Molecular basis and mechanisms of progression of non-alcoholic steatohepatitis. *Trends Mol. Med.* **2008**, *14*, 72–81, doi:10.1016/j.molmed.2007.12.003.

34. Naveed, M.; Hejazi, V.; Abbas, M.; Kamboh, A.A.; Khan, G.J.; Shumzaid, M.; Ahmad, F.; Babazadeh, D.; FangFang, X.; Modarresi-Ghazani, F.; et al. Chlorogenic acid (CGA): A pharmacological review and call for further research. *Biomed. Pharmacother.* **2018**, *97*, 67–74, doi:10.1016/j.biopha.2017.10.064.

35. Arnao, M.B.; Sanchez-Bravo, J.; Acosta, M. Indole-3-carbinol as a scavenger of free radicals. *Biochem. Mol. Biol. Int.* **1996**, *39*, 1125–1134, doi:10.1080/15216549600201302.

36. Shertzer, H.G.; Tabor, M.W.; Berger, M.L. Protection from N-Nitrosodimethylamine-Mediated Damage by Indole-3-carbinol. *Exp. Mol. Pathol.* **1987**, *218*, 211–218.

37. Choi, Y.; Kim, Y.; Park, S.; Lee, K.W.; Park, T. Indole-3-carbinol prevents diet-induced obesity through modulation of multiple genes related to adipogenesis, thermogenesis or inflammation in the visceral adipose tissue of mice. *J. Nutr. Biochem.* **2012**, *23*, 1732–1739, doi:10.1016/j.jnutbio.2011.12.005.

38. Ma, Y.; Gao, M.; Liu, D. Chlorogenic acid improves high fat diet-induced hepatic steatosis and insulin resistance in mice. *Pharm. Res.* **2015**, *32*, 1200–1209, doi:10.1007/s11095-014-1526-9.

39. Zhou, Y.; Ruan, Z.; Wen, Y.; Yang, Y.; Mi, S.; Zhou, L.; Wu, X.; Ding, S.; Deng, Z.; Wu, G.; et al. Chlorogenic acid from honeysuckle improves hepatic lipid dysregulation and modulates hepatic fatty acids composition in rats with chronic endotoxin infusion. *J. Clin. Biochem. Nutr.* **2014**, *54*, 151–160, doi:10.3164/jcbn.14-10.

40. Dhibi, M.; Brahmi, F.; Mnari, A.; Houas, Z.; Chargui, I.; Bchir, L.; Gazzah, N.; Alsaif, M.A.; Hammami, M. The intake of high fat diet with different trans fatty acid levels differentially induces oxidative stress and non alcoholic fatty liver disease (NAFLD) in rats. *Nutr. Metab.* **2011**, *8*, 1–12, doi:10.1186/1743-7075-8-65.

41. Uehara, T.; Ppogribny, I.P.; Rusyn, I. The DEN and CCl4-induced mouse model of fibrosis and inflammation-associated hepatocellular carcinoma. *Curr. Protoc. Pharmacol.* **2015**, *66*, 1–4, doi:10.1002/0471141755.ph1430s66.The.

42. Weber, L.W.D.; Boll, M.; Stampfl, A. Hepatotoxicity and Mechanism of Action of Haloalkanes: Carbon Tetrachloride as a Toxicological Model. *Crit. Rev. Toxicol.* **2003**, *33*, 105–136, doi:10.1080/713611034.

43. Shi, H.; Shi, A.; Dong, L.; Lu, X.; Wang, Y.; Zhao, J.; Dai, F.; Guo, X. Chlorogenic acid protects against liver fibrosis in vivo and in vitro through inhibition of oxidative stress. *Clin. Nutr.* **2016**, *35*, 1366–1373, doi:10.1016/j.clnu.2016.03.002.

44. Ahn, M.; Kim, J.; Yang, D.; Chun, J.-Y.; Kim, G.O.; Shin, T. Indole-3-carbinol alleviates carbon tetrachloride-induced liver injury by inhibiting inflammatory response and regulating lipid metabolism. *Adv. Tradit. Med.* **2021**, *21*, 371–378, doi:10.1007/s13596-020-00452-8.

45. Krajka-Kuźniak, V.; Paluszczak, J.; Szaefer, H.; Baer-Dubowska, W. The activation of the Nrf2/ARE pathway in HepG2 hepatoma cells by phytochemicals and subsequent modulation of phase II and antioxidant enzyme expression. *J. Physiol. Biochem.* 2015, *71*, 227–238.

46. Zamani-Garmsiri, F.; Ghasempour, G.; Aliabadi, M.; Hashemnia, S.M.R.; Emamgholipour, S.; Meshkani, R. Combination of metformin and chlorogenic acid attenuates hepatic steatosis and inflammation in high-fat diet fed mice. *IUBMB Life* **2021**, *73*, 252–263, doi:10.1002/iub.2424.

47. Kono, Y.; Kobayashi, K.; Tagawa, S.; Adachi, K.; Ueda, A.; Sawa, Y.; Shibata, H. Antioxidant activity of polyphenolics in diets Rate constants of reactions of chlorogenic acid and caffeic acid with reactive species of oxygen and nitrogen. *Biochim. Biophys. Acta* **1997**, *1335*, 335–342.

48. Guo, Y.; Wu, X.Q.; Zhang, C.; Liao, Z.X.; Wu, Y.; Xia, Z.Y.; Wang, H. Effect of indole-3-carbinol on ethanol-induced liver injury and acetaldehyde-stimulated hepatic stellate cells activation using precision-cut rat liver slices. *Clin. Exp. Pharmacol. Physiol.* **2010**, *37*, 1107–1113, doi:10.1111/j.1440-1681.2010.05450.x.

49. Bin, L.; Cong, M.; Zhu, Y.; Xiong, Y.; Jin, W.; Wan, Y.; Zhou, Y.; Ao, Y.; Wang, H. Indole-3-Carbinol Induces Apoptosis of Hepatic Stellate Cells through K63 De- Ubiquitination of RIP1 in Rats. *Cell. Physiol. Biochem.* **2017**, *41*, 1481–1490, doi:10.1159/000470650.

50. Miura, K.; Yang, L.; van Rooijen, N.; Ohnishi, H.; Seki, E. Hepatic recruitment of macrophages promotes nonalcoholic steatohepatitis through CCR2. *Am. J. Physiol. - Gastrointest. Liver Physiol.* **2012**, *302*, 1310–1321, doi:10.1152/ajpgi.00365.2011.

51. Kinoshita, M.; Uchida, T.; Sato, A.; Nakashima, M.; Nakashima, H.; Shono, S.; Habu, Y.; Miyazaki, H.; Hiroi, S.; Seki, S. Characterization of two F4/80-positive Kupffer cell subsets by their function and phenotype in mice. *J. Hepatol.* **2010**, *53*, 903–910, doi:10.1016/j.jhep.2010.04.037.

52. Jiang, J.; Kang, T.B.; Shim, D.W.; Oh, N.H.; Kim, T.J.; Lee, K.H. Indole-3-carbinol inhibits LPS-induced inflammatory response by blocking TRIF-dependent signaling pathway in macrophages. *Food Chem. Toxicol.* **2013**, *57*, 256–261, doi:10.1016/j.fct.2013.03.040.

53. Cho, H.J.; Seon, M.R.; Lee, Y.M.; Kim, J.; Kim, J.-K.; Kim, S.G.; Park, J.H.Y. 3,3'-Diindolylmethane Suppresses the Inflammatory Response to Lipopolysaccharide in Murine Macrophages. *J. Nutr.* **2008**, *138*, 17–23, doi:10.1093/jn/138.1.17.

54. Shan, J.; Fu, J.; Zhao, Z.; Kong, X.; Huang, H.; Luo, L.; Yin, Z. Chlorogenic acid inhibits lipopolysaccharide-induced cyclooxygenase-2 expression in RAW264.7 cells through suppressing NF-κB and JNK/AP-1 activation. *Int. Immunopharmacol.* **2009**, *9*, 1042–1048, doi:10.1016/j.intimp.2009.04.011.

55. Younossi, Z.M.; Stepanova, M.; Afendy, M.; Fang, Y.; Younossi, Y.; Mir, H.; Srishord, M. Changes in the Prevalence of the Most Common Causes of Chronic Liver Diseases in the United States From 1988 to 2008. *Clin. Gastroenterol. Hepatol.* **2011**, *9*, 524-530.e1, doi:10.1016/j.cgh.2011.03.020.

56. Panagiotakos, D.B.; Chrysohoou, C.; Pitsavos, C.; Stefanadis, C. Association between the prevalence of obesity and adherence to the Mediterranean diet: the ATTICA study. *Nutrition* **2006**, *22*, 449–456, doi:10.1016/j.nut.2005.11.004.

57. Schwingshackl, L.; Missbach, B.; König, J.; Hoffmann, G. Adherence to a Mediterranean diet and risk of diabetes: a systematic review and meta-analysis. *Public Health Nutr.* **2015**, *18*, 1292–1299, doi:10.1017/S1368980014001542.

Final conclusions

Taken together, we managed to establish a hybrid (by associating WD and CCl_4 protocols) model of fibrosis-associated NASH, featuring severe microvesicular steatosis and increased NAS grading, extensive fibrosis, α-SMA levels (indicative of HSC activation), increased number of $Ki67^+$ and $casp3^+$ hepatocytes, and hepatic $CD68^+$ cells. Additionally, we observed that the Nrf2-Nf-κB exerts a pivotal activity, by unbalancing the redox-inflammatory axis in the hepatic milieu, along with a strain-dependent metabolomic profile. Our findings suggest that the C57BL/6J mice were more susceptible to the model of NASH, rather than BALB/c mice. Further, we assessed the effects of the I3C and/or CGA on C57BL/6J mice submitted to the model of NASH. We observed that the I3C+CGA alleviated NASH, by decreasing the number of hepatic CD68+ cells and HSC activation, besides slightly reducing the hepatic lipid content and collagen fibers deposit (~25% compared to NASH group). Thus, we suggest that the combination I3C and CGA acts on the lipid-inflammatory axis, attenuating the hallmarks of NAFLD and prospecting as a potential preclinical strategy.